WORKING TOWARDS A CANCER CELL SELECTIVE AND BRAIN PENETRATING ANTI GLIOMA DRUG

by Kelsey Middleton

A thesis submitted to the Graduate Council of
Texas State University in partial fulfillment
of the requirements for the degree of
Master of Science
with a Major in Chemistry
August 2016

Committee Members:

Alexander Kornienko, Chair

Todd Hudnall

Karen Lewis

FAIR USE AND AUTHOR'S PERMISSION STATEMENT

Fair Use

Duplication Permission

DEDICATION

Grandma I know you weren't here for the duration of this degree, but I know it was you who kept telling me not to quit. This is for you.

ACKNOWLEDGEMENTS

I would like to thank my research advisor Dr. Kornienko for his guidance and patience throughout this project. I would like to thank my committee members, Dr. Todd Hudnall and Dr. Karen Lewis, for their expertise and input over the past two years. I would also like to thank my lab mates, Derek Medellin and Robert Scott, as well as Dr. Ramesh Dasari for their expertise and assistance with this project.

I would like to thank my colleagues at Texas State who have not only provided input in this project, but have helped ensured its completion. Thank you Karolyn Barker, Rachel Bower, Elyssa Cherry, Kim Ramsdell, and Cally Moore. You are all amazing and words cannot express how grateful I am to have met all of you.

Thank you to the entire Department of Chemistry stockroom for always being able to help me when I was out of options. Thank you to the entire Royall-Burklund clan for taking me under your wing during hard times. Thank you to my sister, Bethany, for always providing an ear to listen to, and to my nephew Gatlin for letting her listen without being too fussy. Thank you to my Dad and stepmom Michelle for being supportive, and for always being able to provide new socks.

Lastly, thank you to Boo for still meeting me at the door at the end of every day, regardless of how late I came home.

TABLE OF CONTENTS

Page

LIST OF TABLES

Table **Page**

LIST OF FIGURES

Figure **Page**

LIST OF ILLUSTRATIONS

Scheme **Page**

LIST OF ABBREVIATIONS

Abbreviation	Description
GBM	Glioblastoma Multiforme
CSC	Cancer stem cells
NSCLC	Non-small cell lung cancer
F-actin	Fibrillar polymerized actin
CNS	Central nervous system
BBB	Blood brain barrier
GLUT1	Glucose 1 transporter
PET	Postrion emission tomography
SGLT	sodium-glucose linked transporters
SCL2A	Solute carrier family 2A
ADME	Absorption, distribution, metabolism, excretion
Lyc	Lycorine
NCS	Narciclasine
DMF	Dimethylformamide
NaH	Sodium hydroxide
NaI	Sodium iodide
DMAP	4-dimethylaminopyridine
EDCI	1-Ethyl-3-(3-dimethylaminopropyl) carbodiimide
DCC	*N,N′*-Dicyclohexylcarbodiimide
MeOH	Methanol
$CHCl_3$	Chloroform
DCM	Dichloromethane
H_2O	Water
MTT	3-(4,5-dimethylthiazol-2-yl)-2,5-diphenyltetrazolium bromide
Formazan	(*E,Z*)-5-(4,5-dimethylthiazol-2-yl)-1,3-diphenylformazan
PTSA	*p*-toluenesulfonic acid
TsCl	Tosylate chloride
CuAAC, “click chemistry”	Copper-Catalyzed Azide-Alkyne Cycloaddition
EtOAc	Ethyl Acetate

ABSTRACT

Glioblastoma multiforme is one of the most fatal and hardest to treat cancers. The main reasons for our failure to treat this type of cancer are the resistance to glioblastoma cells, to their high metastatic potential and poor drug penetration across the blood brain barrier. In previous research we have found that two alkaloids, lycorine and narciclasine, are effective in overcoming cancer cell resistance to apoptosis and potently inhibit glioblastoma cell growth and migration. In current research, described in this thesis, we attempted to take advantage of substrate active transport of lycorine and narciclasine into cancer cells as well as across the blood brain barrier using the GLUT1 transporter. To this end, we attempted to make various conjugates, of lycorine and narciclasine to glucose with the hypothesis that the glucose moiety would be recognized by GLUT1 and facilitate uptake of these molecules into brain cancer cells. Two such conjugates were successfully prepared and tested in cancer cells; however, it was found that these compounds were less potent than their parent alkaloids, suggesting that they were not good GLUT1 substrates.

I. INTRODUCTION

A. Glioblastoma resistance to chemotherapy

Glioblastoma multiforme (GBM) is known to be one of the most common and fatal types of cancers, with a mean period of survival of approximately 14 months from the time of diagnosis.[1] GBM is classified by the World Health Organization as a grade IV tumor, based on observed pathological findings such as necrosis, vascular proliferation, and mitotic activity, at the time of diagnosis.[2] Diagnosis for GBM patients generally occurs late in adulthood, with a mean patient age around 64 years, and has been found to be more common in men than women.[3] Due to lack of specific symptoms, proper symptoms of GBM and other gliomas often goes unnoticed until tumors are already in advanced stages, contributing to poor prognosis, tumor recurrence, and a low survival rate.[4] Current treatment regimens for GBM patients include combined maximal surgical resection, radiotherapy, and chemotherapy with temozolomide, an alkylating agent designed to target DNA replication in cancer cells to induce apoptosis.[1]

However, recurrence of tumors seems standard despite vigorous treatment efforts. Metastasis plays a prominent role in tumor recurrence; glioma cells are unique in that they have the capability of invading and "branching" through surrounding brain tissue (Figure 1), often preventing surgical resections and leading to therapy resistance.[5] Studies have shown that elevated hypoxic areas within well-developed tumors contribute to multidrug resistance (MDR) as well as chemotherapy resistance.[6]

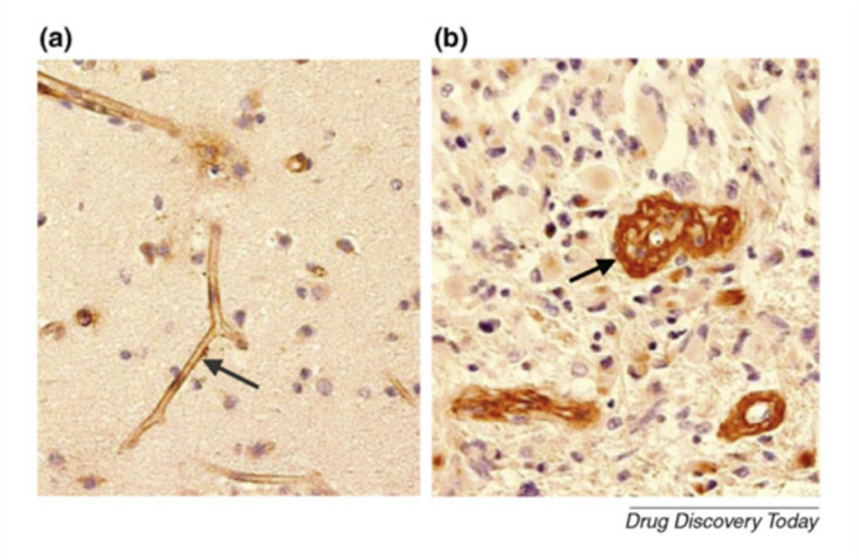

Figure 1. Migration of GBM cells through the parenchyma of the brain. (a) Represents the "branching" characteristics of GBM cells. (b) Represents the solid tumors capable of forming GBM colonies. Taken from Juillerat *et al.*[7]

Cancer stem cells (CSC) within solid tumors play an important role in tumor regrowth, progression, and drug resistance. CSCs are particularly resistant to apoptosis, which constitutes the main mechanism of action of current chemotherapy.[8] The resistance of cancer cells to current therapies demands alternative treatments that are not dependent on the induction of apoptosis. Here we suggest lycorine and narciclasine, cytostatic alkaloids from the plant family *Amaryllidaceae*, as potential candidates.

B. *Amaryllidaceae* alkaloids as potential anti-GBM agents

The medicinal use of plants from the *Amaryllidaceae* family dates as far back as the 4th century B.C., when Hippocrates of Kos treated patients showing symptoms of uterine cancer with daffodil oil extracts.[9] *Amaryllidaceae* plants are extensively used for traditional medicinal purposes in various different countries worldwide, particularly in developing countries with limited medical funds and facilities. The majority of compounds found and isolated from the *Amaryllidaceae* plant family are toxic alkaloids, which despite their adverse side effects, have demonstrated anti-tumor effects repetitively *in vivo*.[10] Here we focus on two alkaloids, lycorine and narciclasine, that have both demonstrated significant anti-tumor effects, for further investigation.

Lycorine, the first *Amaryllidaceae* alkaloid found, was isolated in 1877 from *Narcissus poeticus* and its structure elucidated in 1956 by Nagakawa *et al*.[11],[12] Narciclasine was isolated and characterized in 1967 by Ceriotti *et al* (Figure 2).[13]

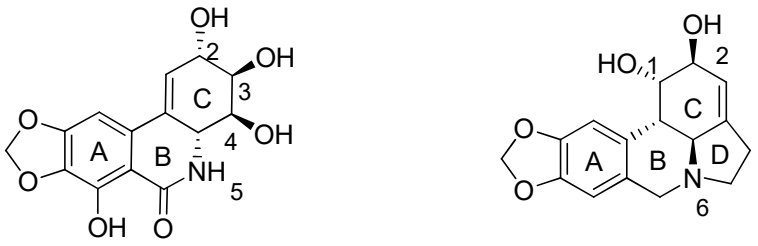

Figure 2. Structures of narciclasine (left) and lycorine (right).

Both lycorine and narciclasine exhibit a variety of pharmacological effects, including anti-tumor, anti-viral, anti-malarial, anti-bacterial, and anti-inflammatory properties.[14] It has been demonstrated that both lycorine and narciclasine inhibit eukaryotic protein synthesis initiation and elongation.[15] It has been further demonstrated

that both lycorine and narciclasine impair actin cytoskeleton rearrangements in cancer cells, and works performed by the Kornienko lab as well as with our collaborators at the University of New Mexico and Free Brussels University has been able to demonstrate the cytostatic activity of these alkaloids against both apoptosis-resistant and apoptosis-sensitive cancer cell lines.[11]

These collaborative *in vitro* studies have demonstrated that lycorine is active against cell lines that are apoptosis-resistant (A549, U373, OE21, and SKMEL-28) and apoptosis-sensitive (Hs683 and B16F10). For lycorine, quantitative video microscopy results were also used to demonstrate this activity. Figure 3 depicts lycorine inhibiting the growth of two known apoptosis-resistant cancer cell lines.[11] Here we stress that lycorine does not induce cell death, but rather inhibits cell growth when assayed at its IC_{50} value (5 μM). Lycorine has also been found to provide significant therapeutic benefits in mice bearing brain grafts of the B16F10 melanoma mouse model at nontoxic doses.[11]

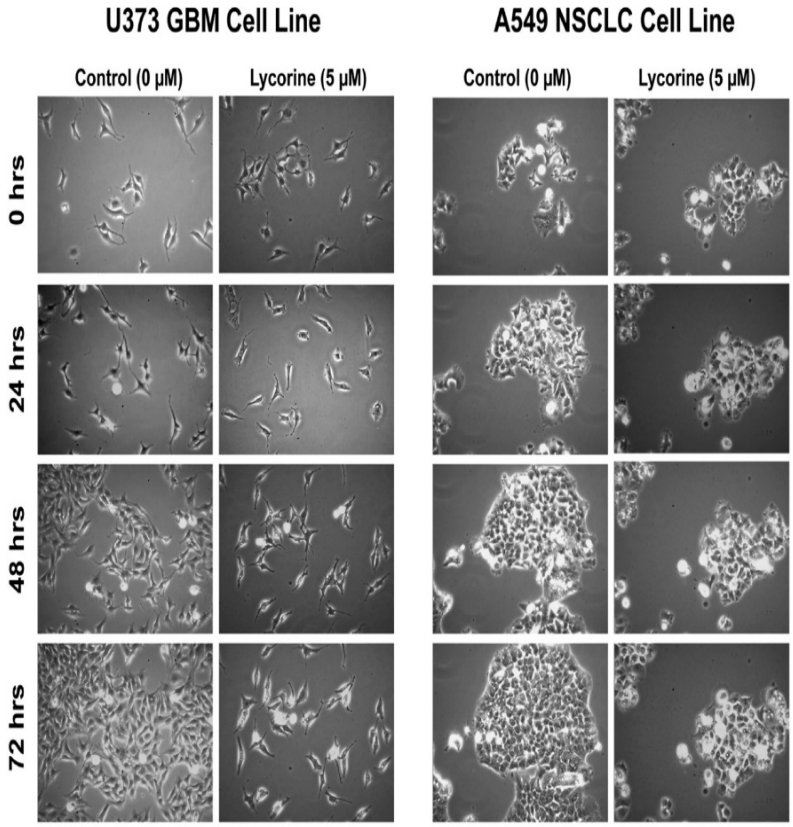

Figure 3. Quantitative video microscopy reported by Lamoral-Theys *et al*.[11] Quantitative video-microscopy was used to analyze and observe the cytostatic effects of lycorine on apoptosis-resistant human U373 glioblastoma and apoptosis-resistant A549 non-small cell lung cancer cells. Cytostatic growth was monitored in both cell lines over a 72 hour time period. Confluency for both control groups was observed within 72 hours, whereas confluency was not reached in the lycorine-treated cell lines within the same time period.

The data in Figure 4 confirm the cytotoxic effects of lycorine on actin cytoskeleton rearrangement in the apoptosis-resistant U373 GBM and A549 non-small cell lung cancer (NSCLC) cell lines.

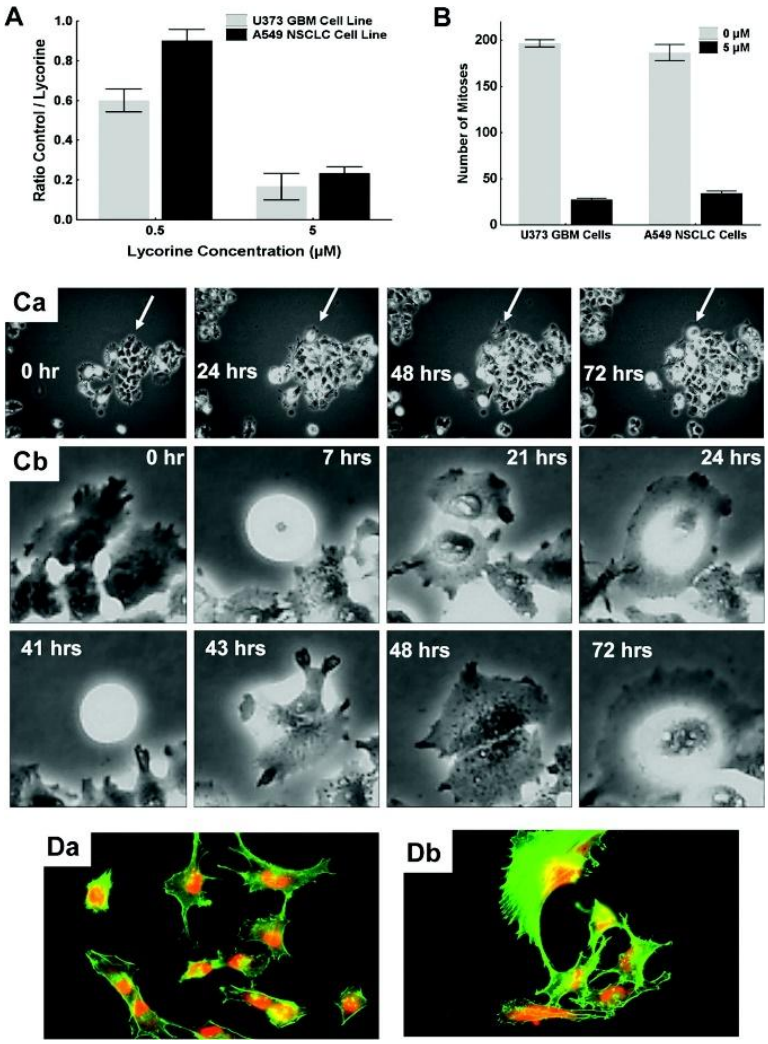

Figure 4. Findings reported by Lamoral-Theys *et al*.[11] (4A) represents a Global Growth Rate (GGR) of 0.2, meaning that 20% of cells grew in the lycorine treated cell lines for both U373 GBM and A549 NSCLC. (4B) represents the amount of cell mitoses decreased in the lycorine vs control cell lines for both U373 and A549 (≥90%). (4Ca) represents a single cell isolated from A549 NSCLC colony treated with 5 µM of lycorine over 72 h. (4Cb) represents this same cell enlarged using phase contrast microscopy. (4D) represents immunofluorescence analysis with green fluorescence (F-actin) and red fluorescence (G-actin) of 5 µM lycorine treated U373 GBM (4Da) verses control (4Db).

It was found that 20% of the lycorine treated cells in both U373 GBM and A549 NSCLC cell lines exhibited cell growth (4A), and that both cell lines exhibited ≥90% decrease in cell mitosis (4B). A single colony from A549 NSCLC cell line treated with 5

μM of lycorine was isolated and observed using computer-assisted phase microscopy at normal (4Ca) and increased magnifications (4Cb). It was observed that the cell isolated entered mitosis 7 hours after treatment with 5 μM of lycorine (4Cb), but failed to enter mitosis after 24 hours (4Cb). After 41 hours, this same cell attempted to enter mitosis once more, but failed by 72 hours. These findings strongly suggest that the lycorine-induced cytostatic effects take place primarily during cytokinesis. To confirm these results, immunofluorescence analyses were used to observe actin cytoskeleton of lycorine treated U373 GBM cell line (4Da) verses a control line (4Db). Lack of the green fluorescent dye in the lycorine treated U373 GBM cell line confirms lycorine-induced cytostatic effects on actin cytoskeleton organization.[11]

Like lycorine, it has been demonstrated that narciclasine also impairs actin cytoskeleton organization. The wound healing assay performed by Ingrassia and colleagues confirm these findings (Figure 5).[16] The results of this assay conclude that in all three cell lines, 10 nM narciclasine did not impair wound healing. However, at 100 nM, narciclasine displayed inhibitory effects in U373 glioblastoma cells and PC-3 prostate cancer cells, but not in normal lung fibroblasts (Ccd-25-Lu). Thus, it can be concluded

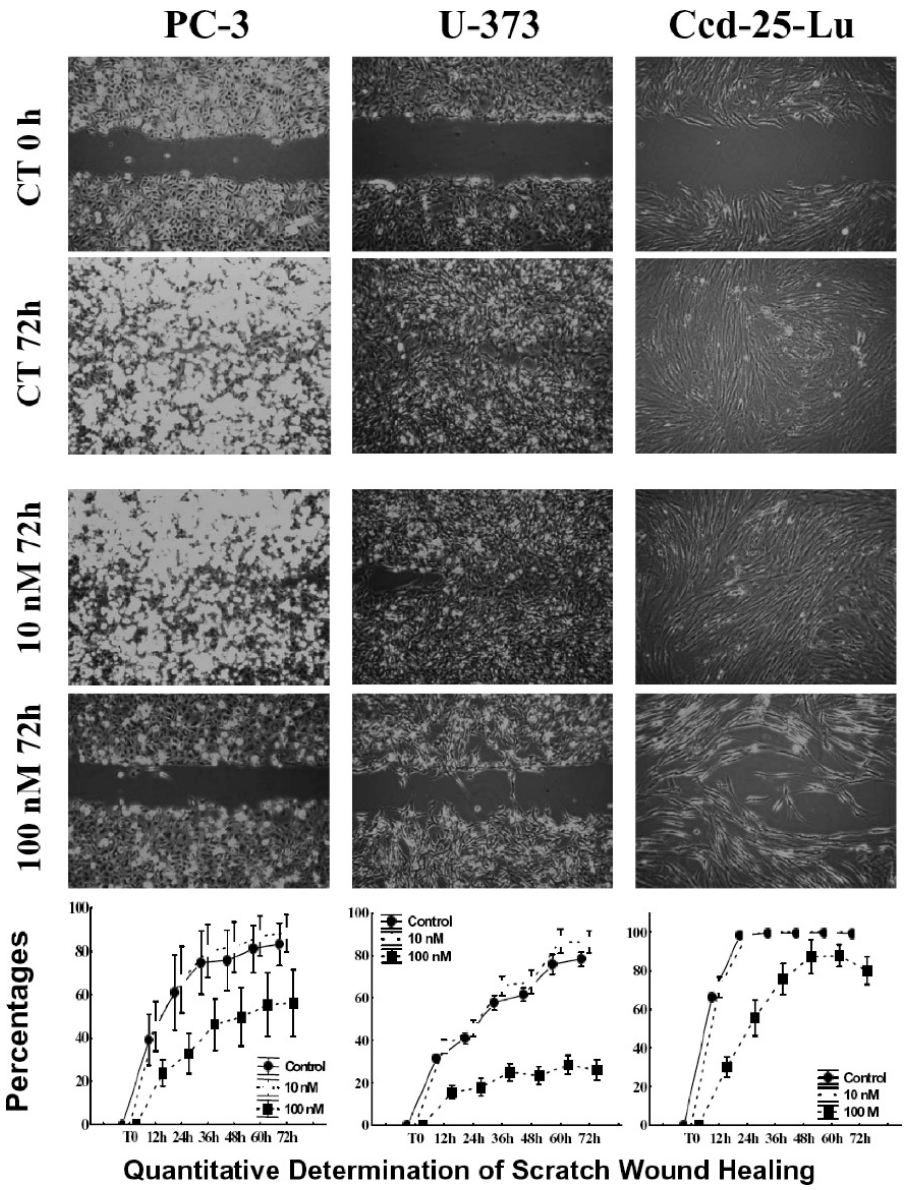

Figure 5. Results of wound healing assays reported by Ingrassia *et al.*[16] Top: results of the wound healing assays with human PC-3 prostate cancer cells, U373 glioblastoma cells, and normal Ccd-25-Lu lung fibroblasts treated for 72 h with 10 or 100 nM narciclasine. CT 0 h represents control group at 0 hr. CT 72 h represents control group after 72 h. 10 nM 72 h and 100 nM 72 h each represent respective concentrations of narciclasine after 72 hours. Bottom: percentage of wound healing for all 3 cell lines over a 72 h period.

that narciclasine appears to inhibit cancer cell migration independent of apoptosis status; as U373 cells are apoptosis-resistant and PC-3 cells are apoptosis-sensitive. Here, the high therapeutic ratio, or ration of specificity for cancer cells versus normal cells, of narciclasine in cancer cells (PC-3 and U373) over normal cells (Ccd-25-Lu) is also confirmed.

Further work performed by Ingrassia and company confirm that narciclasine shows higher *in vitro* antiproliferative activity in cancer cells over normal cells (Figure 6).[16] Here we see that at 100 nM, narciclasine increased the amount of fibrillar polymerized actin, or F-actin, (green fluorescence) in both prostate cancer (PC-3) cells (Figure 6A) and U373 glioblastoma cells (Figure 6B), but not Ccd-25-Lu normal lung fibroblast cells (Figure 6C). This prevalence of F-actin compared to globular actin (red fluorescence), signifies an increase in rigidity of the actin cytoskeleton in cancer cells, and as such can lead to impairment of cancer cell growth and migration. Figure 6D quantitatively represents the levels of F-actin for PC-3, U373, and Ccd-25-Lu cells respectively.

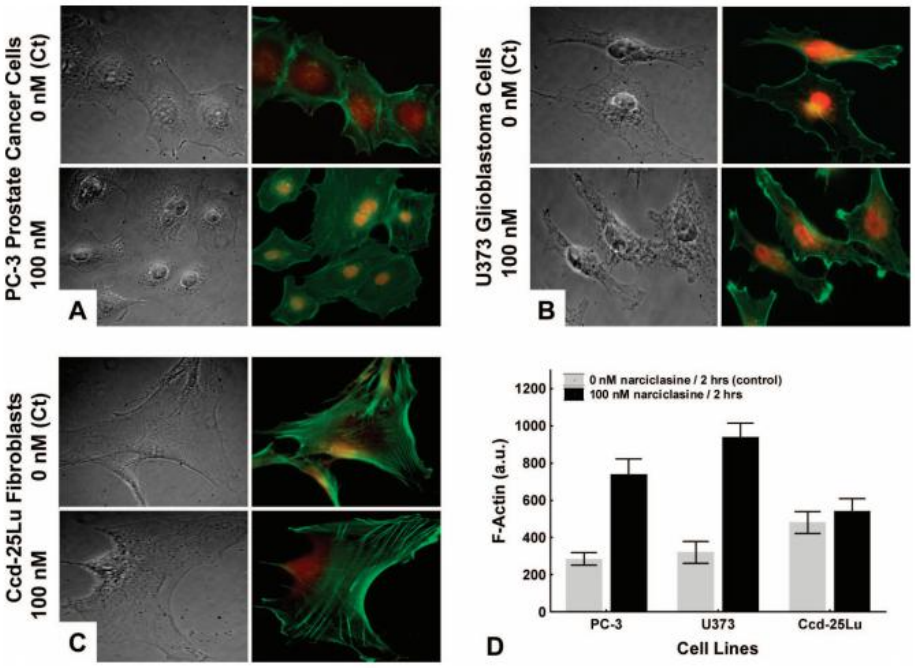

Figure 6. Findings reported by Ingrassia *et al*.[16] Qualitative (A−C) and quantitative (D) determination of narciclasine-induced effects on actin cytoskeleton organization in human prostate cancer cells (PC-3) (A), U373 glioblastoma cells (B), and normal Ccd-25-Lu lung fibroblasts (C). Fibrillar actin appears as green fluorescence, and globular actin appears as red fluorescence. Fibrillar actin levels were quantitatively determined using previously reported computer-assisted fluorescence microscopy.[17]

Further structure-activity relationship studies performed by Ingrassia revealed that few chemical modifications of narciclasine showed improved or equivalent IC_{50} values. However, it was found that esterification of the C2 hydroxyl position (see Figure 2) retained or improved *in vitro* narciclasine activity. These findings assisted in deciding how to appropriately modify narciclasine, as detailed later. However, lycorine's low *Log* P and narciclasine's low solubility make derivatization and delivery of these compounds difficult. We address these issues each respectively here in this project.

C. Challenges with drug delivery to the brain

Polar molecules such as lycorine and narciclasine have a problem with crossing the blood brain barrier (BBB), a highly restrictive and selective biological membrane separating the vascular system and the central nervous system (CNS) (Figure 7).[18] The BBB is composed primarily of highly specialized endothelial cells connected by tight and gap junctions, and maintains internal homeostasis within the CNS as well as limits the risk of blood borne toxins and pathogens accessing the CNS.[19] Passage of essential precursors and substrates to maintain CNS homeostasis through the BBB can occur through various different pathways, as described below and in Figure 7. For the purposes of this particular project, we will focus on both carrier and receptor mediated transport of the blood brain barrier.

The primary mechanisms for carrier-mediated and receptor-mediated transport through the blood brain barrier are shown below in Figure 7. First, the paracellular aqueous pathway (a) located in tight junctions between adjacent epithelial cells allows the passage of water soluble molecules but restricts the passage of polar solutes. Small liposoluble molecules (<400 Da) can be transported via passive diffusion through the transcellular lipophilic pathway (b).[18] The BBB also allows passage of hydrophilic molecules, such as glucose and amino acids, via carrier-mediated transport through the plasma membrane down a concentration gradient (c). Unlike carrier-mediated transport, receptor-mediated transcytosis (d) functions via active transport and is more highly selective, and has high energy requirements for passage of solutes such as insulin, transferrin, and leptin, since passage of these solutes goes against a concentration gradient.[20] Lastly, adsorption-mediated transcytosis (e) allows for passage of

macromolecules and molecules adsorbed and bound to these macromolecules via endocytosis through the endothelial cytoplasm.[21]

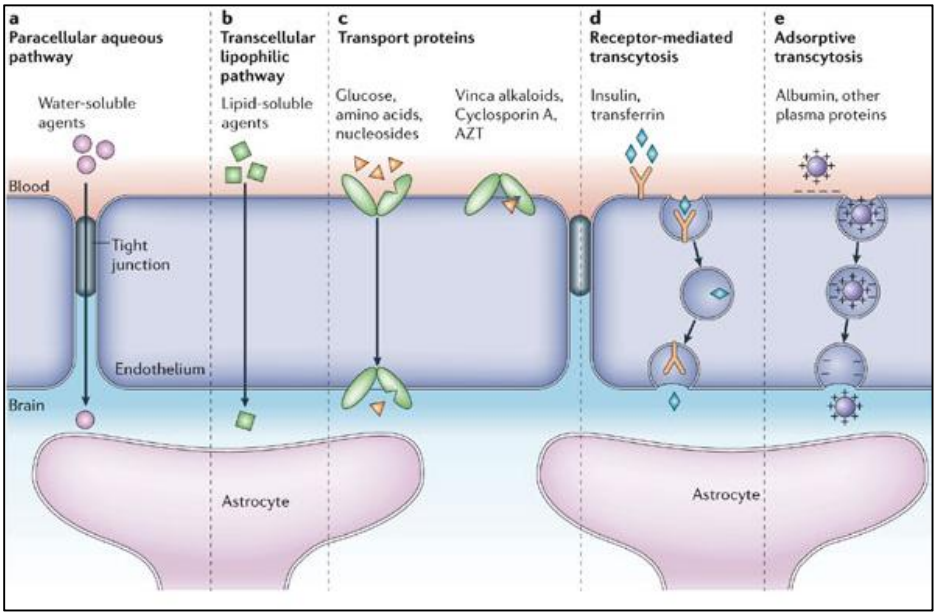

Figure 7. Overview of potential routes for carrier and receptor-mediated transport across the BBB.[8] (a) paracellular aqueous pathway, (b) transcellular lipophilic pathway, (c) transport proteins, (d) receptor mediated endocytosis, (e) adsorptive transcytosis.

Unfortunately, successful treatment of CNS diseases and tumors is limited by the delivery of CNS drugs through the BBB. One possible solution around this is to generate analogs with increased lipophilicity via synthetic modification. Previous studies performed by Dasari *et al*. involved the synthesis of 35 lycorine derivatives, or analogs, modified at the C1 and C2 positions. Many of these showed retention of cytostatic activity, albeit at reduced potencies.[9] Similar studies were performed by Ingrassia *et al.* with narciclasine showed that modification of the parent structure resulted in decreased potency.[16]

Another possible solution includes conjugating drugs to specific molecules known to be capable of crossing the BBB.[7] Coupling of pharmacological agents to naturally occurring substrates, such as amino acids, antibodies, and carbohydrates, has been previously proposed numerous times in literature (Figure 8).

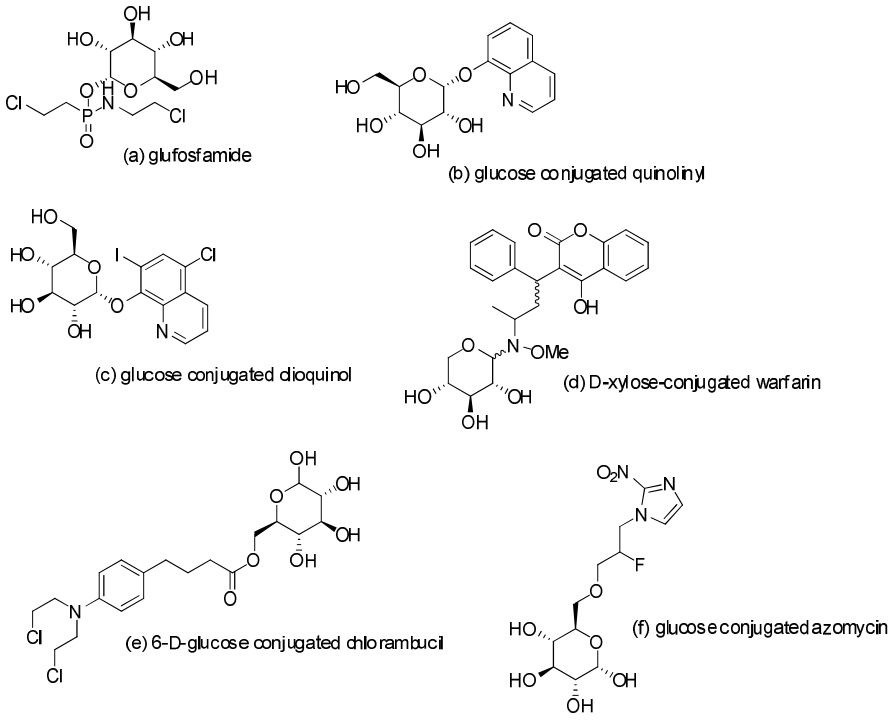

Figure 8. Structures of previously studied and tested glucose derivatives. (a) glufosfamide, initially developed as a cytotoxic anti-cancer compound; (b) glucose conjugated quinolinyl, and (c) clinquinol, both developed to improve tumor cell targeting; (d) D-xylose conjugated warfarin, which showed cytotoxicity in cancer cells; (e) chlorambucil, designed as a DNA alkylator similar to glufosfamide; and (f) glucose linked azomycin, synthesized to improve GLUT 1 uptake.

Both (a) glufosfamide and (e) D-glucose-conjugated chlorambucil, were designed as DNA alkylators. Glufosfamide, reported by Pohl and colleagues in 1995, was the first published example of a glucose-conjugated drug, and was designed initially to decrease cytotoxicity as well as increase selectivity of the cancer-targeting agent ifosfamide, a

DNA alkylating agent.[22] It was later reported by Pohl and colleagues that glufosfamide requires cleavage of the glucose moiety to free the active ifosfamide group, and side effects of the drug included slight renal toxicity.[22] The drug successfully entered human clinical trials in 1997, and has shown success in treating pancreatic cancer patients over the past ten years.[23] However, European clinical studies with glufosfamide has shown very low efficacy in patients with GBM and non-small cell lung carcinoma.[23],[24] The ability of glufosfamide to cross the BBB was not further investigated.[25]

Both Figure 8b and 8c belong to a group of glucose conjugated metal-binding compounds, 8-hydroxyquinolines, which have shown promising preliminary anti-cancer activity due to their ability to forage for Cu (II), a co-factor required for tumor growth and proliferation.[26] This class of compounds acts as a prodrug, requiring intracellular cleavage to free the active quinoline from the glucose complex.[3] However, this class of compounds ultimately failed as this cleavage was not observed during *in vivo* testing with mammalian cells.[3]

Grigsby and colleagues reported preliminary chemical and biological evaluation of a series of azomycin-glucose conjugates in 2012, after failed trials with 2-nitroimidazole compounds that showed toxicity in dose limiting clinical studies.[27] To overcome this toxicity and improve cancer cell selectivity, they attached a glucose moiety. These glucose conjugates were tested in *Xenopus* oocytes that overexpressed glucose 1 transporter (GLUT1) to assess whether drug uptake was GLUT1-mediated. Figure 8f was found to be the strongest competitor for glucose uptake, suggesting partial GLUT1-mediated uptake. Further *in vivo* studies for azomycin-glucose conjugates was not further reported.[25]

Of these compounds, D-xylose-conjugated warfarin (8d) was shown to have the most prominent anti-cancer activity.[28] Peltier-Pain and colleagues initially synthesized a series of warfarin-carbohydrate conjugated drugs to improve warfarin absorption, distribution, metabolism, and excretion (ADME) properties.[28] It was discovered that some conjugates showed cytotoxic effects in cancer cell lines, of which (8d) was reported to have the most anti-cancer potential. However, further studies regarding its ability to cross the BBB were not performed.

One promising method to exploit the results of glycosylated prodrugs is by utilizing GLUT1, which has the highest transport rate of substrates of all the carrier mediated transporters on the BBB, making it an attractive candidate for prodrug delivery.[29]

D. Glucose Transporter 1 (GLUT1)

It has been reported that cancer cells consume elevated levels of glucose, in a phenomenon known as the Warburg Effect.[25],[30] It has been proposed that this is due to upregulation of glycolysis, which is required to meet the high energy demand of rapidly proliferating cells.[31] Previous studies involving positron emission tomography (PET) imaging using 2-deoxy-2-(^{18}F) fluoro-D-glucose (^{18}F-FDG) have also demonstrated increased uptake of glucose into cancerous cells, although whether this was due to overexpression of GLUT1 has yet to be determined.[25]

Studies performed by Zhou and colleagues concerning selective tissue targeting via various families of GLUT transporters have been performed as a systematic approach to improve efficacy and reduce adverse side effects in kidney cancer targeting.[32] It was

found that amongst the reported glucose transporters in the kidney, the sodium-glucose linked transporter family (SGLT2) retained high affinity *in vivo* rat models, showing promise for transporter mediated drug enrichment.[32] Gynther and colleagues also demonstrated successful binding of two glucose bound prodrug moieties to GLUT1, as well as their capability of successfully crossing the BBB.[29] These studies have demonstrated that glucose derivatives are capable of binding to GLUT1.

However, for successful passage of glucose-linked through the BBB, knowledge and understanding of the GLUT1, the primary transporter of glucose through the BBB into the central nervous system, is essential. GLUT1, which is encoded by the solute carrier family 2A (SLC2A) of passive hexose transporters, is a type II integral protein consisting of 12 transmembrane α-helical domains.[31] It regulates facilitative transport of glucose through cell membranes in erythrocytes, and is the main supplier of glucose for the central nervous system. The transporter is roughly 54,000 Da in size and 492 amino acid residues long.[31]

Crystal structures of GLUT1 containing the single point mutation N45T and single missense mutation E329Q were reported by Deng and colleagues in 2014.[31] It was important to isolate these mutations to lock the GLUT1 in certain confirmations to understand its functionality and ensure successful crystallization, as GLUT1 is a highly active transporter that could contain a variety of confirmations. Although the outward open conformation (Figure 9A) has yet to be crystallized, the ligand-bound (9B), inward open (9C), as well as the ligand-free (9D) occluded conformations were successfully characterized.[31] These findings show that the GLUT1 acts as a uniporter to transport D-glucose as well as other hexose moieties across the plasma membrane. This knowledge

not only further assists in understanding substrate binding to the GLUT1 transporter, but can also be used to observe amino acid residue interactions of lycorine-glucose bound analogs within the active site of GLUT1.

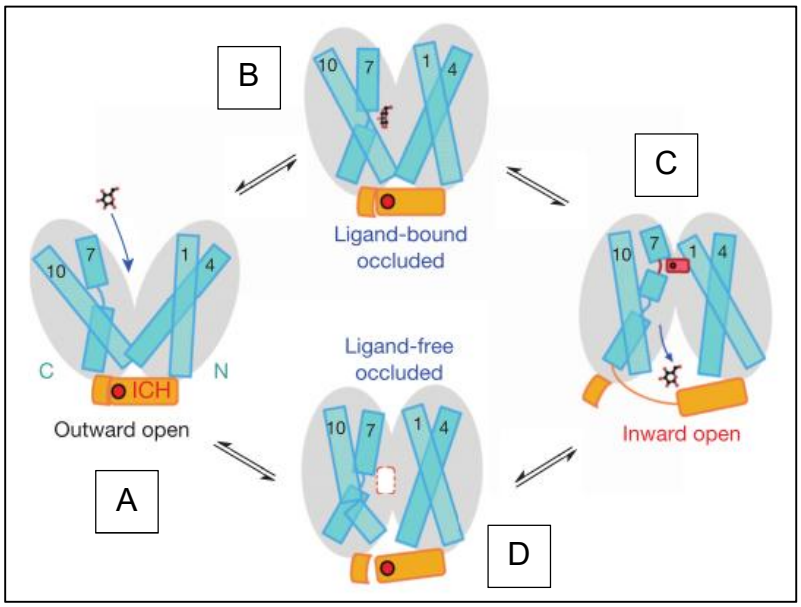

Figure 9. Proposed working model for GLUT1.[31] Structure A, outward open, has yet to be isolated. Structures successfully isolated include B, C, and D.

II. PROJECT GOALS

Here we propose coupling lycorine and narciclasine analogs to glucose based on the discussion above: to enable increased uptake of lycorine through the BBB for more effective CNS targeting. We also want to optimize selectivity against cancer cells using GLUT1. The poor *log* P (measure of lipophilicity) values of lycorine (0.77)[33] and poor water solubility of narciclasine presents an obstacle for CNS tumor targeting. The C1 and C2 hydroxyl groups along with the N6 nitrogen make lycorine too hydrophilic for delivery through the BBB, and the 4 hydroxyl groups along with its amido nitrogen provide the same barrier for narciclasine. As such, we propose to couple these *Amaryllidaceae* alkaloids to glucose to improve absorption, distribution, metabolism, excretion (ADME) characteristics, and cancer cell selectivity that overexpress GLUT1. After generating the desired lycorine (Lyc) and narciclasine (NCS) alkynes (A in Figure 10), they will be attached to glucose azide derivatives (B in Figure 10), utilizing 1,3-dipolar cycloaddition, or "click chemistry"(C in Figure 10), with $CuSO_4$ and sodium ascorbate, as outlined below.

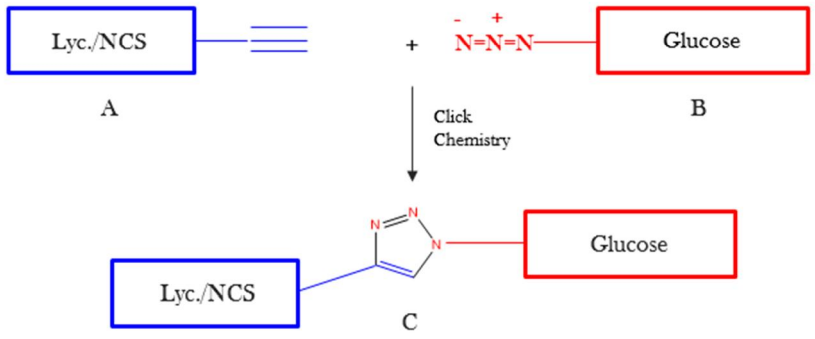

Figure 10. Proposed outline for "click chemistry" with lycorine and narciclasine alkynes (A) and and gluose azides (B) using copper catalyzed alkyne azide click chemsitry.

III. RESULTS AND DISCUSSION

A. Lycorine Analogs

1. Background

Two types of lycorine analogs were synthesized for this project (Figure 11). First, non-cleavable analogs **1** and **2** generated via S_N2 alkylation (left) and second, cleavable analogs **3** and **4** (right) generated via steglich esterification.[9]

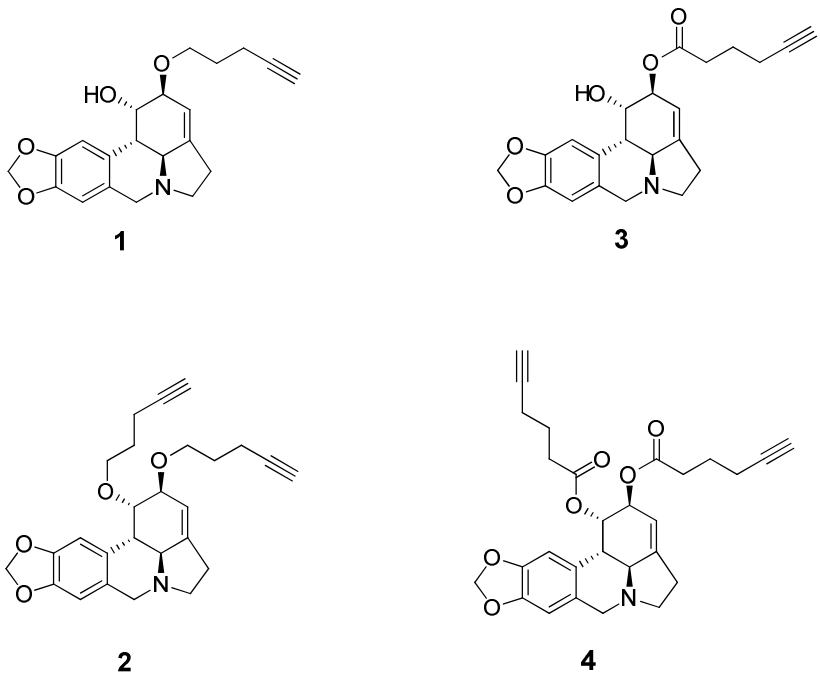

Figure 11. Non-cleavable (compounds **1** and **2**) and cleavable (compounds **3** and **4**) lycorine analogs

Both cleavable and non-cleavable lycorine analogs were prepared to take into consideration the effect of naturally occurring hydrolases and esterases within the body. The cleavable analogs can act as a prodrug, releasing lycorine after esterase-mediated hydrolysis (Figure 12).

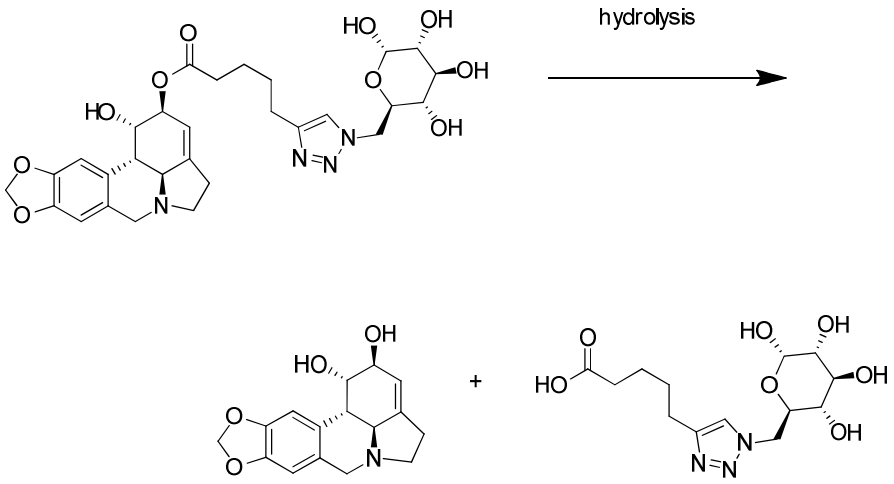

Figure 12. Proposed hydrolysis of prodrug clicked from compounds **3** and **14** via esterases. The hydrolyzed prodrug releases the active lycorine and glucose-carboxylic acid derivative.

The benefit of this cleavage is to release the parent lycorine alkaloid, which then has the potential to have the full antiproliferative effect against GBM cells. However, as there are esterases in other parts of the body, there is risk of hydrolysis outside the CNS, increasing the chances of off-site targeting. The non-cleavable ethers, on the other hand, will not be targeted via esterases, as ethers do not undergo saponification. The benefit of this is that there is no risk of hydrolysis by esterases outside the CNS, reducing off-site target effects. However, as there is no chance of hydrolysis of the non-cleavable compounds, reduced cytostatic activity is possible.

2. Synthesis

Lycorine used in this work was obtained as a crystalline compound from the fields of the Apulia region, Italy. Bulbs of *Sternbergia lutea (L.) Ker-Gawl* were cleaned, dried, then extracted and purified according to the procedure reported by Evidente *et al.*, producing 9.8 g of lycorine.[10] Synthesis of compound **1** was accomplished via S_N2

reaction using 4-pentynyl tosylate, NaH, and NaI in DMF at 85 °C for 12 hr. NaH was necessary to deprotonate the C2 hydroxyl group for alkylation, while NaI was used to react with the 4-pentyl tosylate to produce 5-iodopent-1-yne *in situ*.

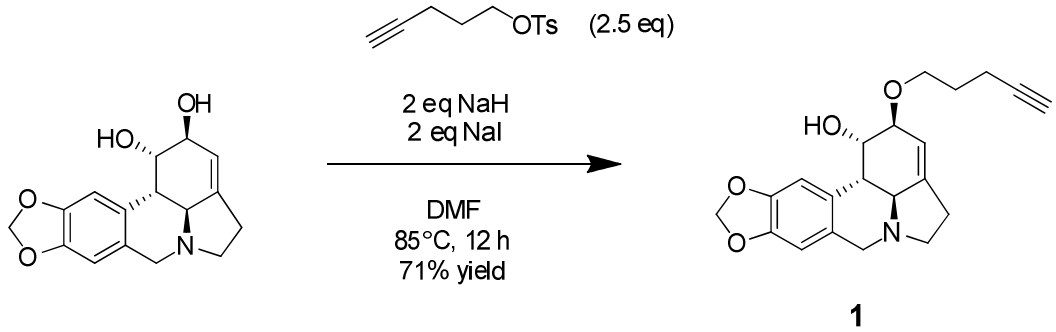

Scheme 1. S_N2 alkylation of lycorine to produce mono-substituted ether lycorine alkyne (**1**).

Here iodide is a preferred leaving group than tosylate for nucleophilic attack by lycorine, and the reaction would proceed slower without including NaI (Figure 13). DMF was chosen as the solvent as it is a polar aprotic solvent, which is necessary for successful S_N2 reactions.

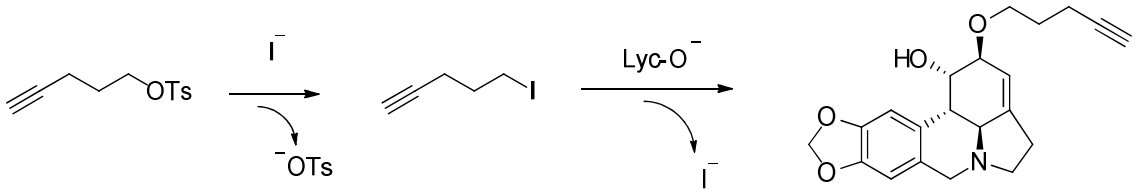

Figure 13. *In situ* reaction of NaI with 4-pentyl tosylate.

Synthesis of the desired di-substituted ether lycorine alkyne (Scheme 2, compound **2**) was generated using similar conditions to compound **1**, with a few alterations. Synthesis of compound **2** required 3 equivalents of 4-pentynyl tosylate, as well as NaH and NaI to produce the desired di-substituted product. Excess NaH over 4 equivalents did not improve the yield of compound **2**.

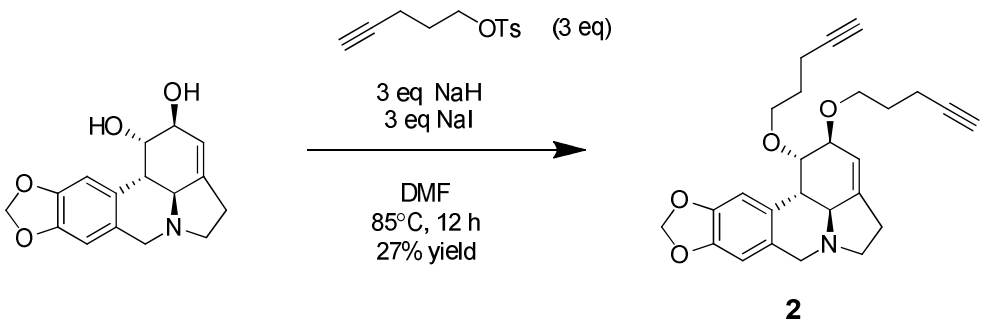

Scheme 2. S_N2 alkylation of lycorine to produce di-substituted lycorine ether alkyne (**2**).

Synthesis of the mono (**3**) and di (**4**)-substituted lycorine ester analogs were performed via steglich esterification using 5-hexynoic acid, DMAP, and EDCI in DMF at room temperature, as shown in Scheme 3. After an aqueous work up with ethyl acetate, purification of both ester analogs was performed similar to the above ether analogs.

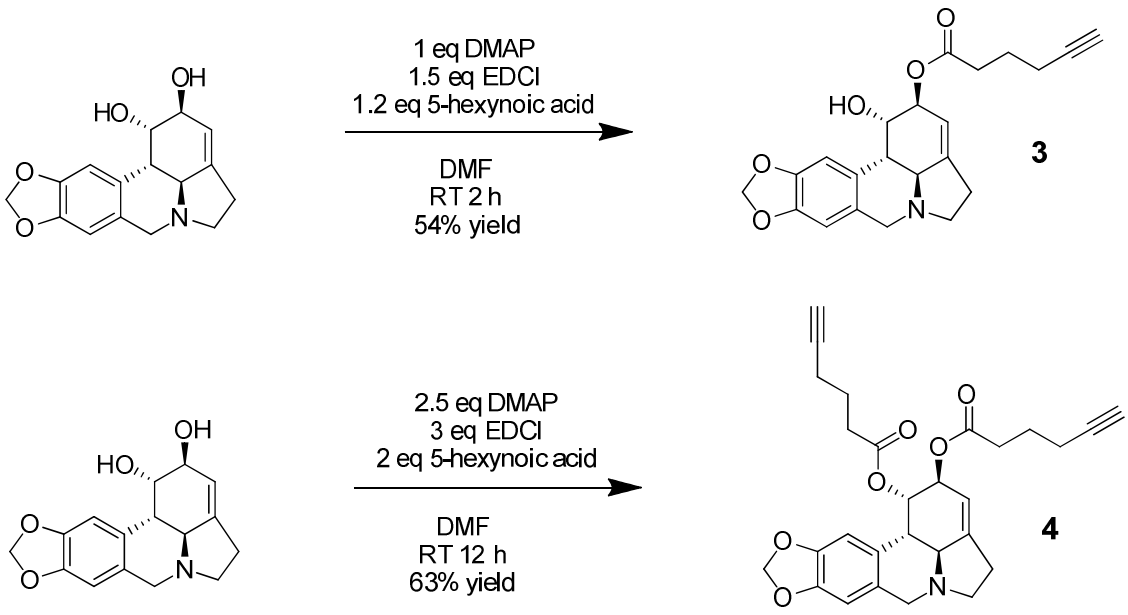

Scheme 3. Steglich esterification of lycorine to produce both mono (**3**) and di (**4**) substituted lycorine ester alkynes.

Here compound **4** was favored as the major product. As a result, different equivalents of 5-hexynoic acid, DMAP, and EDCI were necessary to favor formation of compound **3**. Formation of compound **3** was obtained using 1 equivalent of DMAP, 1.5 equivalents EDCI, and 1.2 equivalent 5-hexynoic acid, and the reaction was not allowed to proceed for longer than 2 hours.

B. Narciclasine Analogs

1. Background

One of the problems with narciclasine was determining a strategy to selectively attach an ester functional group to narciclasine, which contains 4 hydroxyl groups and an N-H group. In order to selectively attach the desired ester group, protecting groups must be utilized. Figure 14 details the process for selectively attaching the desired ester to narciclasine via steglich esterification. First we decided to attach an isopropylidene protecting group on the *cis* C3 and C4 hydroxyl groups. Due to their trans stereochemical relationship, there was no concern about attachment between the C2 and C3 hydroxyl groups. Of the remaining two hydroxyl groups, one being phenolic, we decided to esterify the remaining C2 hydroxyl group, and lastly deprotect the C3 and C4 hydroxyl groups prior to subsequent click reactions.

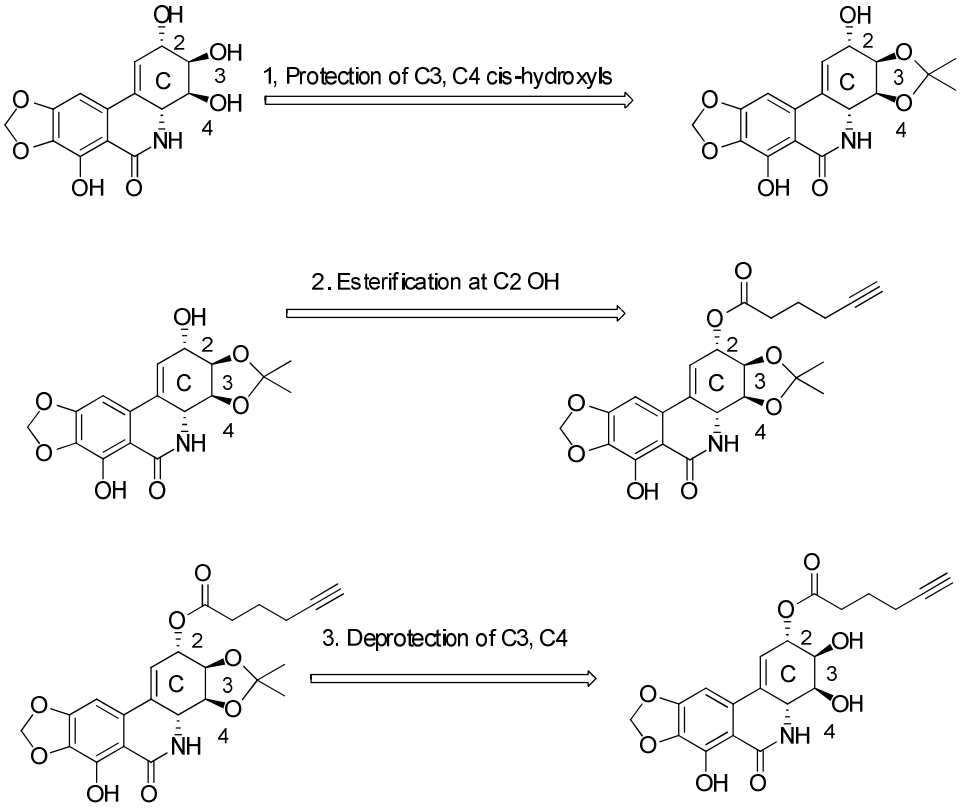

Figure 14. Detailed process for Steglich esterification of narciclasine.

2. Synthesis

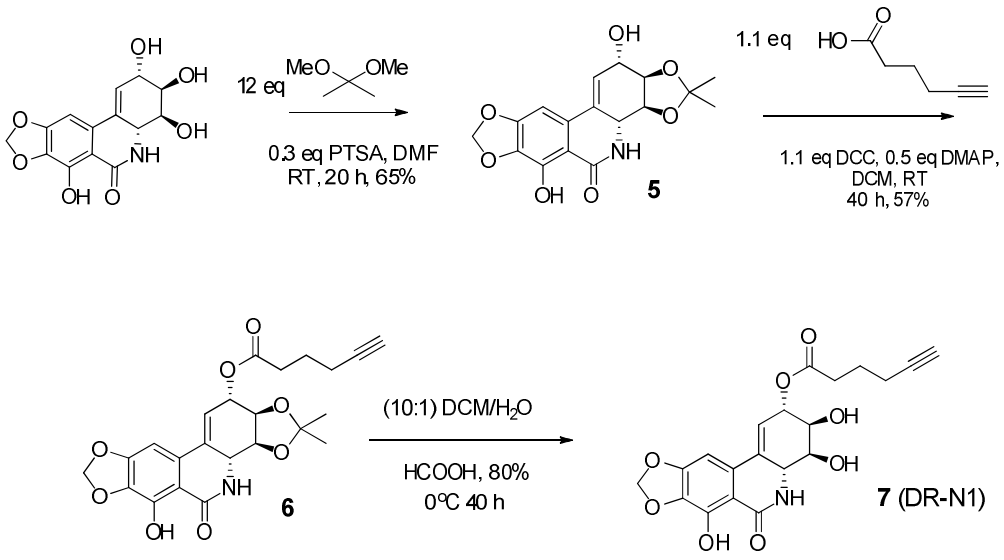

Scheme 4. Steglich esterification of narciclasine to generate narciclasine ester alkyne (**7**).

Due to their *cis* orientation, the C3 and C4 hydroxyl groups of narciclasine were protected with an isopropylidene group, using PTSA in DMF. The reaction was monitored via TLC (5% MeOH/$CHCl_3$), until a new spot ($R_f \sim 0.46$) appeared (visualized under UV). No purification of this protected narciclasine analog (**5**) was perfomed, and the desired protected narciclasine ester (**6**) was produced using the crude material. This was done to ensure no protected narciclasine would be lost during purification.

Unlike compounds **3** and **4**, the esterification of narciclasine was performed using DCC and DMAP rather than EDCI and DMAP. Purification via preparative TLC in a 4% MeOH/$CHCl_3$ yielded compound **6** (57% yield), which was then subjected to deprotection with formic acid in a solution of 10:1 DCM/H_2O for 20 hours at 0 °C. Initially, the deprotection using double the equivalents of formic acid did not work after 20 hours. However, upon addition of two more equivalents of formic acid, for a total of four equivalents, the desired product was formed another 20 hours later, and purified in a

7% MeOH/$CHCl_3$ solvent system (R_f ~0.63) to yield 80% of compound **7**, hereafter referred to as DR-N1.

3. Biological evaluation

DR-N1 was evaluated for antiproliferative effects using the MTT colorimetric assay (Figure 16). Here, soluble 3-(4,5-Dimethylthiazol-2-yl)-2,5-diphenyltetrazolium bromide (MTT) is reduced to insoluble formazan via reductases within the cellular mitochondria, resulting in the formation of dark purple crystals (see Figure 15). Reduction of the MTT dye depends on cellular mitochondrial reductase activity.[34] Therefore, cells with a low metabolic activity will reduce very little of the MTT dye, resulting in low levels of formazan production. This reduction can be measured and quantified using spectrophotometry at certain wavelengths (595 nm), and plotted against concentration of drug utilized for the assay. High absorbance readings signify high cell metabolic function, and thus imply high levels of cell proliferation and cell viability.[34]

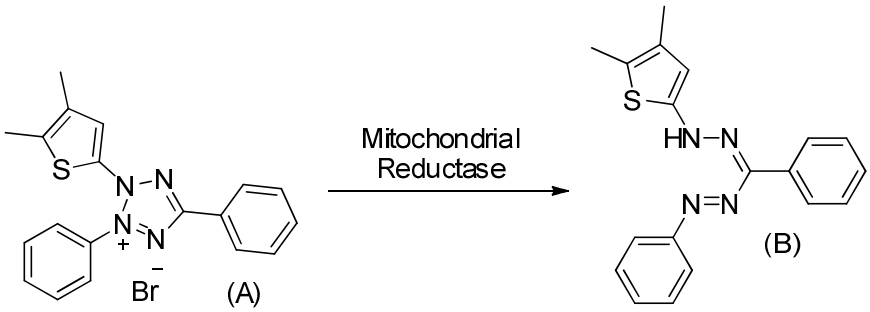

Figure 15. Reduction of MTT reagent to dark purple formazan.

Results show that DR-N1 fully retained the activity of narciclasine (GI_{50} = 40 nM for narciclasine, GI_{50} = 50 nM for DRN1). Here the GI_{50} values represent the concentration of drug required to cause 50% reduction in cancer cell proliferation.[34] To

determine these values, *in vitro* growth inhibitions for both DR-N1 and narciclasine were measured in 5 different cancer cell lines and monitored after 48 hour treatment (Table 1, Figure 16A, 16B).

To confirm the retention of cytostatic, non-cytotoxic mechanism of action, phase-contrast microscopy was utilized to observe cell morphology and the effects of these compounds on actin cytoskeleton organization. It was revealed that in SKMEL-28 melanoma cells at the GI_{50} concentrations listed, DR-N1 does not induce cell death in cancer cells, but exerts pure growth inhibitory properties similar to narciclasine (Figure 16C).

Table 1. IC_{50} *in vitro* growth inhibitory concentrations (MTT assay) of compound **7** (DR-N1) and narciclasine in A549 non-small cell lung cancer, SKMEL-28 melanoma cancer, U373n astroglioma, and HS683 oligodendroglioma cell lines. Assays were performed with our collaborators at Free Univeristy of Brussels.

Compounds	A549 NSCLC	SKMEL-28 (Melanoma)	MCF- 7 (breast)	U373n (astroglioma)	HS683 (oligodendroglioma)	Mean+SEM
DR-N1	0.05	0.02	0.07	0.04	0.04	0.05±0.007
Narciclasine	0.04	0.04	0.06	0.05	0.03	0.04±0.006

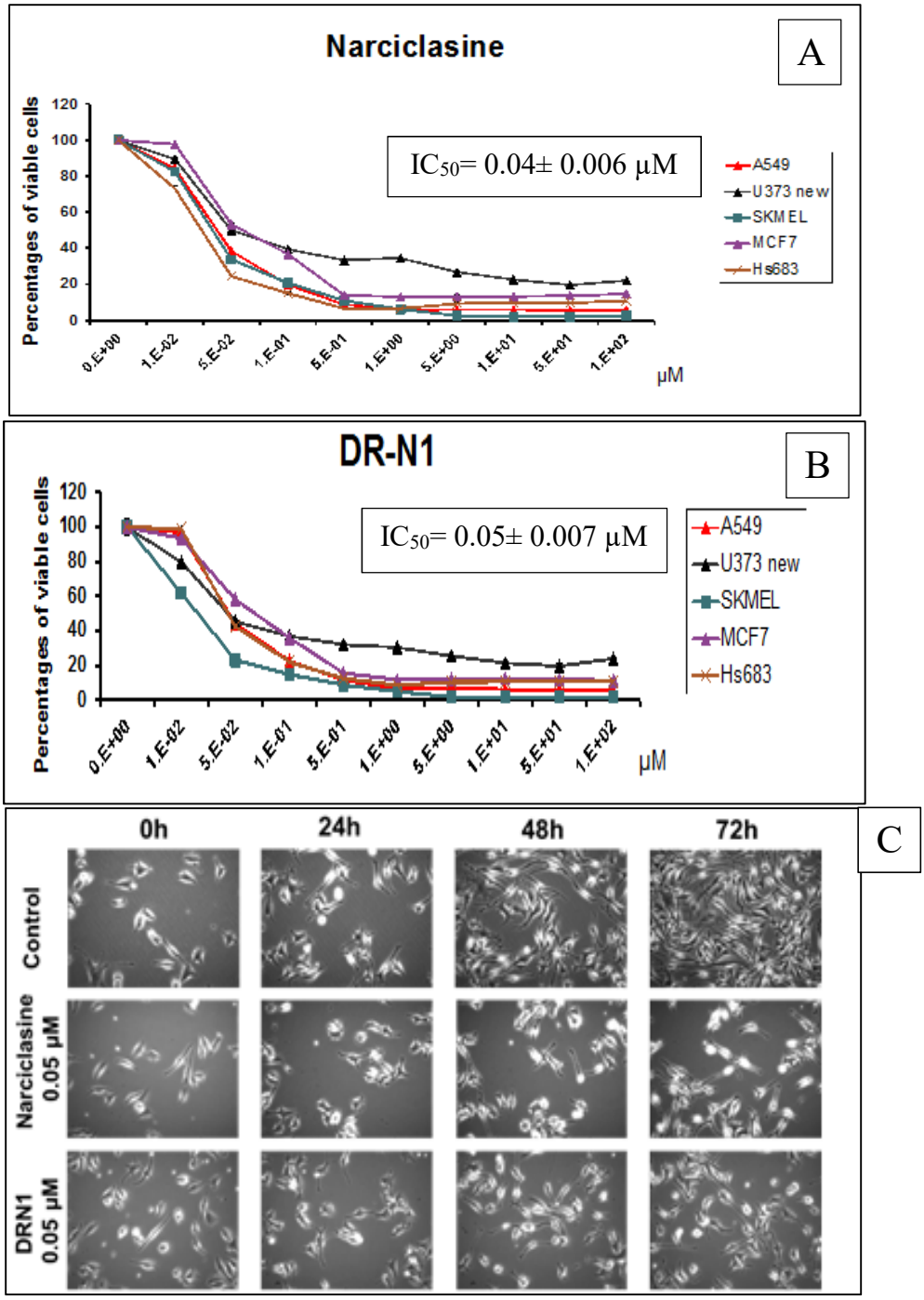

Figure 16. Results of the MTT assay for narciclasine and DR-N1. 16A and 16B represent *in vitro* growth inhibition for narciclasine and DR-N1 utilizing the IC_{50} values listed in Table 1. 16C shows Phase Contrast Microscopy for both narciclasine and DR-N1 in SKMEL-28 melanoma cells over a 72 h period. Here it is important to note the confluency reached in the control group by the 72 h mark, versus the inhibition of growth of both the DR-N1 and narciclasine treated cells. Assays were performed by our collaborators at Free University of Brussels.

C. Glucose Analogs

1. Background

The two positions on glucose which were decided to focus on for attachment of the azide functional group are the C1 and C6 positions (Figure 16).

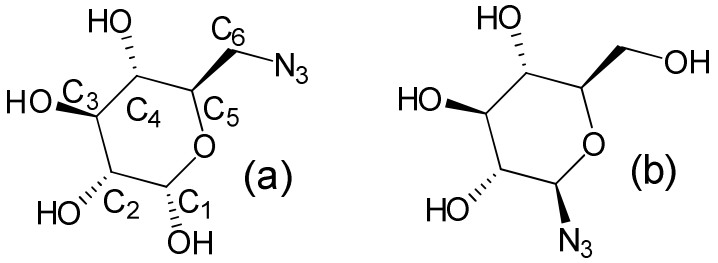

Figure 17. Glucose azide derivatives that will be the main focus for this project: C6 (a) and C1 (b).

Numerous studies have been performed since the early 1990s demonstrating the various derivitazations of these compounds. Tiwari and company published an extensive review in 2016 detailing the numerous ways these compounds have been synthesized, as well as the benefits of utilizing carbohydrate azides.[35] These molecules have been found to be very stable and relatively unreactive in a variety of conditions, which is unusual for azide containing compounds.[35]

For this project, we focused on derivatizing only the C1 and C6 positions on glucose for a number of reasons. First, the reactions at the C1, or anomeric, postion on glucose are easier to control because of the anomeric effect, as described in further detail below. Anomeric glucose azides have also been successfully reported on large scales.[36] The C6 position on glucose is also convenient synthetically as this postion is less sterically hindered and more open to S_N2 reactions.

Second, the C6 position is important for the recognition of the ligand by the GLUT1 binding site, as a previous study performed by Fernandez and colleagues showed that ligand uptake was strongly inhibited for dopamine-linked glucose conjugated at the 6th position.[37] Using a GLUT1 theoretical model, Mueckler and Makepeace noted in 2008 that the C6 hydroxyl on glucose enters a hydrophobic pocket in the GLUT1 binding site, and unlike positions C1-C5, does not form a hydrogen bond with GLUT1 that is essential for substrate affinity.[29],[38] Later studies performed by Gynther and company demonstrated the ability of C6 glucose conjugated prodrugs to cross the blood brain barrier via the GLUT1 transporter.[29] Radiolabelling studies with ^{14}C glucose in an *in situ* rat brain models not only successfully demonstrated that these prodrugs crossed the BBB, but also that the uptake was GLUT1-mediated.[29]

2. Synthesis

Sugar residues are common for exhibiting a phenomenon known as the anomeric effect, a stereochemical phenomenon that refers to the propensity of polar substituents bonded to an anomeric center to prefer the α position rather than the β position (Figure 18).[2] This effect is due to electrostatic interactions from the lone pairs of electrons on the sugar heteroatom on the C1 position of glucose.[39]

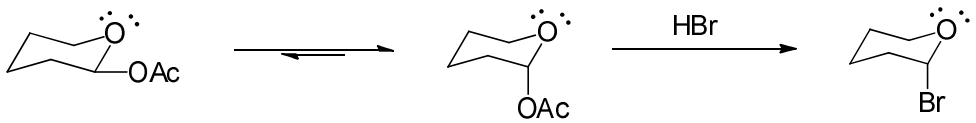

Figure 18: Results of the anomeric effect on sugar.

First, acetylation of the C2 through C6 hydroxyl groups (Scheme 5) protects them from bromination with HBr.

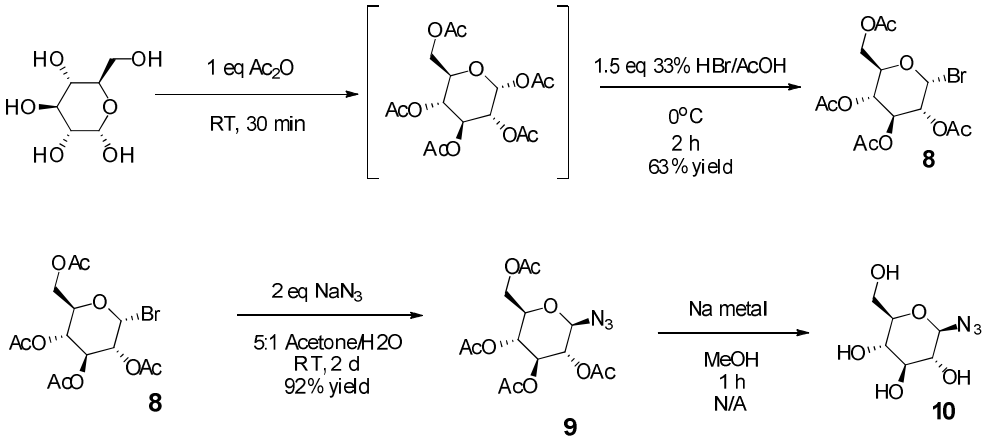

Scheme 5. Synthesis of anomeric glucose derivatives. Courtesy of Kumar and colleagues.[40]

The crude material (**8**) was treated with 2 equivalents of sodium azide in the 5:1 acetone/H_2O mixture, yielding 92% of the desired product (**9**). Once again, the anomeric effect facilitated the formation of this product by assisting the bromide departure.

To achieve successful synthesis of glucose containing an azide functional group at the C6 position, α-D-methoxyglucoside (**11**) was selected as the starting material in which the anomeric carbon is blocked to prevent subsequent synthesis. The sterically accessible C6 carbon on glucose, makes the position ideal for S_N2 chemistry. This property is taken advantage of for both the tosylation as well as the azide synthesis, as shown in Scheme 6.

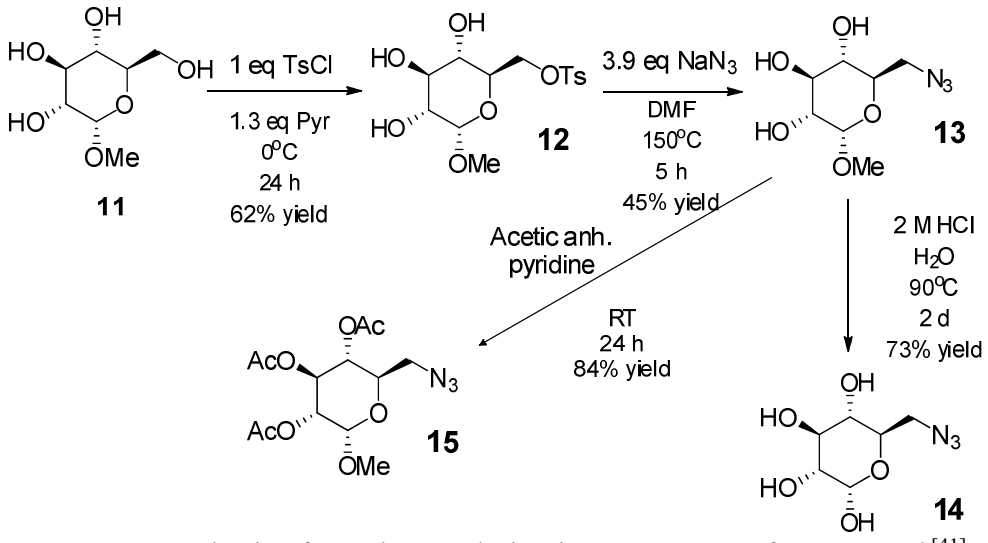

Scheme 6: Synthesis of C6 glucose derivatives. Courtesy of Wang *et al.*[41], Overend *et al.*[42], and Matsuda *et al.*[43]

Unlike the synthesis of compounds **8**-**10**, which were protected with acetyl groups, no aqueous work up was used. Due to the unprotected hydroxyl groups on the C3, C4, and C5 positions, there was a significant risk of losing the desired products to the aqueous layer after each subsequent step. Instead, co-distillation with H_2O and toluene were taken to ensure no significant product loss.

The purification of both the tosylated product (**12**) and the azide product (**13**) proved to be successful in a MeOH/$CHCl_3$ solvent system in which the MeOH content was no more than 4%. However, isolating the demethylated azide product (**14**), obtained by hydrolysis of compound **13**, proved more challenging. After cooling the reaction to room temperature, sodium bicarbonate was added to neutralize excess HCl. Once the crude product was co-distilled with H_2O and toluene, the resulting crude material was filtered with methanol.

This filtered crude material was redissolved in methanol, and purified via conventional flash column chromatography on silica gel with a 5%-30% MeOH/$CHCl_3$

solvent system. However, due to a significant product loss (~10%) an improved column procedure was developed that included washing the crude material with 10% MeOH/$CHCl_3$ on the silica gel and increasing the polarity of the eluting solvent stepwise by 5% MeOH. Compound **14** was successfully isolated using a 20% MeOH/$CHCl_3$ solvent system.

However, due to the high polarity of compound **14**, which might potentially make purification of subsequent click conjugates difficult, we also decided to prepare acetylated C6 methoxy glucose azide (**15**). The preparation of compound **15** involved treating compound **13** with Ac_2O and pyridine at room temperature. The acetylated product was obtained at ~10% higher yield than its deacetylated counterpart, as the acetyl protecting groups prevented loss of product during purification.

D. *Amaryllidaceae* Alkaloid-Glucose Click Conjugates

1. Background

First introduced by Sharpless in 2001, this Copper-Catalyzed Azide-Alkyne Cycloaddition (CuAAC) produces 1,4 regioselective triazole rings.[44] This "click chemistry" is a stereospecific, high-yield reaction that can incorporate various different functional groups, and can be performed over a broad pH range. [45],[46] Click chemistry is an attractive tool for medicinal chemistry purposes, as the triazole linkage provides a rigid link between the desired compounds to be combined, and cannot subsequently be oxidized, reduced, or hydrolytically cleaved.[46] For these reasons, click chemistry has found widespread applications in the realm of drug discovery, notably in the carbohydrate area.

The mechanism of copper-catalyzed click chemistry has been proposed by Fokin in 2013, and is shown below (Figure 19).[47]

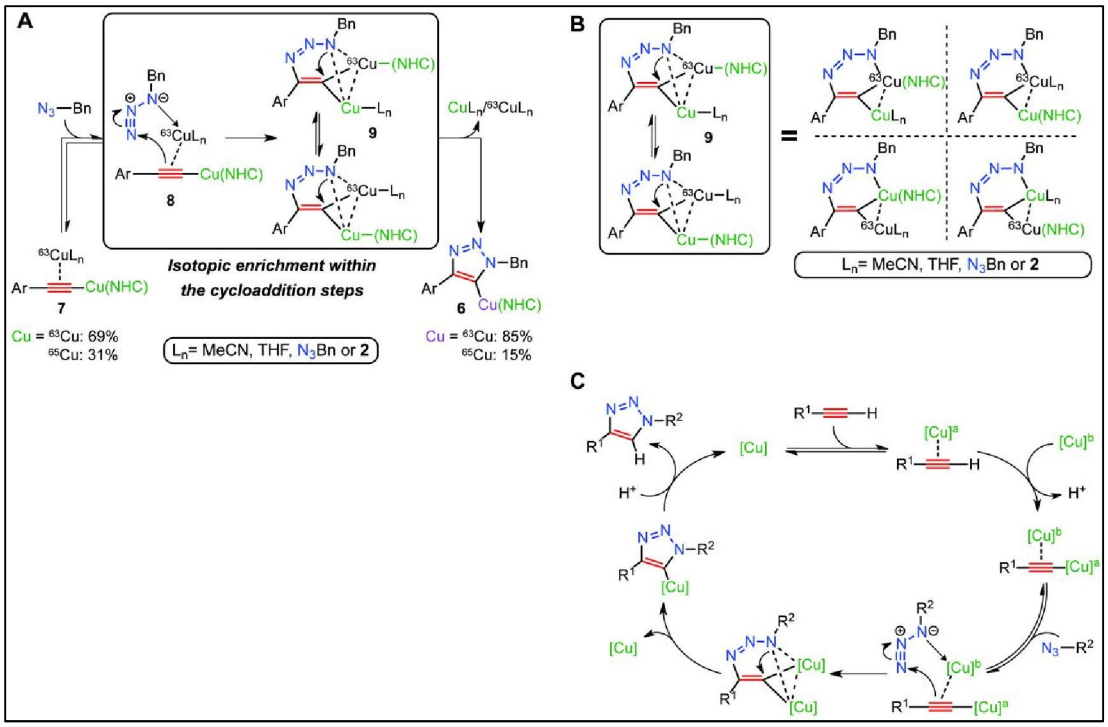

Figure 19. Mechanism of CuAAC as proposed by Fokin *et al*.[47] Kinetic studies with radiolabeled ^{63}Cu and ^{65}Cu were used to validate and confirm that two equivalents of Cu are necessary (A, B). The complete mechanism is shown in C.

Fokin successfully confirmed the necessary presence of 2 equivalents of Cu (I) catalyst, and that the two Cu atoms utilized are functionally exchangeable, despite producing a 1,4 regioselective product. To do this, Fokin and company first successfully established the necessity for a second Cu (I) atom by observing the reaction rates of catalytically activated alkyne-triazole cycloadditions vs non-catalyzed reactions. It was discovered that not only did the catalytically activated reaction rapidly reach completion, but that there was a direct correlation with a lower catalyst concentration and a decrease in the maximum rate of the reaction.[47]

Next, Fokin established the respective roles of each Cu (I) atom by utilizing kinetic and isotope labelling studies with ^{63}Cu and ^{65}Cu (Figure 19A). Radiolabelled Cu atoms were used to observe whether the Cu atoms acted in conjuction or independently of each other. Here, lack of enrichment of the resulting triazolide ring would support the hypothesis that the two copper species act independently.[47] It was hypothesized that one equivalent of Cu (I) catalyst would act as a σ bond ligand to the acetylide intermediate (Figure 19B), while the other Cu (I) eqivalent operates through weak π bonding interactions catalytically activating the acetylide intermediate. Using these labeling experiments along with time-of-flight mass spectrometry, Fokin and company were able to confirm the hypothesized roles for each Cu (I) atom that were found to work exchangeably to both stabilize the acetylide intermediate and activate it for nucleophilic attack by the azide.[47]

2. Synthesis of anomeric glucose derivatives

For the click reactions containing the anomeric azide (compound **10**), we decided to use compounds **1** and **7** (DR-N1) (Schemes 7 and 8). Copper sulfate pentahydrate was used as the main Cu (I) catalyst source since under the reaction conditions Cu (II) undergoes reduction to Cu (I) with sodium ascorbate.

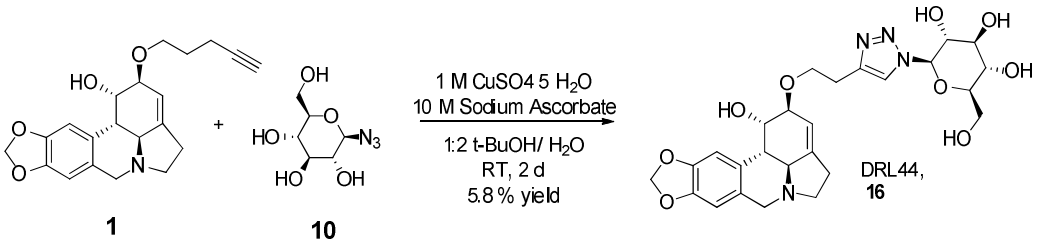

1 10

Scheme 7. CuAAC of mono-ether lycorine alkyne (**1**) to β-azido-deoxy-glucoside (**10**). Courtesy of Dr. Ramesh Dasari.

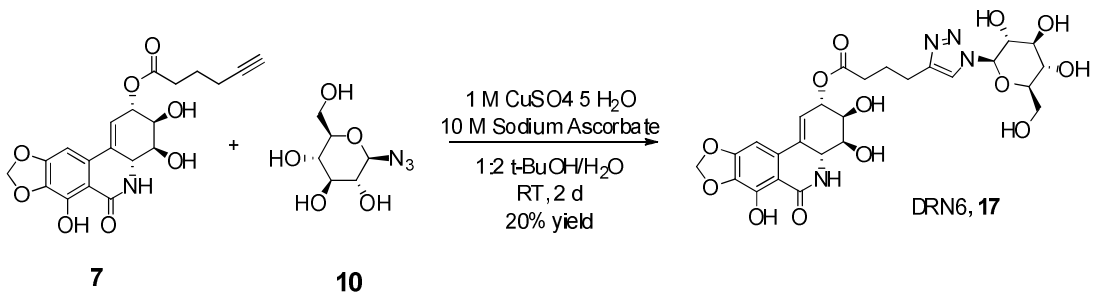

7 10

Scheme 8. CuAAC of narciclasine ester alkyne (**7**) to β-azido-deoxy-glucoside (**10**). Courtesy of Dr. Ramesh Dasari.

For these reactions, compound **7** had a higher yield than compound **1**. One likely reason for this could be solubility of the starting materials. The former appeared to be more soluble in the 1:2 *t*-BuOH/H_2O solvent system used for these reactions.

3. Biological evaluation

Figures 20 and 21 and Table 2 contain the MTT assay data for both lycorine (lyc) and compound **16** (DRL44) in both HeLa and MCF-7 breast cancer cell lines. For compound **16**, the IC_{50} values for both HeLa and MCF-7 (Figures 21C and 21D) increased significantly compared to the parent alkaloid (Figures 20A and 20B). From these results we can conclude that compound **16** did not retain nor improve the original biological compared to the parent alkaloid.

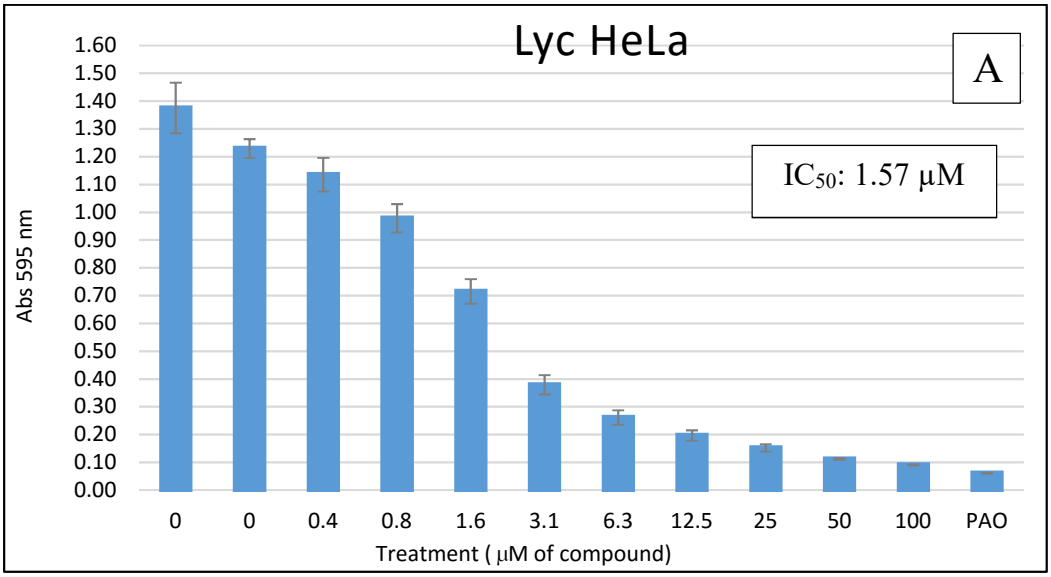

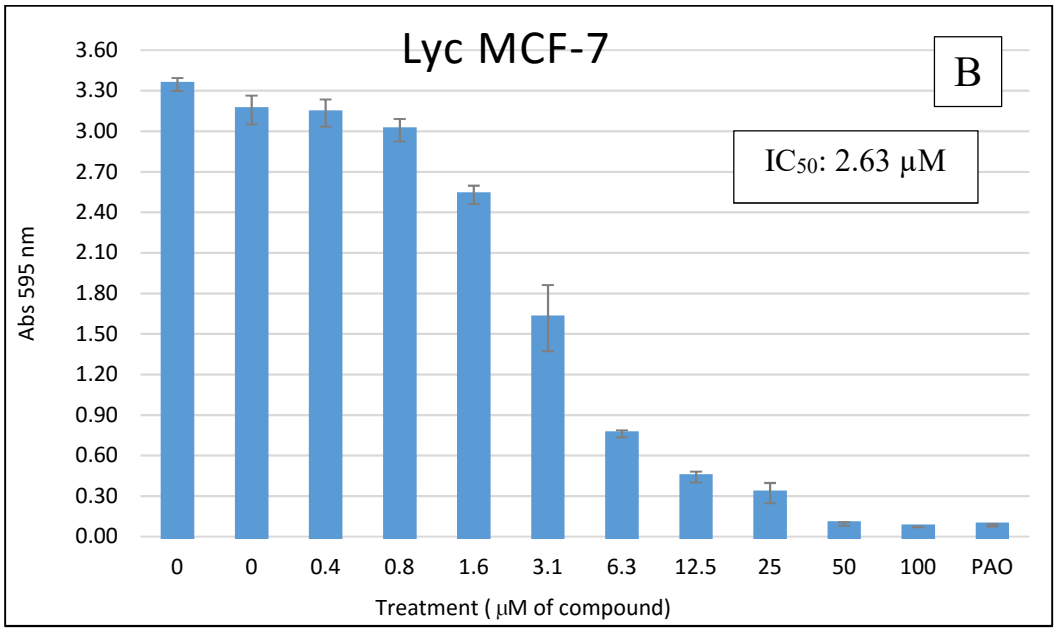

Figure 20. MTT assay evaluation of lycorine (lyc). Results show lycorine for antiproliferative activity of against HeLa (A) and MCF-7 (B) cells. The data were obtained using the MTT assay. PAO = phenyl arsene oxide was used as the positive control. Biological data courtesy of our collaborators at University of New Mexico Tech.

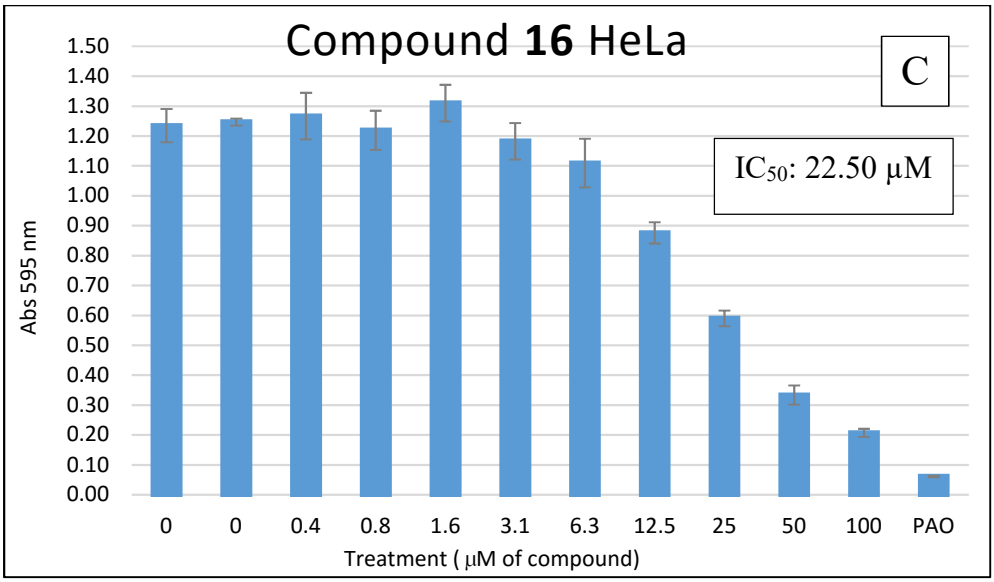

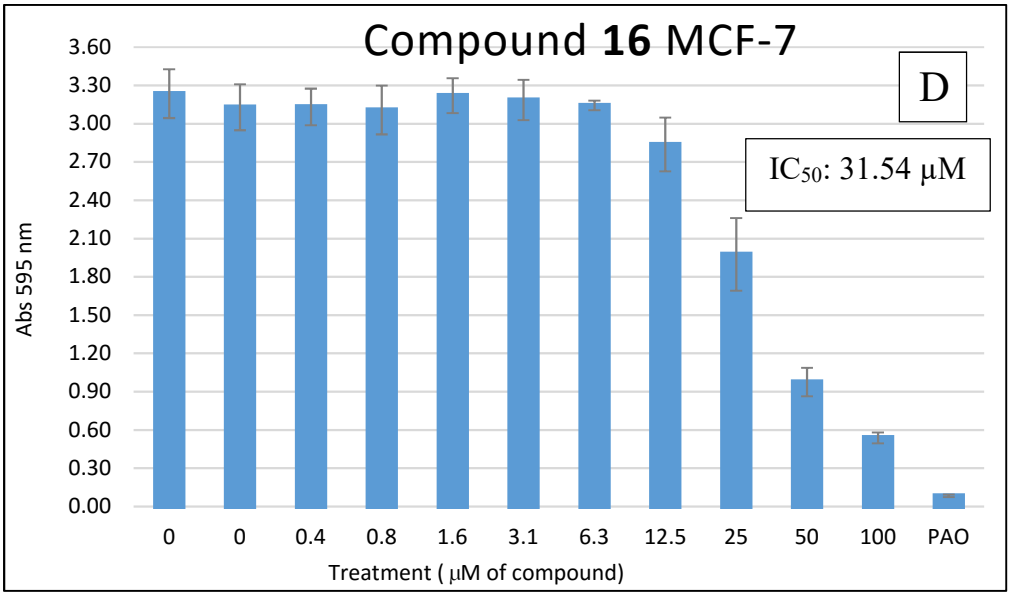

Figure 21. MTT assay evaluation of compound **16**. Results show **16** for antiproliferative activity of against HeLa (C) and MCF-7 (D) cells. The data were obtained using the MTT assay. PAO = phenyl arsene oxide was used as the positive control. Biological data courtesy of our collaborators at University of New Mexico Tech.

Table 2. MTT assay results for lycorine (Lyc) and Compound **16** in both HeLa cervical cancer and MCF-7 breast cancer cells. Biological data courtesy of University of New Mexico Tech.

Compound	Cell Line	IC_{50} (μM)	SD (μM)	TreatedHrs
Lyc	HeLa	1.57	0.193	48
Lyc	MCF7	2.63	0.720	96
16	HeLa	22.50	0.881	48
16	MCF7	31.54	6.026	96

Figure 22 and Table 3 present the MTT assay obtained for compound **17** compared to narclasine against HeLa cervical cancer cells. Figure 22A shows a dose-dependent effect of narciclasine, while Figure 22B depicts the results of with compound **17**. Using these curves, the IC_{50} values were obtained and they are shown in Table 2, as well as for each compound in their respective graphs. Unfortunately for these results, we do not have the data to show detailed narciclasine data for MCF-7 cells, and thus we excluded Compound **17** MCF-7 MTT results.

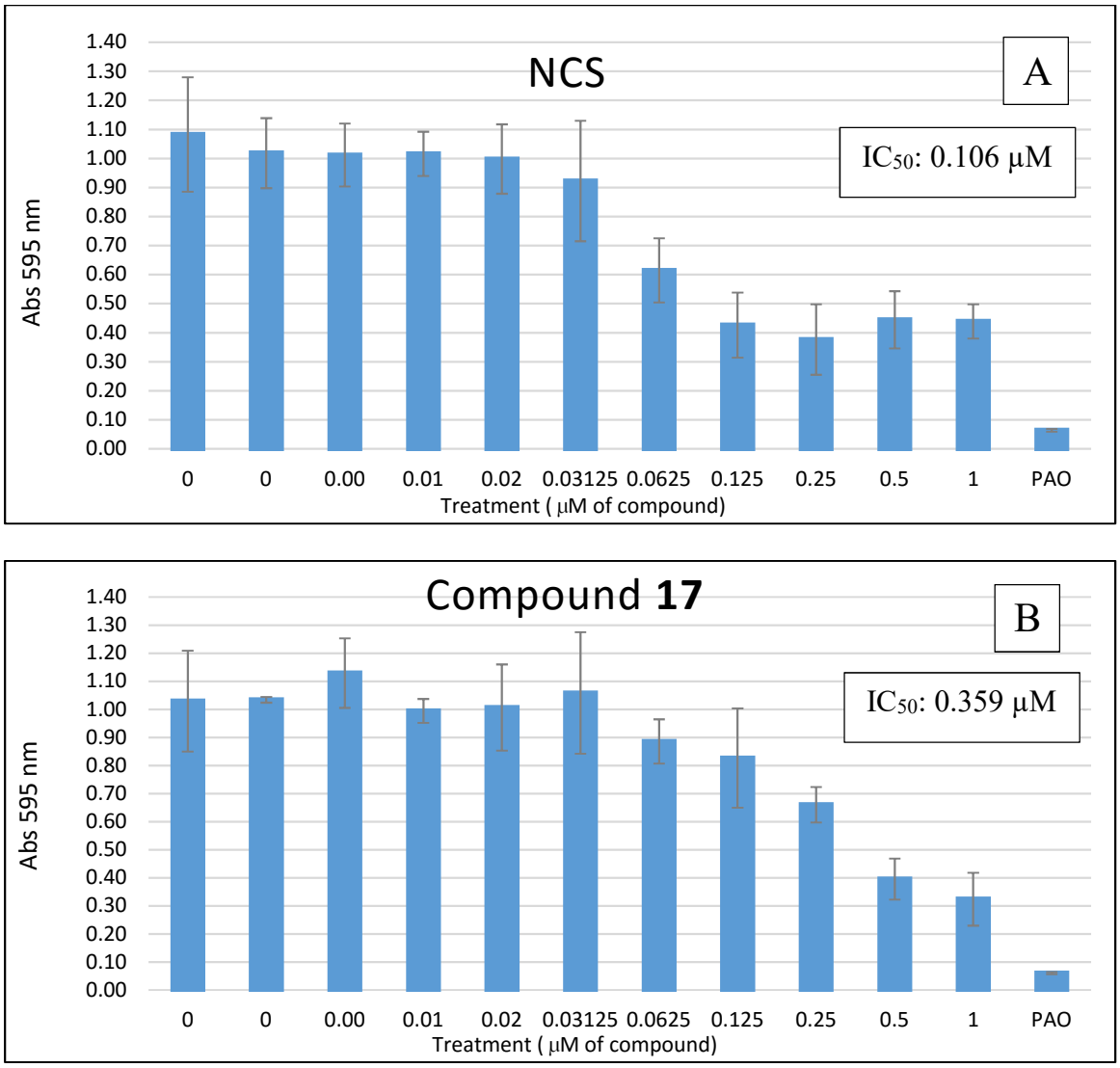

Figure 22. Assessment of compound **17** in HeLa cells (22A) compared to narciclasine (NCS) in HeLa cells (22B) at 595 nm absorbance over 48 h. Biological data courtesy of our collaborators at University of New Mexico Tech.

Table 3. MTT assay results for narciclasine (NCS) and compound **17** in HeLa cervical cancer cells. Biological data courtesy of University of New Mexico Tech.

Compound	Cell Line	IC_{50} (µM)	SD (µM)	TreatedHrs
NCS	HeLa	0.106	0.032	48
17	HeLa	0.359	0.032	48

The results of the above MTT assays ultimately show that the anomeric glucose click compounds did not lead to equal or improved potencies compared to lycorine or narciclasine. Thus, if the glucose conjugate transport into cancer cells was facilitated with GLUT1, we should have seen higher potency at least for compound **17** since as we demonstrated that the derivatization at position C2 for compound **7** does not lead to a drop in potency. These disapponting results are thus likely due the derivatization at the wrong position on glucose to provide sufficient intake through the GLUT1 transporter and the hydrogen bonding at the C1 position. As a result, we decided to focus on the synthesis of C6 glucose derivatives for the remainder of this project.

4. Synthesis of C6 glucose-lycorine derivatives

Outlined below are the details for the click reactions of compounds **1** to compounds **14** (Scheme 9). Due to the limited availability of compound **7**, we decided to first focus on forming C6 click conjugates with compounds **1-4**.

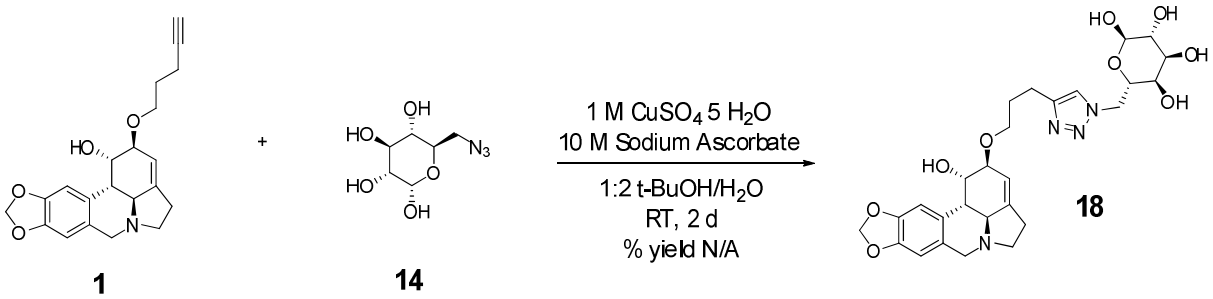

Scheme 9. CuAAC of mono-ether lycorine alkyne (**1**) to 6-azido-D-glucopyranose (**14**).

The set up for the click reactions with compound **14** was very similar to the one performed with compound **10**. Copper sulfate pentahydrate was used as the Cu (I) catalyst source and sodium ascorbate was used to convert Cu (II) to Cu (I). A 1:2 *t*-BuOH/H_2O solvent system was used to fully solubilize the starting materials for the

cycloaddition.

Mass spectrometry was performed before purification of each click compound to determine the formation of each desired triazole product. For the crude product in Scheme 9, the desired molecular ion for the mono-substituted product was found (m/z: 559.28, mol. mass: 558.23). After purification, mass spectrometry was performed once again on the isolated spot (R_f ~0.1) at 20% MeOH/$CHCl_3$, as it fluoresced similar to the starting material, however no desired molecular ion was found. ^{1}H NMR analysis of the same isolated spot showed only the starting material peaks, and not the desired C-H signal of the triazole ring. It was concluded that the desired product was lost during purification.

Schemes 10-12 portray similar procedures to scheme 9, but performed on compounds **2-4** respectively.

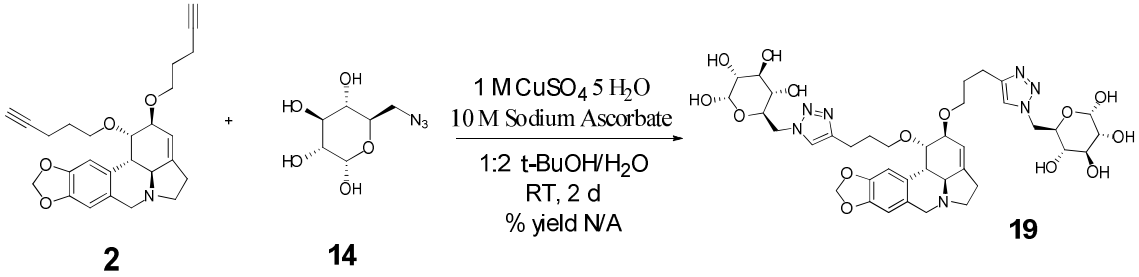

Scheme 10. CuAAC of di-ether lycorine alkyne (**2**) to 6-azido-D-glucopyranose (**14**).

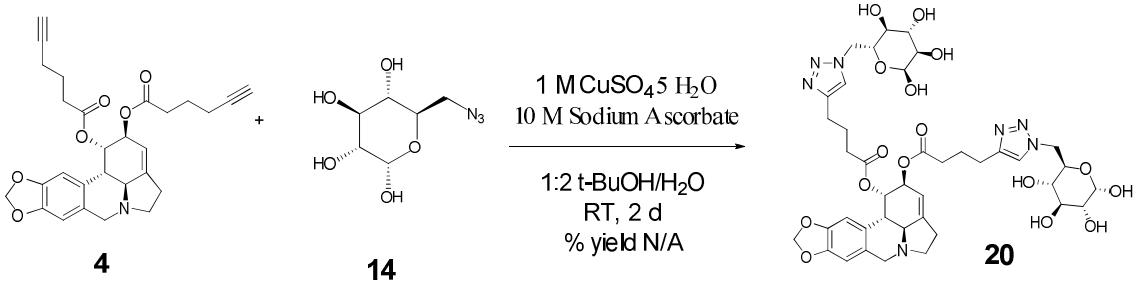

Scheme 11. CuAAC of di-ester lycorine alkyne (**4**) to 6-azido-D-glucopyranose (**14**).

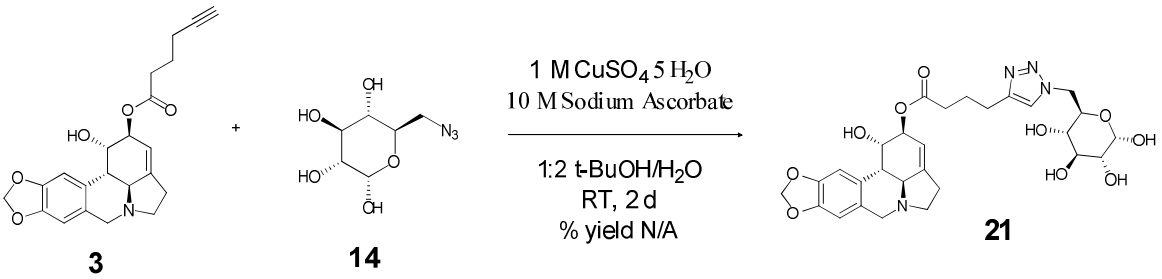

Scheme 12. CuAAC of mono-ester lycorine alkyne (**3**) to 6-azido-D-glucopyranose (**14**).

Unlike Scheme 9, purification of the products from Schemes 10-12 were not performed. For reasons that have yet to be validated, re-purification of the lycorine-glucose click products yielded streaked bands on preparatory thin layer chromatography plates that made isolation of the desired products difficult. One possible reason for this is the high MeOH concentrations necessary for purification of already incredibly polar products on silica gel. Up to 40% MeOH was necessary to separate residual sodium ascorbate from the desired fluorescent bands on the prep-TLC plate.

Another possibility is the low yields from each reaction, as shown by the mass spectrometry. While mass spectrometry is not an adequate indicator of purity of product (due to the ionization potential of different compounds), relative peak size can give an indication of amount of product present in the crude material. For Scheme 10, mass spectrometry of the crude material showed no formation of compound **19**. For Scheme 11, mass spectrometry of the crude material showed compound **20** (m/z: 587.23, mol. mass: 586.23 g/mol). Lastly, for Scheme 12, mass spectrometry of the crude material showed formation of compound **21** (m/z: 886. 34, mol. mass: 885.34 g/mol).

As purification was the main hindrance for these click reactions, we decided to attempt a click synthesis with compounds **1** and **2** and compound **15** (Scheme 13).

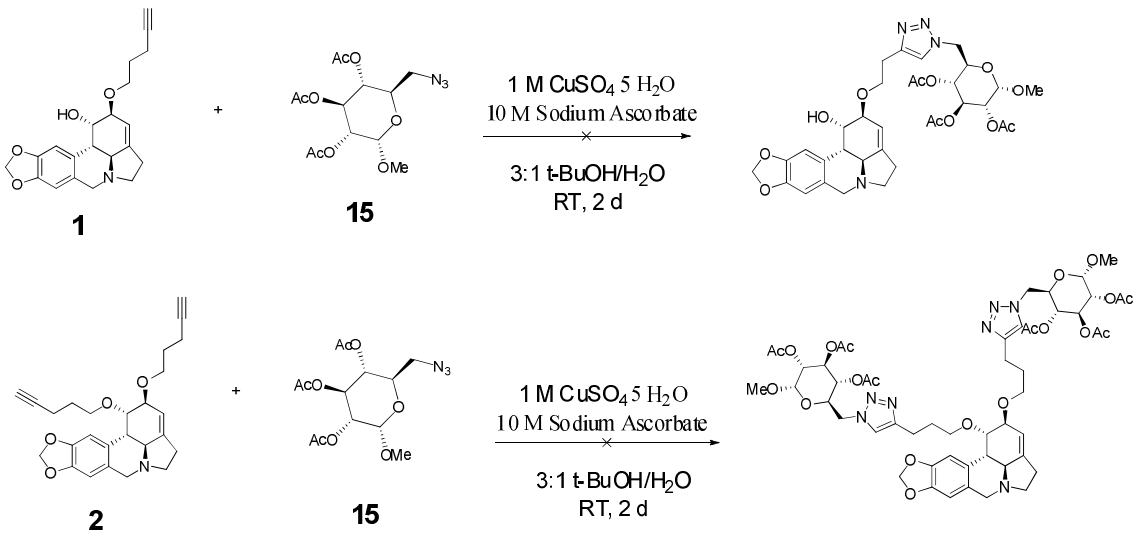

Scheme 13. CuAAC of mono-ether lycorine alkyne (**1**) to 2,3,4-Tri-O-acetyl-6-azido-6-deoxy-α-glucopyranoside (**15**).

Unfortunately, the reaction did not successfully form the desired product. Likely, the reason for this is the low solubility of compound **15** in the 1:2 *t*-BuOH/H_2O solvent system listed for the aforementioned click reactions. To overcome this, the amount of *t*-BuOH was increased threefold to the amount of H_2O present. Unfortunatley, the reaction was still unsuccessful, and ^1H NMR of the crude materials showed no desired C-H triazole peak. Due to time restraints and lack of alkyne availability, we decided not to further pursue this series of click products for the purposes of this project.

As a last resort to obtain C6 conjugated click products, we decided to click compound **7** to compound **14** (Scheme 14).

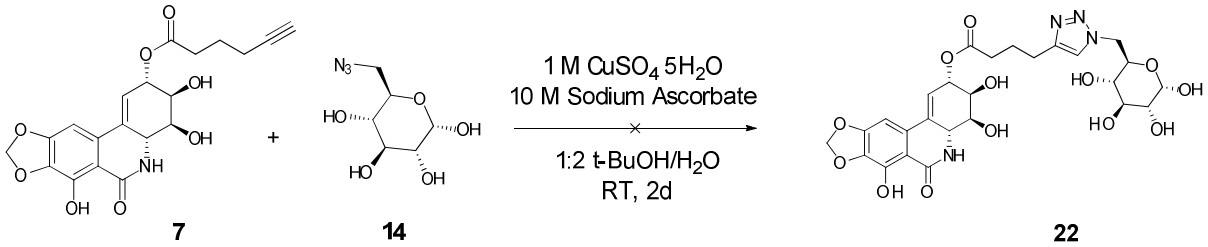

Scheme 14. CuAAC of narciclasine ester alkyne (**7**) to 6-azido-D-glucopyranose (**14**).

Unlike the lycorine click products, narciclasine could be purified multiple times to try and successfully isolate the desired click product. Initial TLC of the crude mixture showed that the starting materials did not appear under UV (R_f~ 0.5 for **7**, R_f~ 0.1 for **14**) (20% MeOH/$CHCl_3$). Unlike compounds **19-21**, we had a TLC reference (compound **17**) for compound **22** (due to the low yield of compound **16**, all product obtained was sent for biological testing). Encouraged by finding a similar spot in crude compound **22** to compound **17**, we decided to purify the entirety of the crude material (0.9 mL total) to obtain a very polar UV active band (R_f~0.05) in a 15% MeOH/$CHCl_3$ solvent system. However, this spot was surrounded by other polar impurities (i.e. ascorbate), thus further purification was encouraged.

Three more purifications on preparatory TLC were performed again in 15% MeOH/$CHCl_3$, until the desired UV-active band was isolated and vacuum filtered. ^{1}H NMR in DMSO showed compounds **7** and **14**, but did not show the desired triazole proton signifying product formation. It was concluded that the reaction did not proceed to the compound **22**.

IV. CONCLUSION

The original goal for this project was to produce anti-cancer compounds with *Amaryllidaceae* alkaloids utilizing glucose as a delivery mechanism. An assessment of the data show that while glucose is an ideal substrate to utilize as a drug delivery system for cancer cell specific targeting, it is not an ideal substrate to utilize in concert with *Amaryllidaceae* alkaloid derivatives for a number of reasons.

Synthesis of the lycorine and narciclasine alkynes and glucose azides proved initially challenging,, but eventually fruitful. Extensive experimentation with the solvent systems led to successful purification for both alkyne and azide compounds. While the C6 glucose azides initially proved challenging to purify, stepwise increases in the polar eluting solvent (~2% MeOH) ensured efficient product purification. The same techniques held true for the synthesis of the *Amaryllidaceae* alkynes: thorough aqueous work ups with subsequent purification using the previously mentioned solvent systems (3-15% MeOH/$CHCl_3$ for lycorine and narciclasine respectively) ensured effective purification. We were able to successfully derive and characterize 4 novel ester compounds: lycorine **3** and **4**, and narciclasine **6** and **7** (see Figure 11 and Scheme 4 respectively).

Synthesis and purification of the click conjugates proved much more difficult for a variety of reasons. Solubility of some starting materials in the *t*-BuOH/H_2O solvent system proved challenging, especially for click reactions with compound **15** (see Scheme 12). Because of the acetyl protecting groups, it is likely compound **15** was not soluble in the *t*-BuOH/H_2O solvent system, and thus the click reaction was unable to proceed. A likely solution to this problem would be to increase the ratio of *t*-BuOH/H_2O, but due to

limited availability of the alkyne starting materials, this option was not further explored.

While compounds **16** and **17** were successfully synthesized, purified, and tested for biological activity, the yields for these reactions, particularly for compound **16**, were incredibly low. Similarily, compounds **19-21** were unable to be effectively purified, though mass spectrometry confirmed formation of product. Unfortunately, due to time constraints as well as availability of starting material, we were not able to successfully reproduce the click reaction with compound **7** and compound **14**.

The method of purification utilized for these compounds is likely a vital reason for the low yields obtained. While normal phase column chromatography and preparatory thin layer chromatography are the commonly accepted standards for compound purification in organic synthesis, this method of purification is not ideal for highly polar compounds. In order to effectively purify these highly polar compounds, high levels of eluting solvent (MeOH) were required. This was an issue in terms of purification, as high levels of methanol have been known to dissolve the solid phase silica gel. Rather, purification with reverse phase column chromatography as well as high performance liquid chromatography would be a more suitable form of purification for these compounds, and could potentially solve these problems. Unfortunately, due to time constraints and lack of availability, these alternative approaches were not pursued. One possibility that could be pursued would be to design lycorine and narciclasine analogs using a different less-polar biological moiety, such as amino acid derivatives, that would prove easier to pruify. Such directions are currently being pursued in the Korneinko lab.

The design and synthesis of properly funcitional pharmacological agents and glucose azides for their subsequent coupling is key to successful drug delivery projects.

Despite not producing the desired *Amaryllidaceae*-glucose click conjugates, valuable insight into the chemistry and drug delivery of glucose based drug delivery conjugates were obtained.

V. EXPERIMENTAL

General:

All reagents, solvents, and catalysts were purchased from various commercial sources (Sigma-Aldrich, Acros Organics) and used without further purification. All reactions were performed in oven dried flasks under nitrogen and monitored via thin layer chromatography (TLC) on TLC pre-coated (250 µm) silica gel 60 F_{24} glass backed plates. Visualization of TLCs were accomplished with UV light, *p*-anisaldehyde, and iodine stains. ^{1}H NMR and ^{13}C spectra were recorded on a Bruker 400 spectrometer. Chemical shifts (δ) are reported in ppm relative to the TMS internal standard. Abbreviations for characterizations are as follows: s (singlet), d (doublet), t (triplet), q (quartet), m (multiplet).

Compound 1:

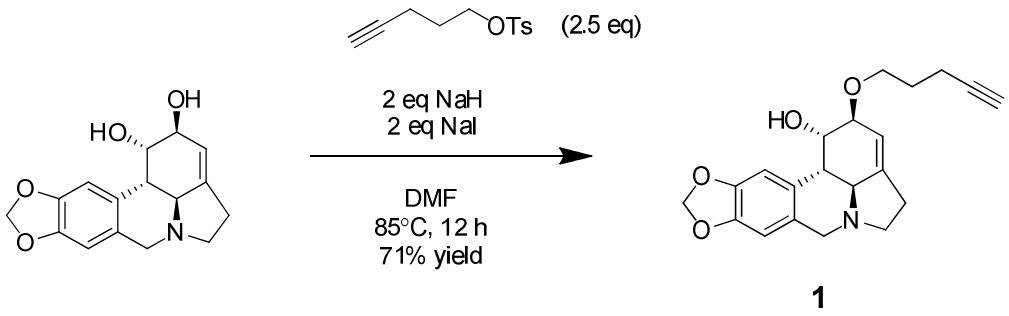

1

To a solution of lycorine (60 mg, 0.208 mmol), in dry DMF (3 mL) were added 2.5 eq of 4-pentyl tosylate (60.6 mg, 0.522 mmol), 2 eq NaH (10 mg, 0.417 mmol), and 2 eq NaI (93.9 mg, 0.417 mmol). The reaction was refluxed at 85 °C for 12 h. After completion of the reaction as monitored by TLC (10% MeOH/$CHCl_3$), an aqueous work

up was performed with EtOAc, and the organic layer was dried using Na_2SO_4 and concentrated down under reduced pressure. The crude product was purified via preparatory TLC (3% MeOH/$CHCl_3$) to obtain 48% yield of compound **1**.

^{1}H NMR ($CDCl_3$): δ= 6.85 (s, 1 H), 6.59 (s, 1 H), 5.92 (d, J = 4 Hz, 2 H), 5.56 (s, 1H), 4.60 (s, 1 H), 4.11 (m, 1 H), 3.96 (s, 1 H), 3.69-3.72 (m, 2 H), 3.55 (d, J = 13.6, 1 H), 3.29-3.34 (m, 1 H), 2.72 (d, J =1.2 Hz 2 H), 2.62 (s, 2 H), 2.44-2.40(m, 2 H), 2.03 (s, 1 H).

Compound 2:

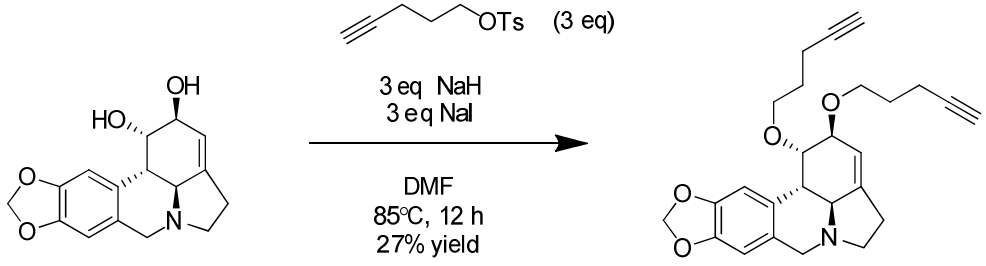

2

To a solution of lycorine (60 mg, 0.208 mmol), in dry DMF (3 mL) were added 3 eq of 4-pentyl tosylate (72.7 mg, 0.626 mmol), 3 eq Na H (15 mg, 0.626 mmol), and 3 eq Na I (93.5 mg, 0.623 mmol). The reaction was refluxed at 85 °C for 12 h. After completion of the reaction as monitored by TLC (10% MeOH/$CHCl_3$), an aqueous work up was performed with EtOAc, and the organic layer was dried using Na_2SO_4 and concentrated down under reduced pressure. The crude product was purified via preparatory TLC (3% MeOH/$CHCl_3$) to obtain 27% yield of compound **2**.

^{1}H NMR ($CDCl_3$): δ= 6.84 (s, 1 H), 6.56 (s, 1 H), 5.92 (d, J = 1.28, 2 H), 5.53 (s, 1 H), 4.17 (s, 1 H), 4.07-4.10 (d, J = 13.9 Hz, 1 H), 3.96 (s, 1 H), 3.77 (m, 1 H), 3.73-3.72 (m, 2 H), 3.51 (s, 1 H), 3.30-3.31 (m, 1 H), 2.72-2.69 (q, J = 11.4, 3 H), 2.58-2.60 (d, J = 6.88, 2 H), 2.29-2.32 (m, 3 H), 2.01-2.10 (m, 2 H), 2.00 (t, J = 0.12, 1 H), 1.91 (t, J = 0.16 Hz,

1 H), 1.66-1.91 (m, 3 H), 1.59-1.66 (m, 3 H).

Compound 3:

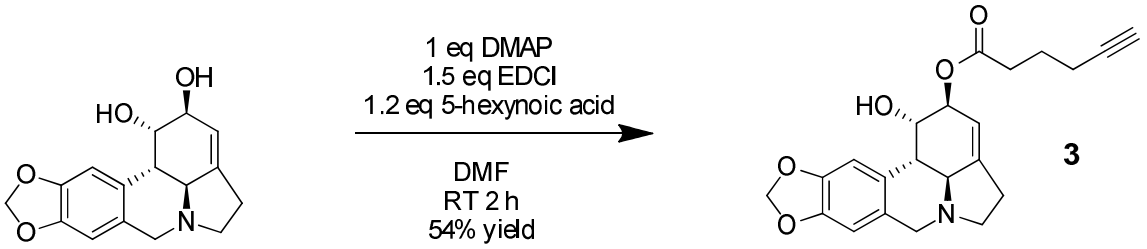

To a solution of lycorine (60 mg, 0.208 mmol), in dry DMF (3 mL) were added 1.2 eq of 5-hexynoic acid (28.4 µL, 0.250 mmol), 1.5 eq EDCI (59.8 mg, 0.312 mmol), and 1 eq DMAP (23.3 mg, 0.209 mmol). The mixture was stirred at room temperature for 2 h. After completion of the reaction as monitored by TLC (10% MeOH/$CHCl_3$), 10 mL of saturated $NaHCO_3$ solution was added to the reaction mixture, and stirred for 10 min. An aqueous work up was performed with EtOAc, and the organic layer was dried using Na_2SO_4 and concentrated down under reduced pressure. The crude product was purified via preparatory TLC (3.5% MeOH/$CHCl_3$) to obtain 54% yield of compound **3**.

^{1}H NMR ($CDCl_3$): δ= 6.81 (s, 1 H), 6.62 (s, 1 H), 5.94-5.95 (d, J = 6.4 MHz, 2 H), 5.49 (s, 1 H), 5.36 (s, 1 H), 4.53 (s, 1 H), 4.18-4.14 (d, J = 14 Hz, 1 H), 3.59-3.36 (d, J = 14 Hz, 1 H), 3.39-3.36 (m, 1 H), 2.92-2.81 (m, 1 H), 2.88-2.85 (d, J = 13.6 Hz, 1 H), 2.75-2.72 (m, 1 H), 2.50 (t, J = 1.6 Hz, 2 H), 2.32-2.28 (m, 2 H), 1.99 (t, J = 0.8 Hz, 1 H), 1.90-1.86 (m, 2 H).

^{13}C ($CDCl_3$): δ= 172.5, 146.6, 146.4, 127.1, 113.7, 113.7, 107.7, 104.6, 101.0, 83.1, 73.6, 69.3, 60.7, 56.9, 53.7, 41.8, 33.1, 28.7, 23.6, 17.8.

Compound 4:

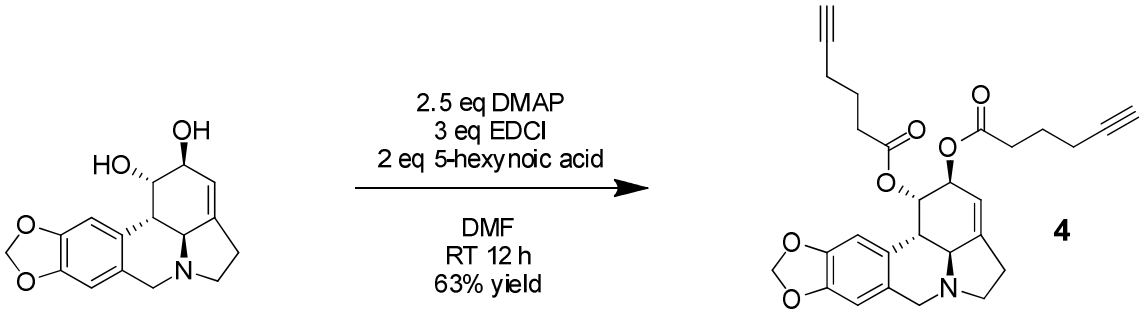

To a solution of lycorine (60 mg, 0.208 mmol), in dry DMF (3 mL) were added 2 eq of 5-hexynoic acid (47.5 µL, 0.418 mmol), 2.5 eq EDCI (99.6 mg, 0.520 mmol), and 1.5 eq DMAP (30.1 mg, 0.312 mmol). The mixture was stirred at room temperature for 12 h. After completion of the reaction as monitored by TLC (10% MeOH/$CHCl_3$), 10 mL of saturated $NaHCO_3$ solution was added to the reaction mixture, and stirred for 10 min. An aqueous work up was performed with ethyl acetate, and the organic layer was dried using Na_2SO_4 and concentrated down under reduced pressure. The crude product was purified via preparatory TLC (3.5% MeOH/$CHCl_3$) to obtain 54% yield of compound **4**.

^{1}H NMR ($CDCl_3$): δ= 6.71 (s, 1 H), 6.57 (s 1 H), 5.91 (s, 2 H), 5.74 (s, 1H), 5.52 (s, 1 H), 5.26 (s, 1 H), 4.11-4.10 (d, J = 4 Hz, 1 H), 3.6 (s, 1 H), 3.39 (s, 1 H), 2.88 (d, J = 4 Hz, 1 H), 2.66 (s, 2 H), 2.50-2.40 (m, 2 H), 2.32-2.31 (m, 2 H), 2.27-2.26 (m, 3 H), 2.09-2.07 (m, 2 H), 1.97 (t, J = 1.2 Hz, 1 H), 1.89 (t, J = 1.3 Hz, 1 H).

^{13}C ($CDCl_3$): δ= 172.1, 171.9, 146.6, 126.6, 107.5, 105.2, 101.2, 83.3, 83.2 70.9, 69.4, 69.2, 61.3, 53.8, 49.9, 40.5, 34.3, 34.1, 32.9, 31.0, 25.4, 25.7, 25.6, 25.5, 25.1, 24.8, 23.9, 17.9.

HRMS (ESI): *m/z* calculated for $C_{28}H_{29}NO_6$ + H (M + H): 476.2073. Found: 476.2075.

Compound 5:

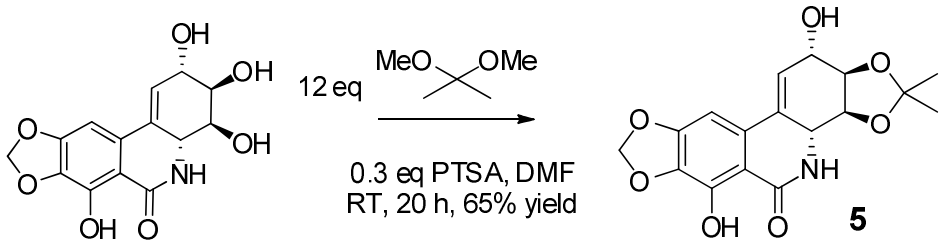

To a solution of narciclasine (10 mg, 0.0326 mmol), in dry DMF (0.5 mL) were added 12 eq of 2,2-dimethoxypropane (4.7 µL, 3.91 mmol), and 0.3 eq PTSA (1.8 mg, 0.0097 mmol). The mixture was stirred at room temperature for 20 h. After completion of the reaction as monitored by TLC (5% MeOH/$CHCl_3$), 3 drops of pyridine were added and the reaction was left to stir at room temperature for an additional hour. 0.3 mL H_2O were added, and the entire contents of the reaction mixture was concentrated down under reduced pressure and co-distilled with toluene. Product was sufficiently pure for the next reaction without purification.

Compound 6:

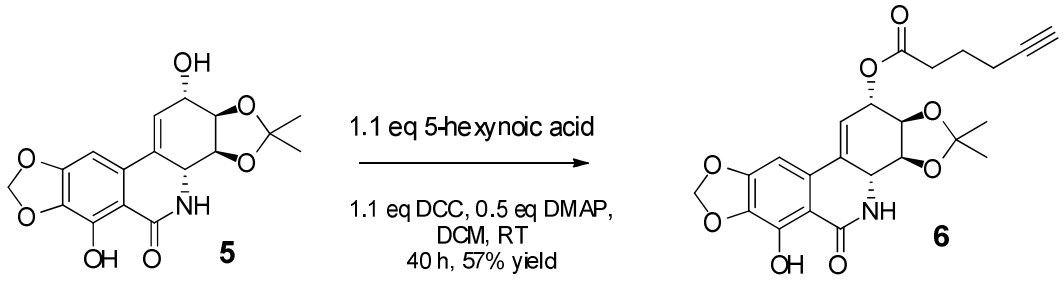

To a solution of **5** (5.9 mg, 0.017 mmol), in dry DMF (0.5 mL) were added 1.1 eq of 5-hexynoic acid (2.1 µL, 0.0183 mmol), 0.5 eq DMAP (1.0 mg, 0.0085 mmol), and 1.1 eq DCC (3.85 mg, 0.0187 mmol). The mixture was left to stir at room temperature for 2

days. After completion of the reaction as monitored by TLC (5% MeOH/$CHCl_3$), the mixture was diluted with 1 mL of dichloromethane. 0.5 mL 1 M HCl, and 0.5 mL H_2O. An aqueous work up was performed, and the organic layer was dried using Na_2SO_4 and concentrated down under reduced pressure. The crude product was purified via preparatory TLC (4% MeOH/$CHCl_3$) to obtain 57% yield of compound **6**.

^{1}H NMR ($CDCl_3$) for **6**: δ= 12.85 (s, 1 H), 6.66 (s, 1 H), 6.44 (s, 1 H), 6.10 (s, 1 H), 5.40 (s, 1 H), 4.33-4.30 (m, 1 H), 4.13-4.11 (m, 1 H), 3.48 (s, 1 H), 2.62-2.59 (m, 2 H), 2.34-2.32 (m, 2 H), 2.30 (s, 1 H), 2.00- 1.99 (m, 3 H), 1.92 (s, 3 H), 1.53 (s, 3 H), 1.39 (s, 2 H).

^{13}C ($CDCl_3$) for **6**: N/A

HRMS (ESI): *m/z* calculated for $C_{23}H_{23}NO_8$ + H (M + H): 442.1424. Found: 442.1545.

Compound 7:

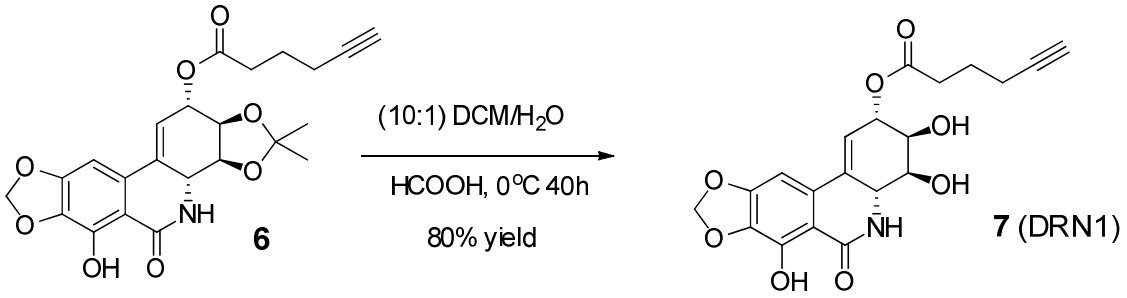

To a solution of **6** (5.9 mg, 0.013 mmol) redissolved in a (10:1) DCM/H_2O at 0 °C were added 0.5 mL formic acid. The mixture was left to stir at 0 °C for 2 days. After completion of the reaction as monitored by TLC (10% MeOH/$CHCl_3$), the reaction was brought to room temperature, concentrated down under reduced pressure and co-distilled with toluene. The crude product was purified via preparatory TLC (7% MeOH/$CHCl_3$) to obtain 80% yield of compound **7**.

^{1}H NMR ($CDCl_3$) for **7**: δ= 12.56 (s, 1 H), 6.63 (s, 1 H), 6.05 (s, 3 H), 5.40 (s, 1 H), 4.45

(s, 1 H), 4.09 (s, 1 H), 3.90 (s, 1 H), 2.49-2.48 (m, 2 H), 2.26-2.27 (m, 2 H), 1.85 (s, 1 H), 1.64-1.62 (t, 2 H), 1.25-1.24 (m, 2 H).

HRMS (ESI): *m/z* calculated for $C_{29}H_{19}NO_8$ + Na (M + Na): 424.1111. Found: 424.1019.

Compound 8:[40]

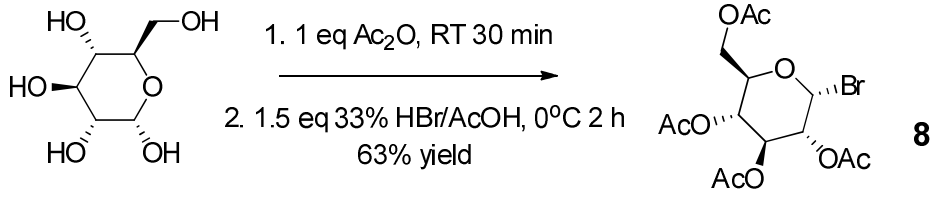

8

To a solution of D-glucose (1 g, 5.55 mmol), 1 eq of Ac_2O (0.61 mL, 5.54 mmol) was added and left to stir at room temperature for 30 min. 1.5 eq of 33% HBr/AcOH (0.912 mL, 0.00832 mmol) was then added at 0 °C and the reaction was left to stir for 2 hours. After completion of the reaction as monitored by TLC (30% EtOAc/hexanes), the reaction was brought to room temperature, and 30 mL saturated $NaHCO_3$ was added to the reaction flask. An aqueous work up was performed with EtOAc, and the organic layer was dried with Na_2SO_4 and concentrated down *in vacuo*. The crude material was purified using normal phase flash chromatography (1:10 to 1.5:10 ethyl acetate/hexanes) to obtain 63% yield of compound **8**.

^{1}H NMR ($CDCl_3$) for **8**: δ= 6.61 (s, 1 H), 5.58 (t, J = 9.64 Hz, 1 H), 5.18 (t, J = 9.48 Hz, 1 H), 4.85-4.82 (d, J = 12 Hz, 1 H), 4.33-4.31 (m, J = 10.7 Hz, 2 H), 4.13-4.12 (d, J = 4 Hz, 2 H), 2.03-2.10 (m, 9 H).

Compound 9:[40]

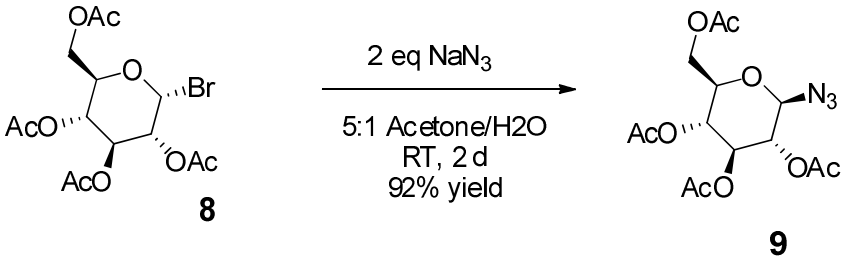

To a solution of **8** (1.5 g, 3.66 mmol) in a 5:1 acetone/H_2O mixture, 2 eq of sodium azide (0.47 g, 7.32 mmol) was added and left to stir at room temperature for 2 days. After completion of the reaction as monitored by TLC (30% ethyl acetate/hexanes), an aqueous work up was performed with ethyl acetate, and the organic layer was dried with Na_2SO_4 and concentrated down *in vacuo*. The crude material was purified using normal phase flash column chromatography, and compound **9** was obtained at 15% ethyl acetate/hexanes at 63% yield.

^{1}H NMR ($CDCl_3$) for **9**: δ= 5.20 (t, J = 8 Hz, 1 H), 5.09 (t, J = 7.4 Hz, 1 H), 4.64-4.63 (d, J = 4 Hz, 1 H), 4.20-4.17 (dd, J = 24.9 Hz, 4.8 Hz, 2 H), 3.81-3.77 (M, 1 H), 2.06-1.99 (m, 13 H).

Compound 10:

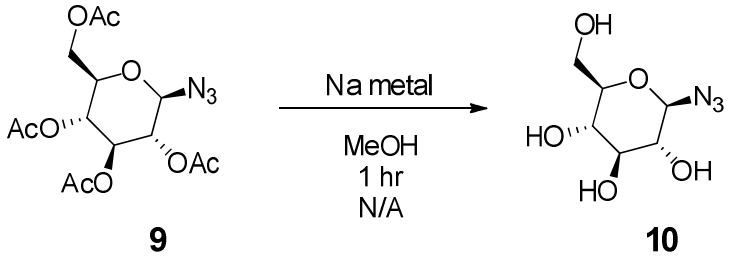

To a solution of **9** (5.0 mg, 0.0134 mmol) redissolved in 2 mL dry MeOH, 5 mg of Na metal was added to obtain NaOMe solution at pH 8, and the solution was left to stir

for 30 min. After 30 min, the pH of the solution was checked again, and Dowex® was added until the pH became neutral. The Dowex® was filtered off via vacuum filtration with 20% H_2O/MeOH, and the remaining solution was concentrated down. Crude material was used for compounds **16** and **17** without purification.

Compound 12: [41]

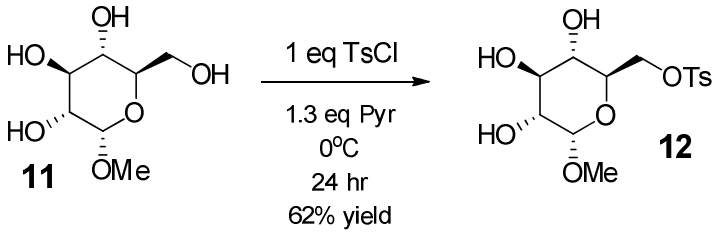

To a solution of **1,** (1.0 g, 5.15 mmol), 1.0 eq TsCl (0.98 g, 5.15 mmol) and 1.3 eq of pyridine (0.52 mL, 6.69 mmol) 0 °C, and left at 4 °C for 24 h. After completion of the reaction as monitored by TLC (10% MeOH/$CHCl_3$), 15 mL of hexane was added, and the mixture was left to stir at 0°C for 1 h. No organic work up was performed for this reaction, and the mixture was concentrated down under reduced pressure and co-distilled with toluene. The crude mixture was purified using flash column chromatography, and the desired product (**12**) was obtained at 4% MeOH/$CHCl_3$ at 62% yield.

^{1}H NMR ($CDCl_3$) for **12**: δ= 7.76-7.78 (d, J = 8 Hz, 2 H), 7.32-7.30 (d, J = 8 Hz, 2 H), 4.63 (s, 1 H), 4.25 (s, 2 H), 4.12 (s, 3 H), 3.71-3.69 (d, J = 8 Hz, 2H), 3.46-3.43 (m, 2 H), 3.38 (s, 3 H), 3.30 (s, 3 H), 2.94-2.86 (d, J = 32 Hz, 2 H), 2.40 (s, 3 H).

Compound 13: [41],[48]

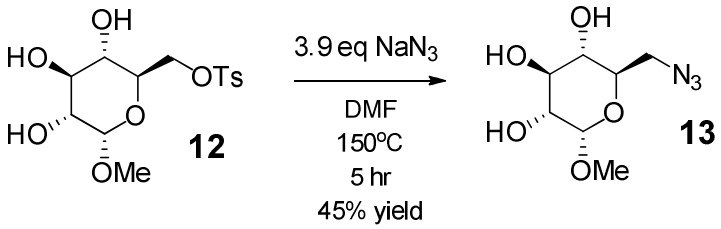

To a solution of **12** (100 mg, 0.287 mmol) in dry DMF (1 mL), 3.9 eq of sodium azide (72.7 mg, 0.120 mmol) and refluxed for 5 h at 150 °C. After completion of the reaction as monitored by TLC (10% MeOH/$CHCl_3$), the reaction was cooled to room temperature and 10 mL benzene was added. The mixture was concentrated down under reduced pressure and co-distilled with toluene. The crude material was purified using flash column chromatography, and compound **13** was isolated at 3.5% MeOH/$CHCl_3$, at 45% yield.

^{1}H NMR ($CDCl_3$) for **13**: δ= 3.86-4.85 (d, J = 4 Hz, 1 H), 3.84-3.81 (m, 2 H), 3.75-3.69 (dd, J = 12 Hz, 2.4 Hz, 1 H), 3.69-3.67 (d, J = 8 Hz, 1 H), 3.63-3.57 (m, 2 H), 3.5 (s, 3 H)

Compound 14: [42],[49]

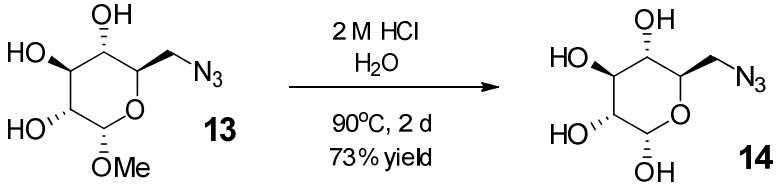

To a solution of **13** (50 mg, 0.228 mmol) redissolved in 2 mL H_2O, 2 mL of 2 M HCl was added, and the mixture was left to stir for 2 days at 90 °C. After completion of the reaction as monitored by TLC (20% MeOH/$CHCl_3$), the reaction was cooled to room temperature, and 20 mL of saturated sodium bicarbonate solution was added. The mixture was then concentrated *in vacuo* and co-distilled with MeOH, and re-precipitated NaCl

was filtered out via vacuum filtration. The crude material was purified normal flash column chromatography, and compound **14** was isolated at 15% MeOH/$CHCl_3$ at a 73% yield.

^{1}H NMR ($CDCl_3$) for **14**: δ= 5.30 (s, 1 H), 4.71-4.69 (d, J = 8 Hz, 1 H), 4.00-3.97 (m, 1 H), 3.73-3.71 (m, 2 H), 3.62-3.57 (m, 2 H), 3.52-3.49 (m, 2H), 3.49-3.47 (m, 1 H), 3.47-3.45 (m, 1 H), 3.32-3.29 (m, 1 H).

Compound 15:[43]

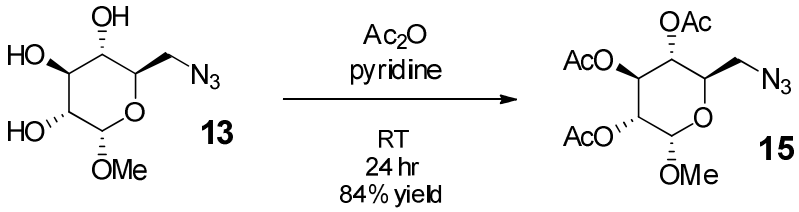

To a solution of **13** (50 mg, 0.228 mmol) 0.2 mL Ac_2O and 1.5 mL pyridine was added at room temperature and stirred for 24 hours. After completion of the reaction as monitored by TLC (30% ethyl acetate/hexane), 30 mL H_2O were then added to the reaction mixture, and and aqueous work up was performed with ethyl acetate. The organic layers were combined, dried with Na_2SO_4, and concentrated down under reduced pressure. Compound **15** was purified at 16% ethyl acetate/hexane via flash column chromatography at 84%.

^{1}H NMR ($CDCl_3$) for **15**: δ= 5.46-5.41 (m, 1 H), 4.98-4.93 (m, 1 H), 4.86-4.83 (1 H), 3.95-3.92 (m, 1 H), 3.48 (s, 3 H), 3.49-3.35 (m, 2 H), 2.12-2.04 (m, 1 H), 2.00-1.97 (m, 9 H).

Compound 16 (DRL44):

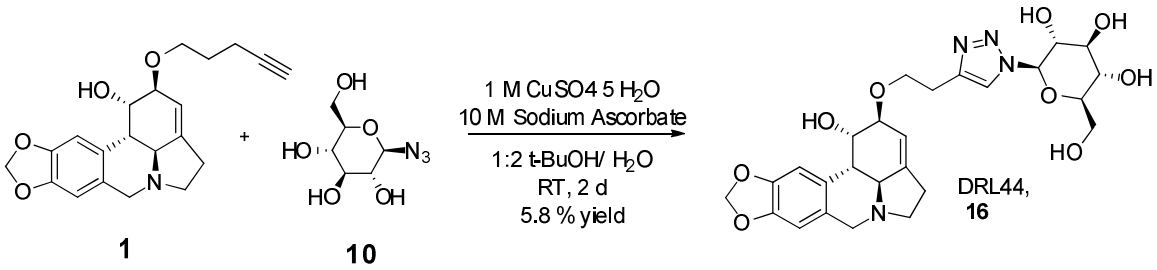

Compound 17 (DRN6):

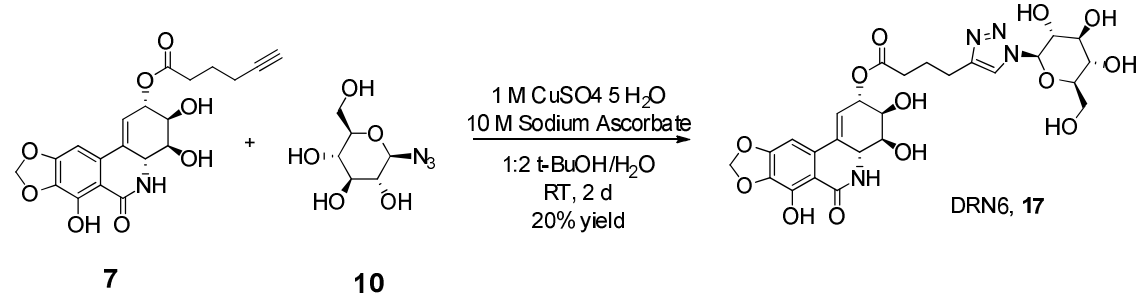

General Procedure for Compounds **16** and **17**:

5 mg of alkyne (compounds **1** and **7**) was added to to a dry, tare 1 mL flask containing 5 mg of azide (**10**) and 0.3 mL *t*-BuOH and 0.6 mL H_2O. Preparation of the reducing agent: A 1M $CuSO_4$•5 H_2O (0.998 g) and 10M sodium ascorbate (0.125 g) solution was added to 1 mL H_2O, and left to stir for 15 min until the mixture turned a light brown. 30 μL of this solution was added to the vial containing both alkyne and azide, and the reaction was left to stir for 2 days.

The reactions were monitored via TLC (20% MeOH/$CHCl_3$) until no starting material was viewed either under UV (R_f ~ 0.63 for **7**, R_f~ 0.71 for **1**) or with a *p*-anisaldehyde stain (R_f ~ 0.12 for **14**). The molecular weights of the desired products were confirmed via mass spectrometry. The entire contents of the reaction mixtures were then

directly plated onto a preparatory TLC plate and run on 15% MeOH/$CHCl_3$ solvent system.

^{1}H NMR (DMSO) for **16**: δ= 8.0 (s, 1 H), 7.0 (s, 1 H), 6.7 (s, 1 H), 6.0 (s, 2 H), 5.6-5.55 (m, 2 H), 5.5 (s, 1 H), 5.1 (s, 3 H), 4.7 (s, 1 H), 4.0-3.5 (m, 6 H), 3.1 (s, 1 H), 2.8-2.7 (m, 1 H), 2.0 (1 H).

^{13}C NMR (DMSO) for **16**: Unable to obtain clear NMR for compound **16**. Sample had to little amount.

^{1}H NMR (DMSO) for **17**: δ= 8.1 (s, 1 H), 7.0 (d, J = 12.4 Hz, 2 H), 6.34-6.32 (d, J = 8 Hz, 1 H), 6.1 (s, 1 H), 6.0 (s, 1 H), 5.8-5.5 (m, 2 H), 5.2-5.1 (m, 2 H), 4.9 (s, 1 H), 4.4 (s, 1 H), 4.2-4.0 (m, 5 H).

^{13}C NMR (DMSO) for **17**: δ= 172.4, 146.5, 121.5, 119.8, 87.9, 80.3, 72.5, 71.4, 70.1, 40.2, 20.0, 39.8, 39.6, 39.4, 33.5, 24.8, 24.7.

General Synthesis of C6 click analogs:

5 mg of lycorine alkynes **1-4** and narciclasine alkyne **7** were added to 5 mg of compound **14** (1:1 eq), in a 0.3 mL *t*-BuOH and 0.6 mL H_2O mixture. Preparation of the reducing agent: a 1M $CuSO_4$•5 H_2O (0.998 g) and 10M sodium ascorbate (0.125 g) solution was added to 1 mL H_2O, and left to stir for 15 min until the mixture turned a light brown. 30 μL of this solution was added to the vial containing compounds both alkyne and azide, and the reaction was left to stir for 2 days.

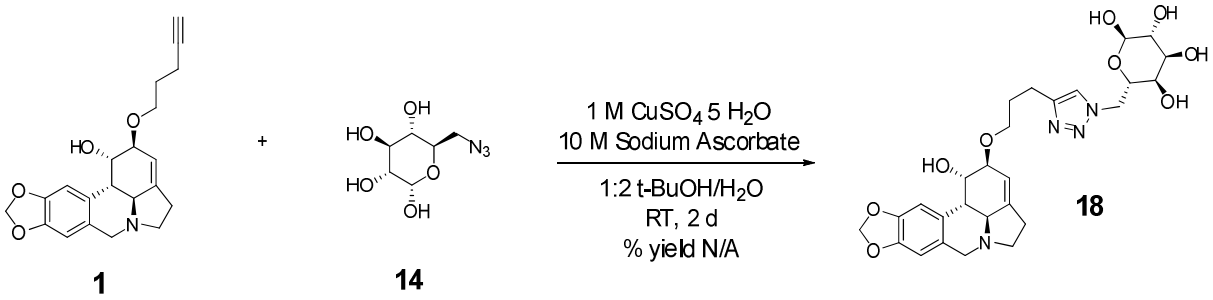

1 **14** **18**

The reaction was monitored by TLC (20% MeOH/$CHCl_3$), until no starting material was viewed either under UV (R_f ~0.76 for **1**) or via *p*-anisaldehyde stain (R_f ~ 0.12 for **14**). After confirming the molecular weight of compound **18** (m/z: 559.28, mol. mass: 558.23 g/mol) the entire contents of the reaction mixture were then plated onto a preparatory TLC plate and run on an 8% MeOH/$CHCl_3$ solvent system. However, it was decided that this solvent system was not polar enough (due to impurities seen on the prep plate), and 15% MeOH/$CHCl_3$ was used. A polar spot (R_f ~0.13) was isolated as it fluoresced similar to the starting material, and mass spec of this spot confirmed the absence of the desired molecular weight. Analysis via ^{1}H NMR of this isolated spot showed only starting material peaks, and not the desired C-H peak on the triazole ring, as well as sodium ascorbate impurities.

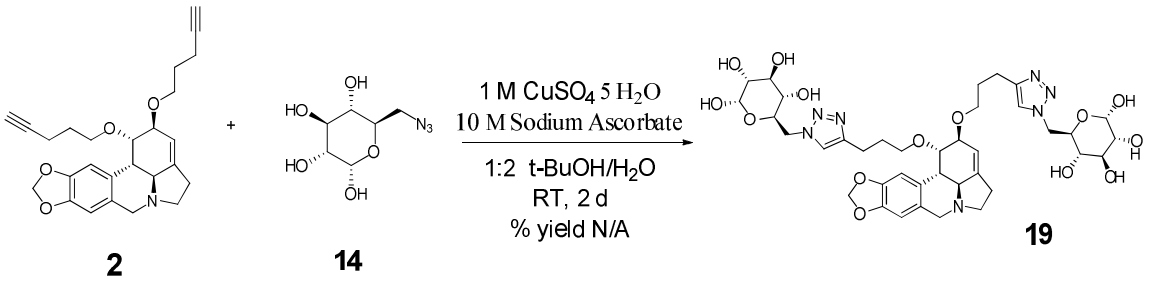

2 **14** **19**

The reaction was monitored via TLC (20% MeOH/$CHCl_3$) until no starting materials were viewed either under UV (R_f ~ 0.82 for **2**) or via *p*-anisaldehyde stain (R_f ~ 0.12 for **14**). Mass spectrometry of the crude material showed no formation of Compound

19. As such, no purification of this crude material was conducted.

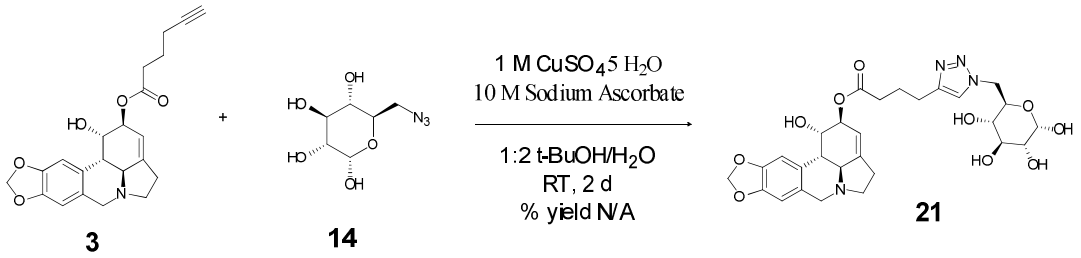

3 **14** **21**

The reaction was monitored via TLC (20% MeOH/$CHCl_3$) until no starting materials were viewed either under UV (R_f ~0.61 for **3**) or via *p*-anisaldehyde stain (R_f ~ 0.12 for **14**). Mass spectrometry of the crude material showed formation of compound **21** (m/z: 587.24 g/mol). However, as with the previous click reactions, purification of the crude material was not conducted.

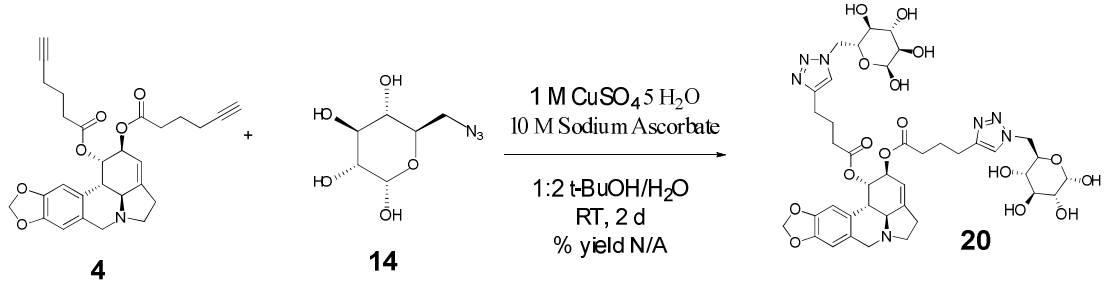

4 **14** **20**

The reaction was monitored via TLC (20% MeOH/$CHCl_3$) until no starting materials were viewed either under UV (R_f ~0.84 for **4**) or via *p*-anisaldehyde stain (R_f ~ 0.12 for **14**). Mass spec of the crude material showed formation of compound **21** (m/z: 587.24 g/mol) and compound **20** (m/z: 886.33 g/mol). Purification of the crude material was not performed.

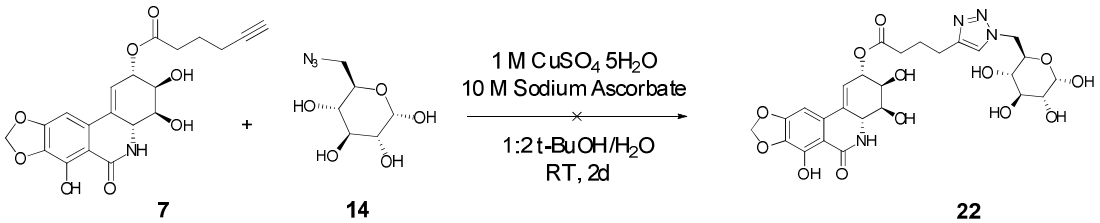

7 **14** **22**

The reaction was monitored via TLC (20% MeOH/$CHCl_3$) until no starting materials were viewed either under UV (R_f~ 0.73 for **7**) or via *p*-anisaldehyde stain (R_f~ 0.47 for **15**). No aqueous workup was performed. The entire contents of the reaction mixture were then plated onto a preparatory TLC plate and run on a 15% MeOH/$CHCl_3$ solvent system. The desired UV active band was surrounded by other polar impurities, so the prep plate was purified further in the same solvent system until this band was isolated (3x more purification on the same plate). ^{1}H NMR of this spot in DMSO showed very dirty starting alkyne and azide starting materials. Mass spectrometry of this same sample showed no desired product. Due to limited alkyne availability, this reaction was not reproduced.

General Synthesis of acetylated click analogs:

10 mg of compounds **1** and **2** was added to a dry, tared flask containing 10 mg of compound **14** (1:1 eq), and 0.3 mL *t*-BuOH and 0.6 mL H_2O were added to the mixture. The reducing agent was prepared (1M $CuSO_4$•5 H_2O (0.998 g) and 10M sodium ascorbate (0.125 g) solution in1 mL H_2O) and left to stir for 15 min until the mixture turned a light brown. 30 µL of this solution was added to the vial containing both azide and alkyne, and the reaction was left to stir for 2 days. The reactions were monitored via TLC (20% MeOH/$CHCl_3$) until no starting materials were viewed either under UV (R_f~ 0.48 for **1**, 0.6 for **2**) or via *p*-anisaldehyde stain (R_f~ 0.47 for **15**).

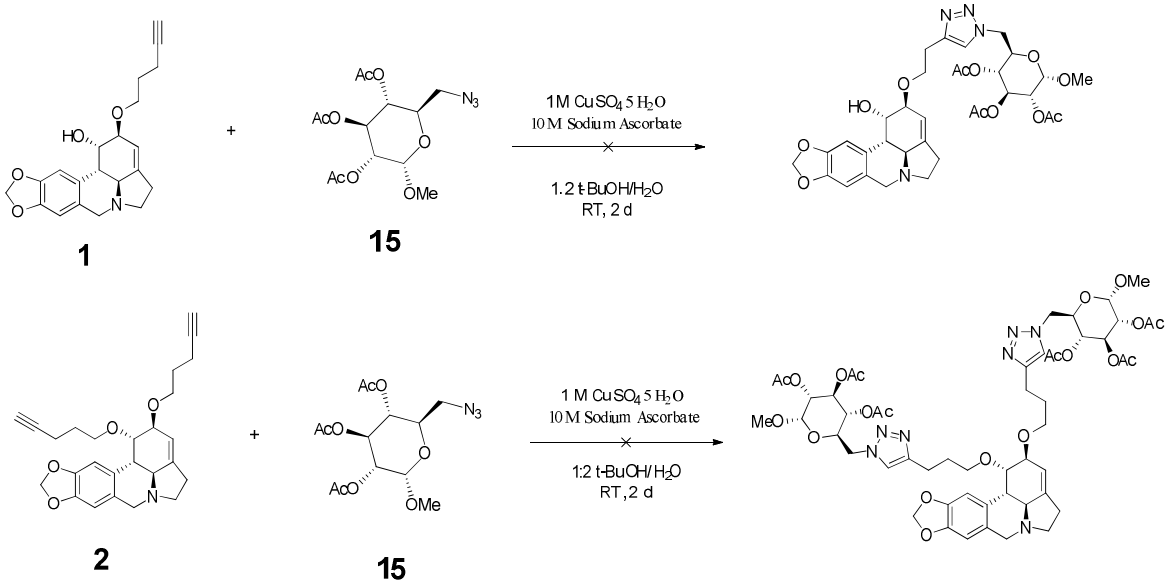
1
15
1M CuSO4 5 H2O
10 M Sodium Ascorbate
1.2 t-BuOH/H2O
RT, 2 d
2
15
1 M CuSO4 5 H2O
10 M Sodium Ascorbate
1:2 t-BuOH/ H2O
RT, 2 d

VII. SPECTRA

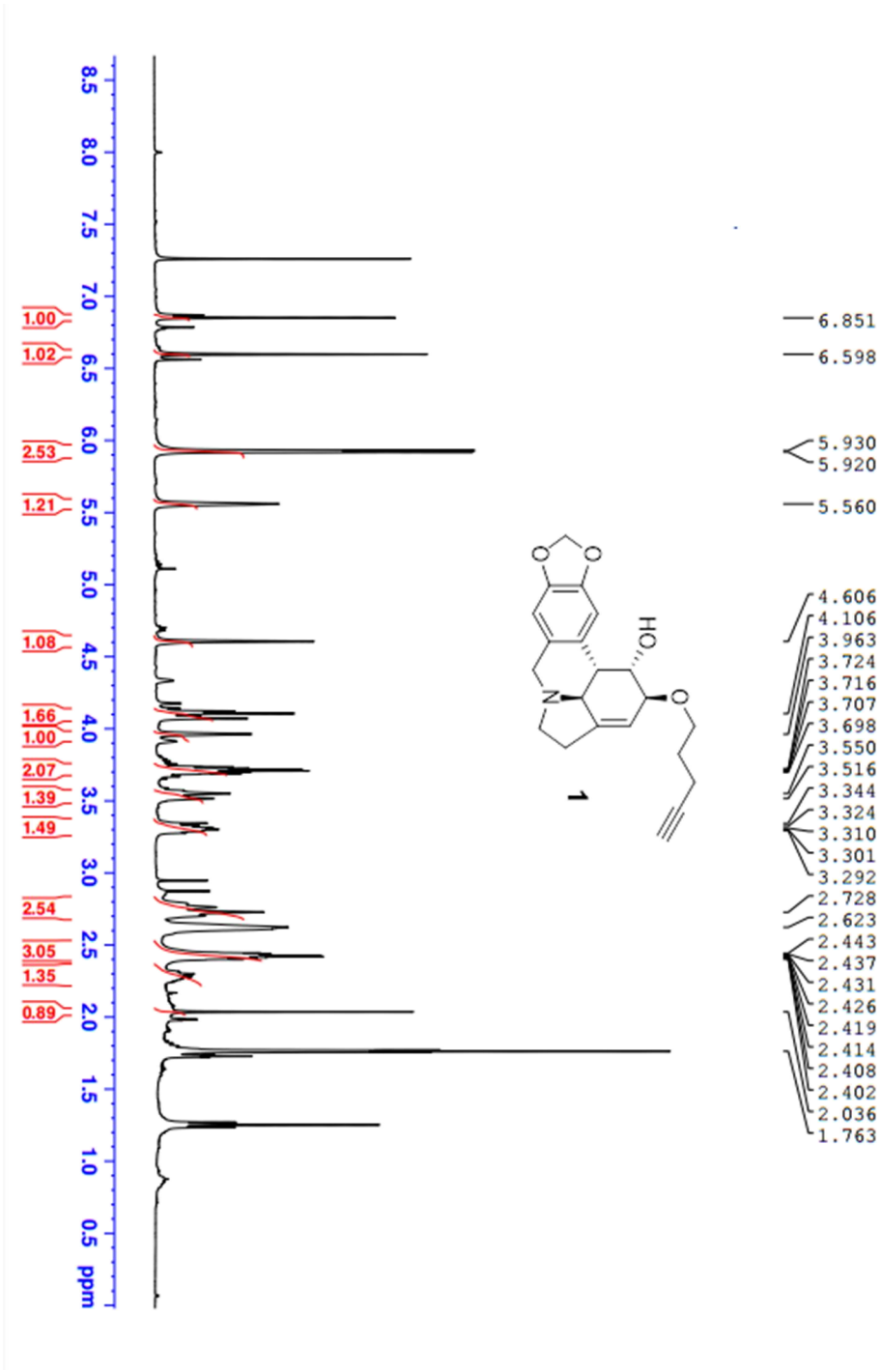
8.5
8.0
7.5
7.0
6.5
6.0
5.5
5.0
4.5
4.0
3.5
3.0
2.5
2.0
1.5
1.0
0.5
ppm
1.00
1.02
2.53
1.21
1.08
1.66
1.00
2.07
1.39
1.49
2.54
3.05
1.35
0.89
6.851
6.598
5.930
5.920
5.560
4.606
4.106
3.963
3.724
3.716
3.707
3.698
3.550
3.516
3.344
3.324
3.310
3.301
3.292
2.728
2.623
2.443
2.437
2.431
2.426
2.419
2.414
2.408
2.402
2.036
1.763
HO
N
O
O
O
1

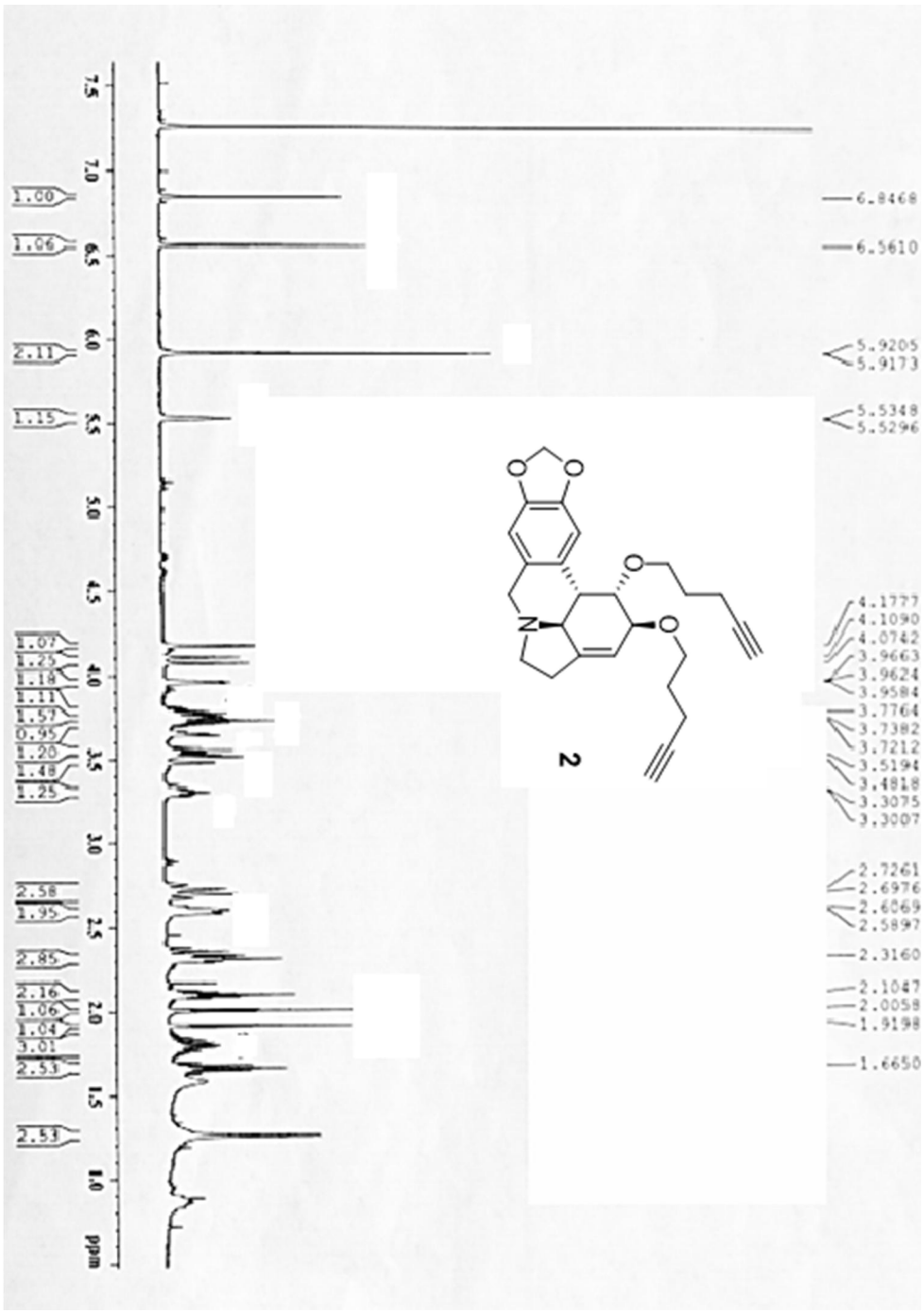
6.8468
6.5610
5.9205
5.9173
5.5348
5.5296
4.1777
4.1090
4.0742
3.9663
3.9624
3.9584
3.7764
3.7382
3.7212
3.5194
3.4818
3.3075
3.3007
2.7261
2.6976
2.6069
2.5897
2.3160
2.1047
2.0058
1.9198
1.6650
2
ppm

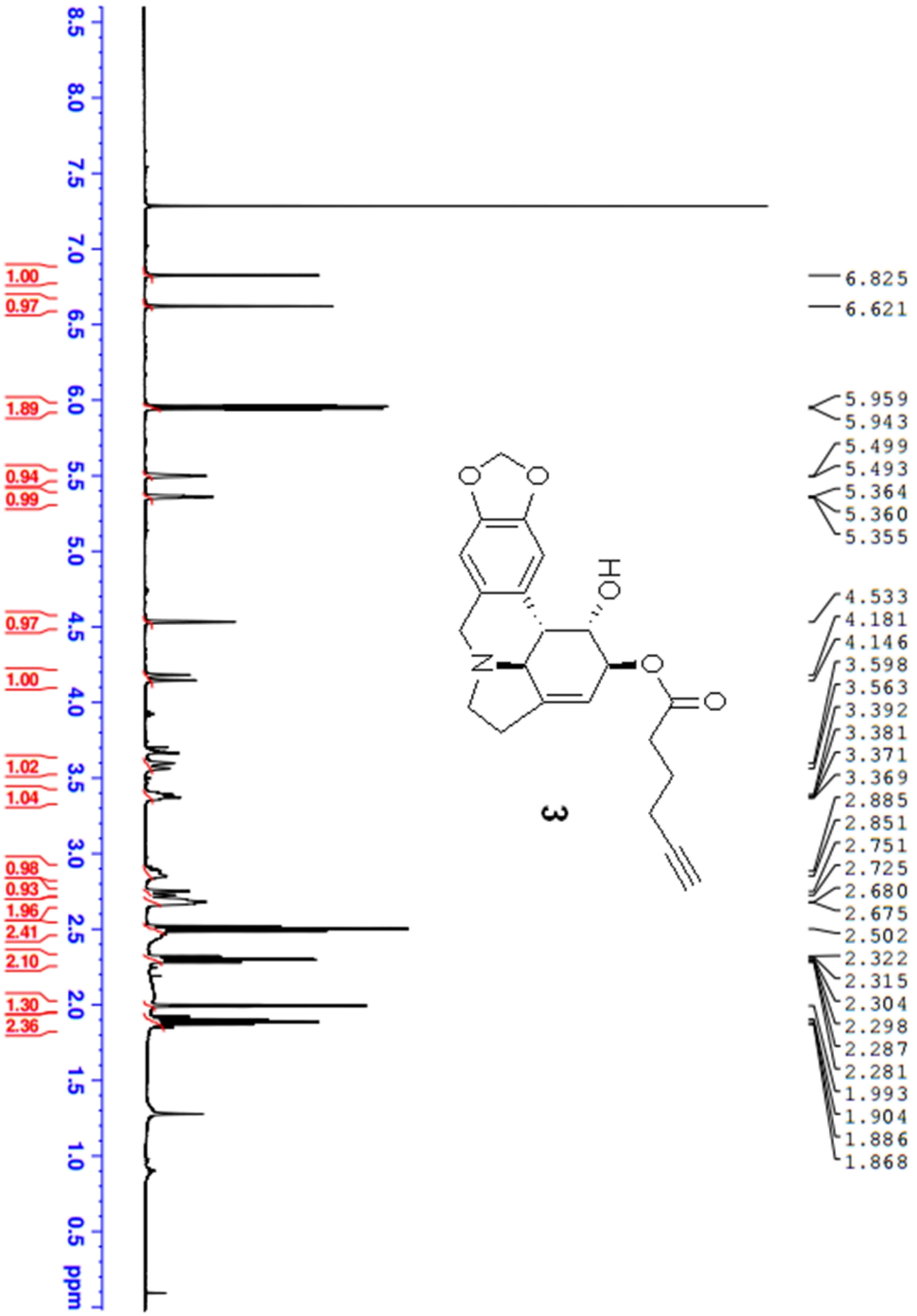
8.5
8.0
7.5
7.0
6.5
6.0
5.5
5.0
4.5
4.0
3.5
3.0
2.5
2.0
1.5
1.0
0.5
ppm
1.00
0.97
1.89
0.94
0.99
0.97
1.00
1.02
1.04
0.98
0.93
1.96
2.41
2.10
1.30
2.36
6.825
6.621
5.959
5.943
5.499
5.493
5.364
5.360
5.355
4.533
4.181
4.146
3.598
3.563
3.392
3.381
3.371
3.369
2.885
2.851
2.751
2.725
2.680
2.675
2.502
2.322
2.315
2.304
2.298
2.287
2.281
1.993
1.904
1.886
1.868
HO
N
O
O
O
O
3

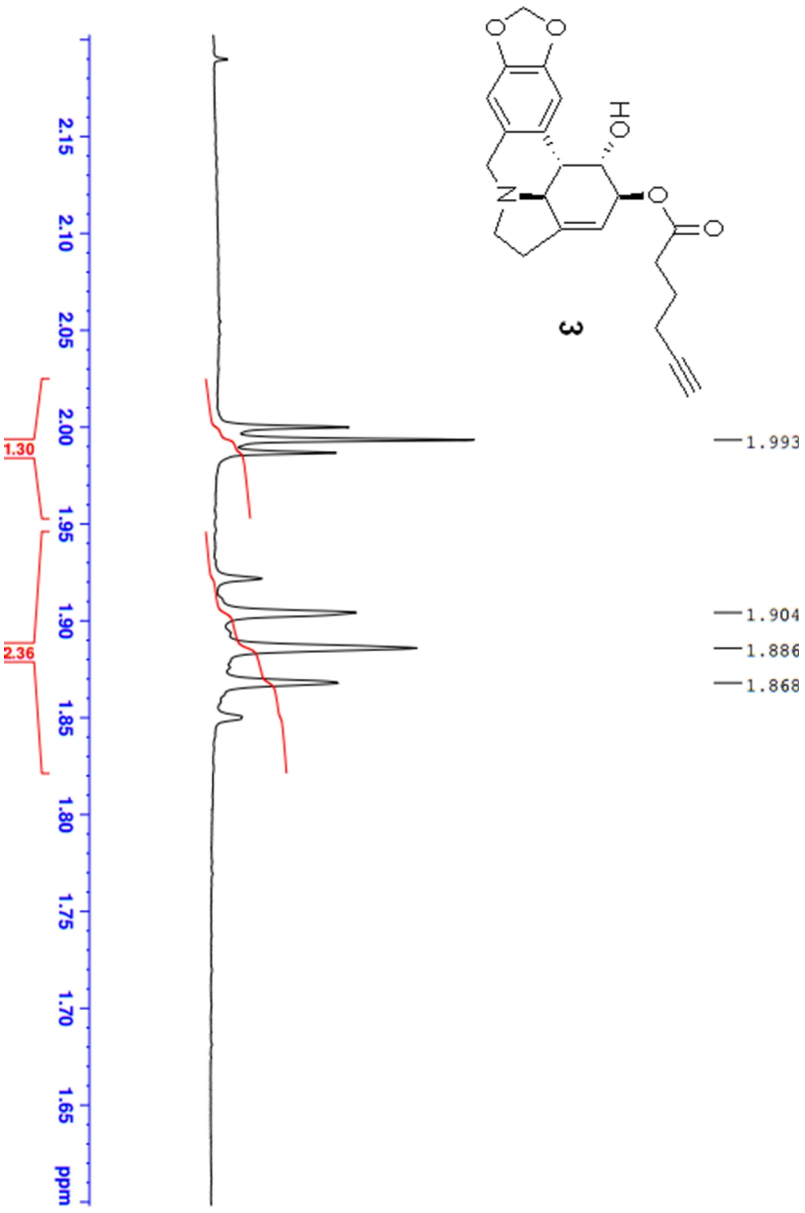
2.15
2.10
2.05
2.00
1.95
1.90
1.85
1.80
1.75
1.70
1.65
ppm
1.30
2.36
1.993
1.904
1.886
1.868
HO
N
O
O
O
O
3

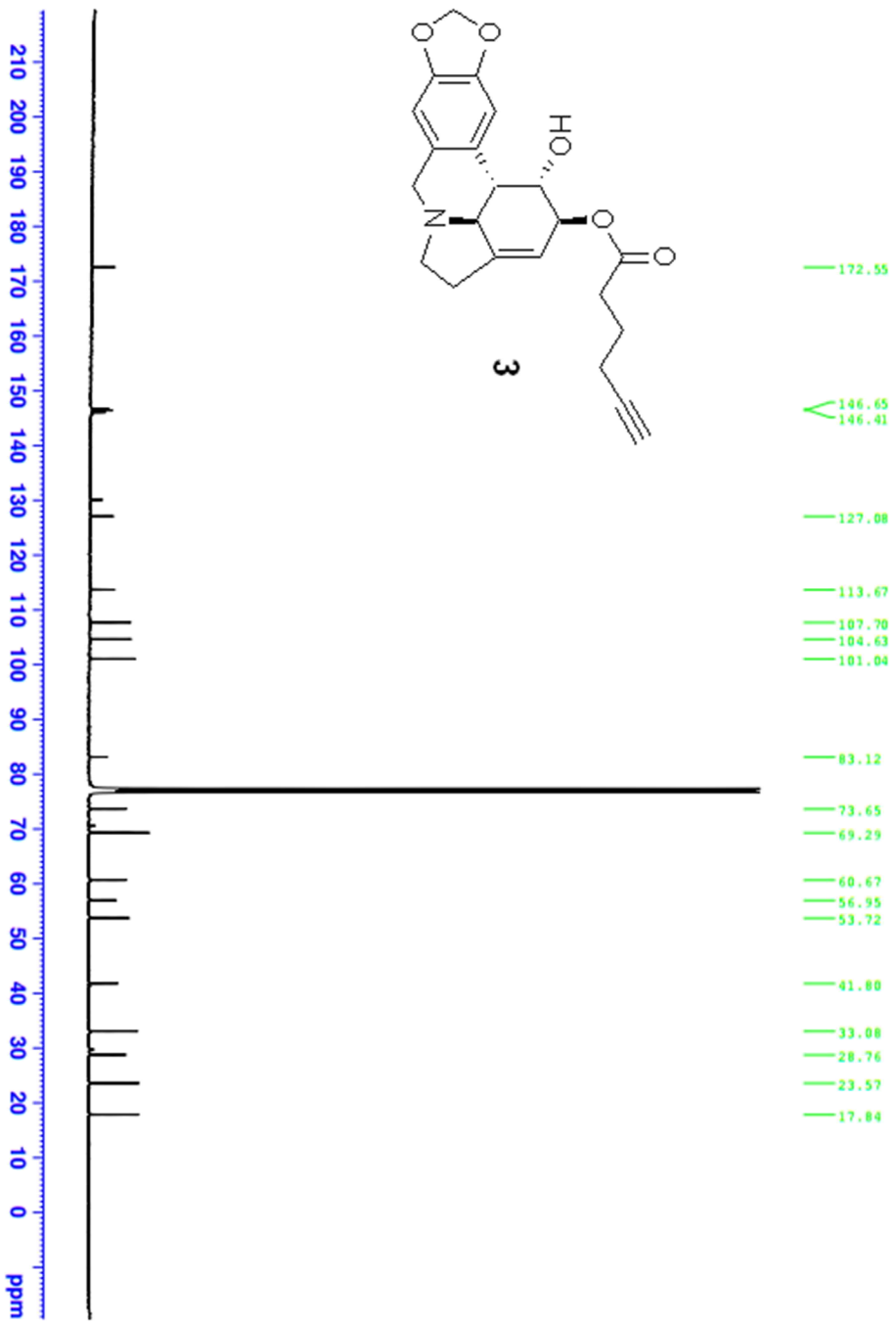
210 200 190 180 170 160 150 140 130 120 110 100 90 80 70 60 50 40 30 20 10 0 ppm
HO
N
O
O
O
O
3
172.55
146.65
146.41
127.08
113.67
107.70
104.63
101.04
83.12
73.65
69.29
60.67
56.95
53.72
41.80
33.08
28.76
23.57
17.84

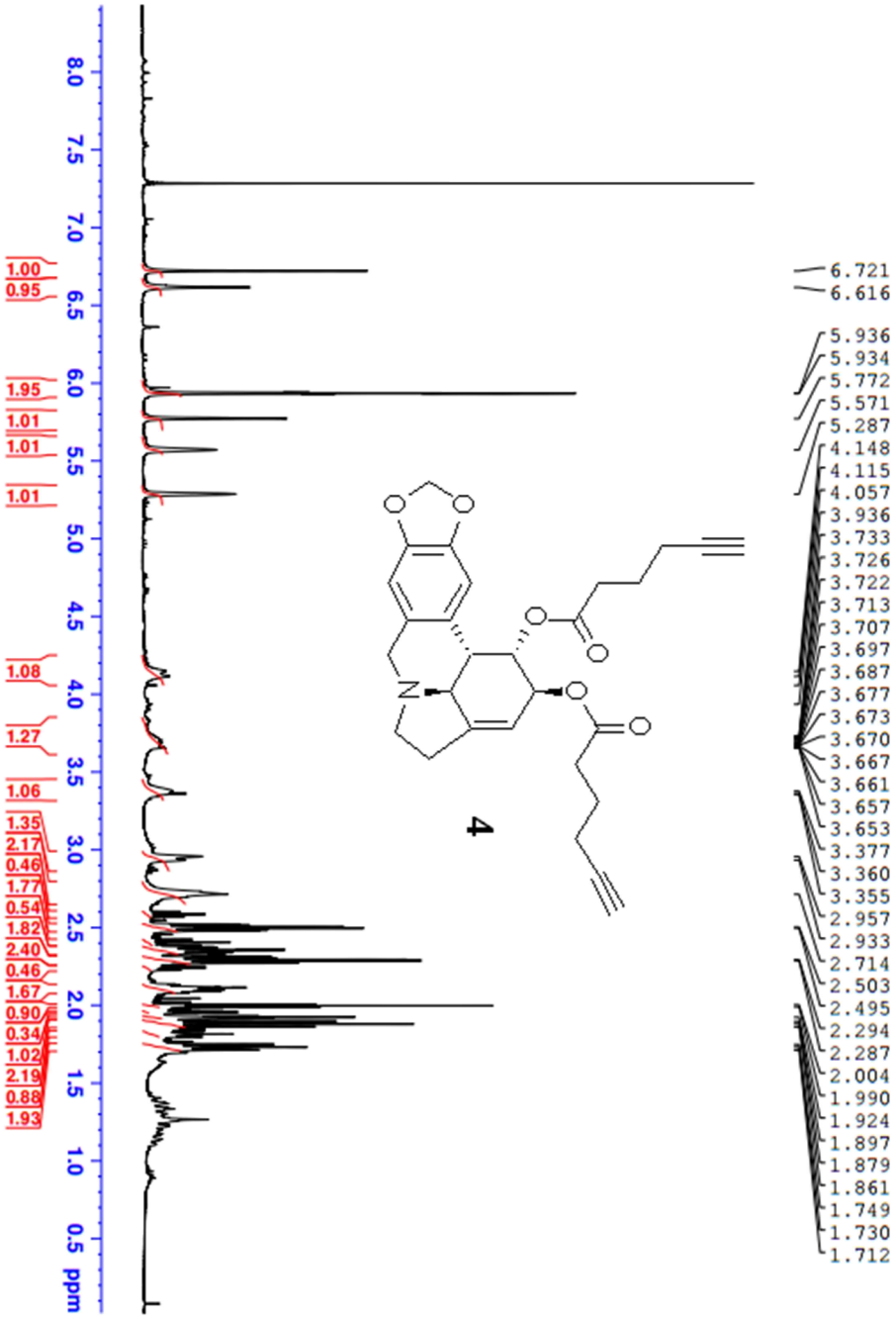
8.0
7.5
7.0
6.5
6.0
5.5
5.0
4.5
4.0
3.5
3.0
2.5
2.0
1.5
1.0
0.5
ppm
1.00
0.95
1.95
1.01
1.01
1.01
1.08
1.27
1.06
1.35
2.17
0.46
1.77
0.54
1.82
2.40
0.46
1.67
0.90
0.34
1.02
2.19
0.88
1.93
6.721
6.616
5.936
5.934
5.772
5.571
5.287
4.148
4.115
4.057
3.936
3.733
3.726
3.722
3.713
3.707
3.697
3.687
3.677
3.673
3.670
3.667
3.661
3.657
3.653
3.377
3.360
3.355
2.957
2.933
2.714
2.503
2.495
2.294
2.287
2.004
1.990
1.924
1.897
1.879
1.861
1.749
1.730
1.712
4

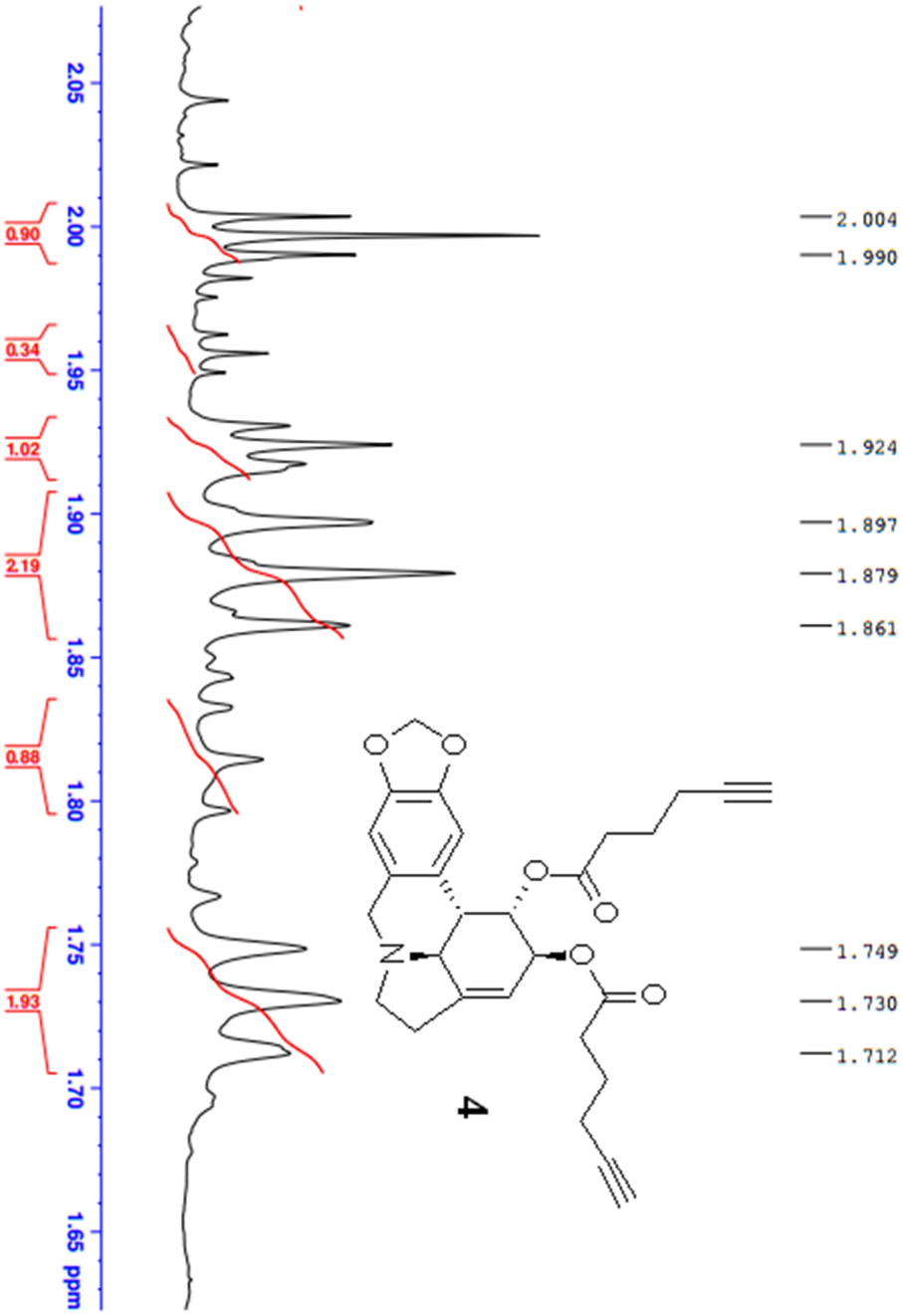
2.05
2.00
1.95
1.90
1.85
1.80
1.75
1.70
1.65 ppm
0.90
0.34
1.02
2.19
0.88
1.93
2.004
1.990
1.924
1.897
1.879
1.861
1.749
1.730
1.712
4

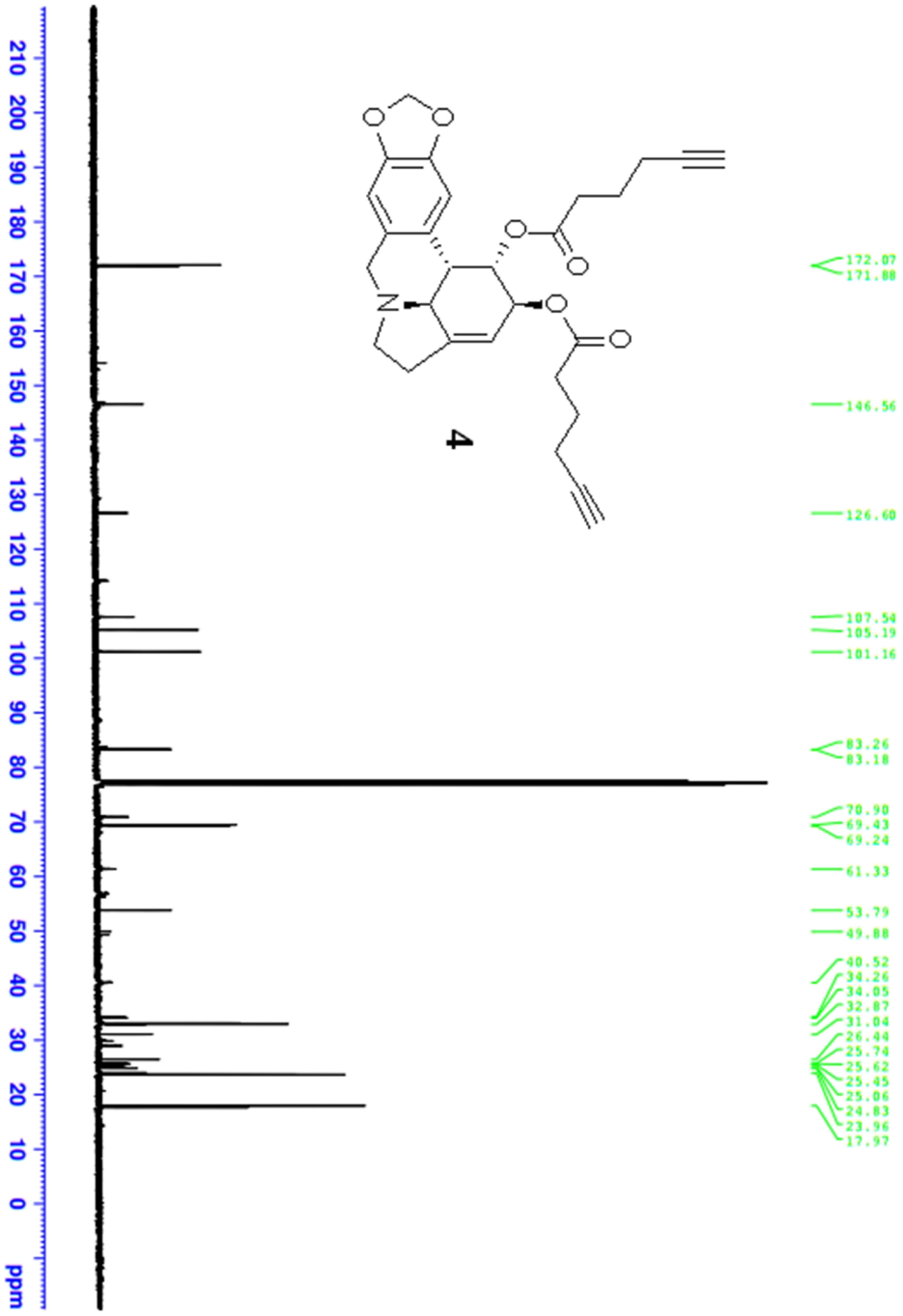
210 200 190 180 170 160 150 140 130 120 110 100 90 80 70 60 50 40 30 20 10 0 ppm
172.07
171.88
146.56
126.60
107.54
105.19
101.16
83.26
83.18
70.90
69.43
69.24
61.33
53.79
49.88
40.52
34.26
34.05
32.87
31.04
26.44
25.74
25.62
25.45
25.06
24.83
23.96
17.97
4

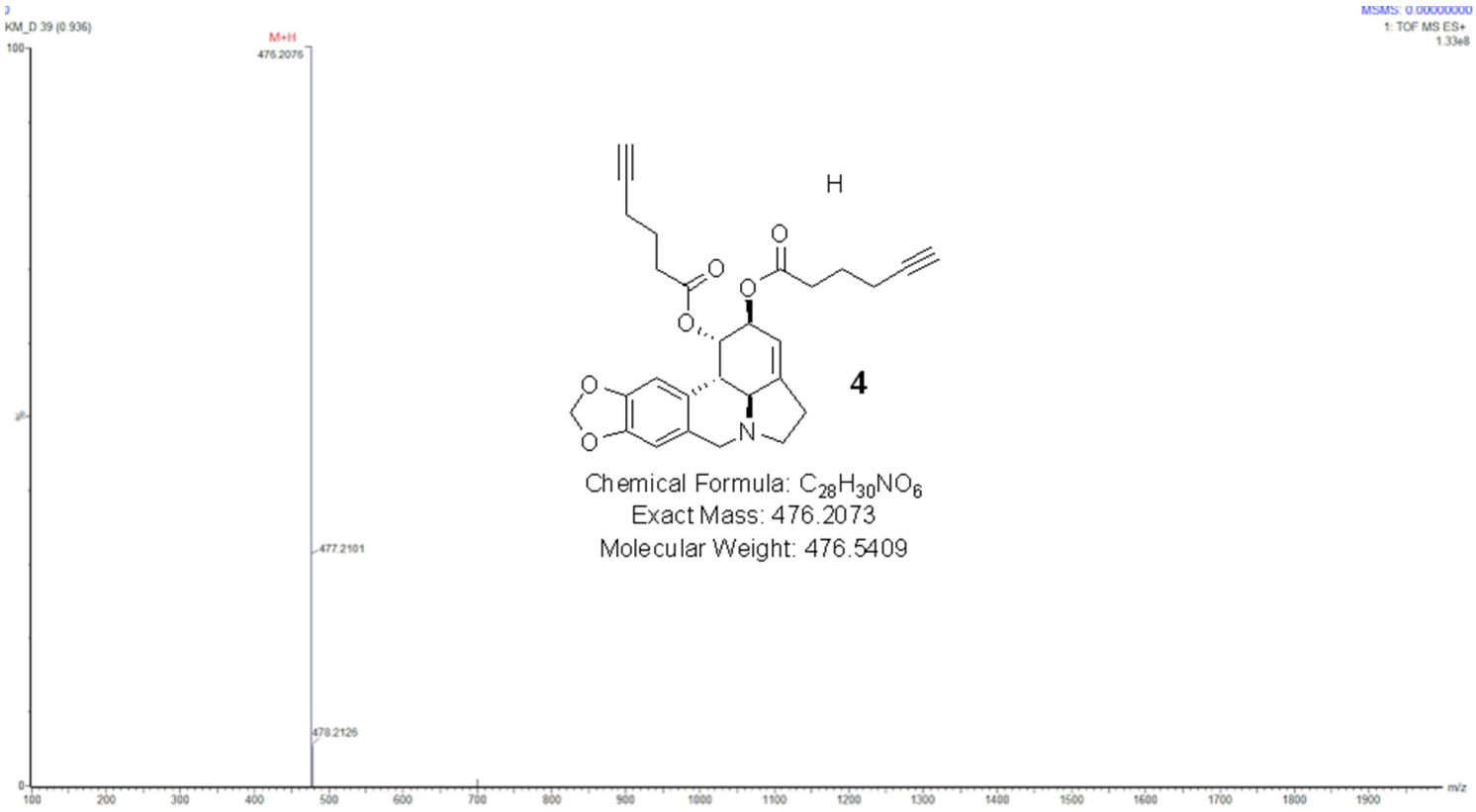

4

Chemical Formula: $C_{28}H_{30}NO_6$
Exact Mass: 476.2073
Molecular Weight: 476.5409

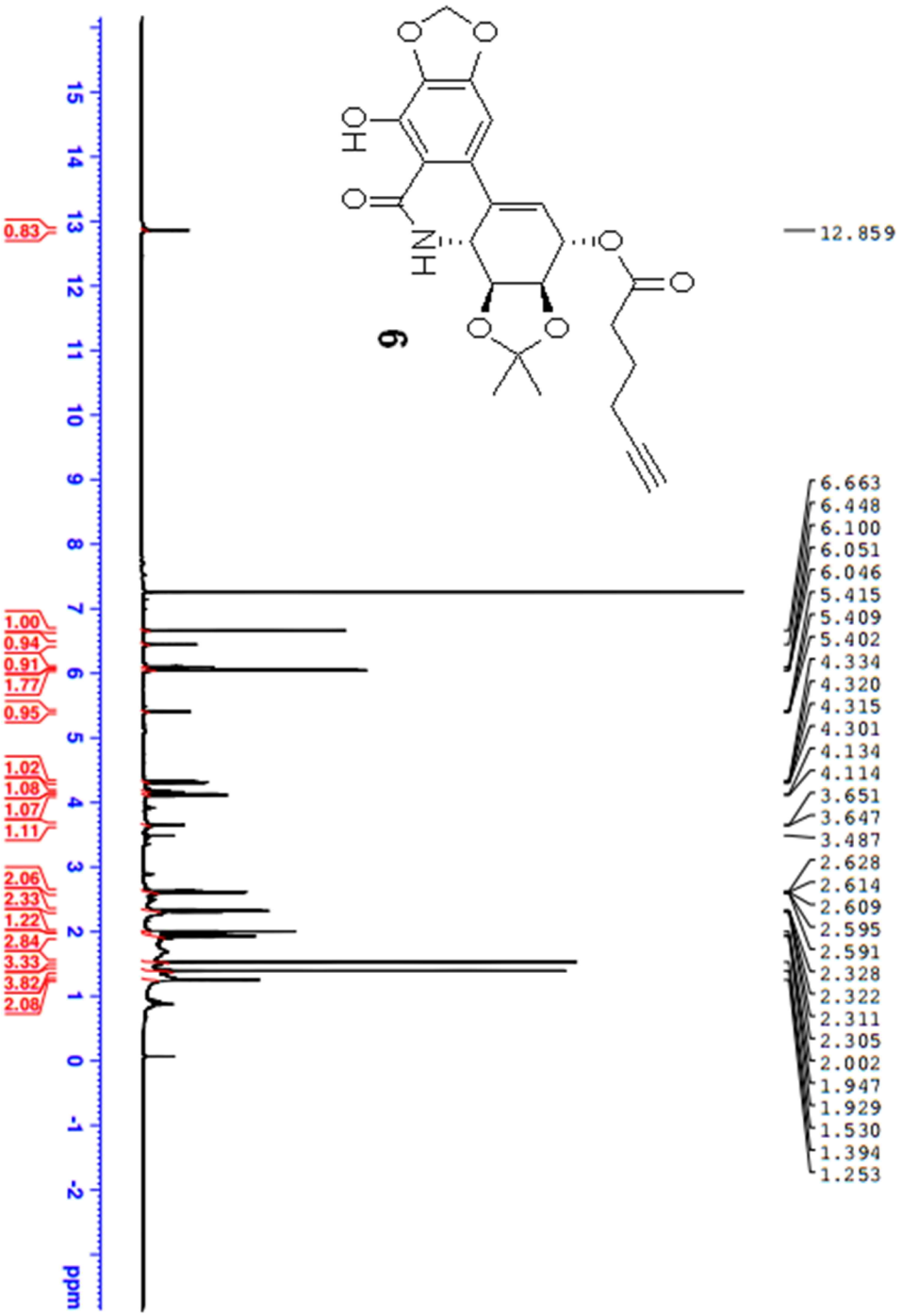
6
12.859
6.663
6.448
6.100
6.051
6.046
5.415
5.409
5.402
4.334
4.320
4.315
4.301
4.134
4.114
3.651
3.647
3.487
2.628
2.614
2.609
2.595
2.591
2.328
2.322
2.311
2.305
2.002
1.947
1.929
1.530
1.394
1.253
0.83
1.00
0.94
0.91
1.77
0.95
1.02
1.08
1.07
1.11
2.06
2.33
1.22
2.84
3.33
3.82
2.08
ppm

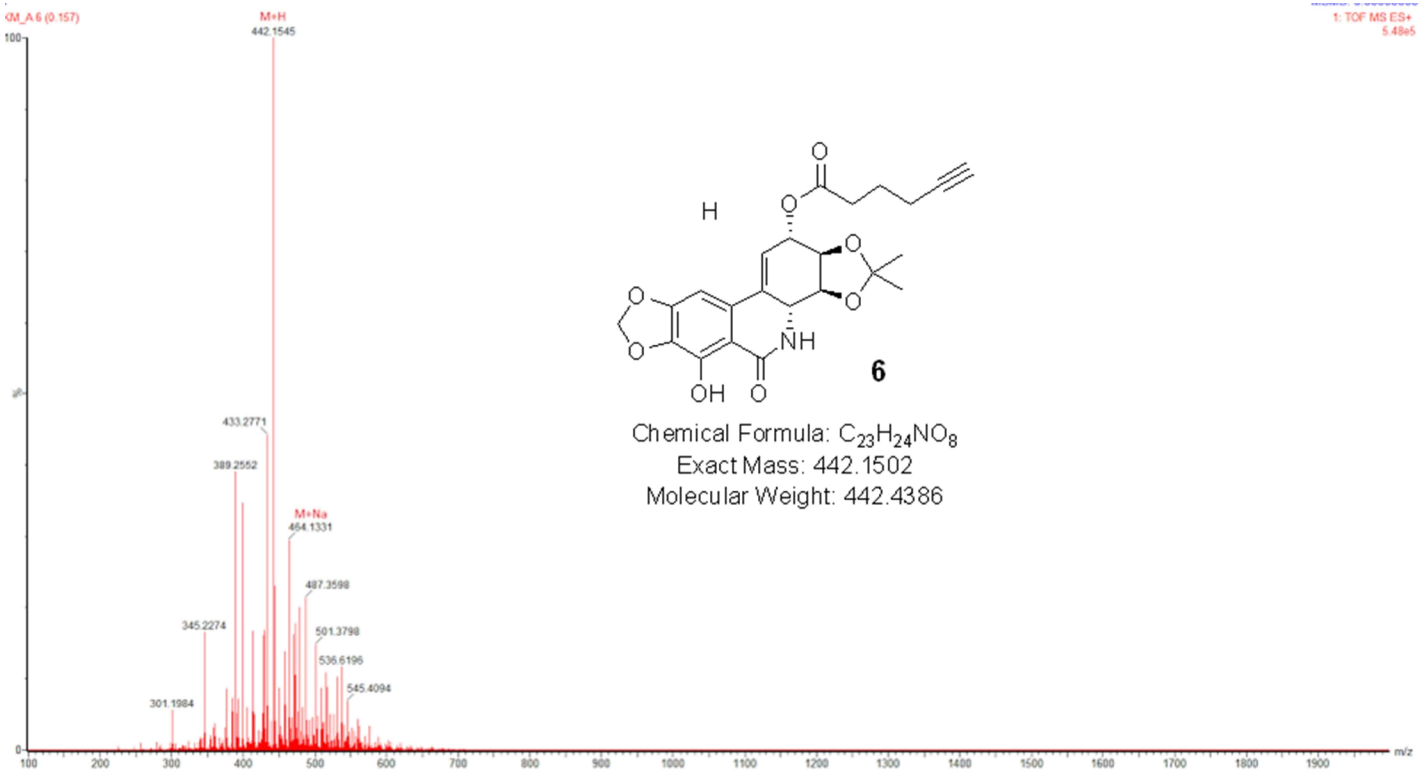

6

Chemical Formula: $C_{23}H_{24}NO_8$
Exact Mass: 442.1502
Molecular Weight: 442.4386

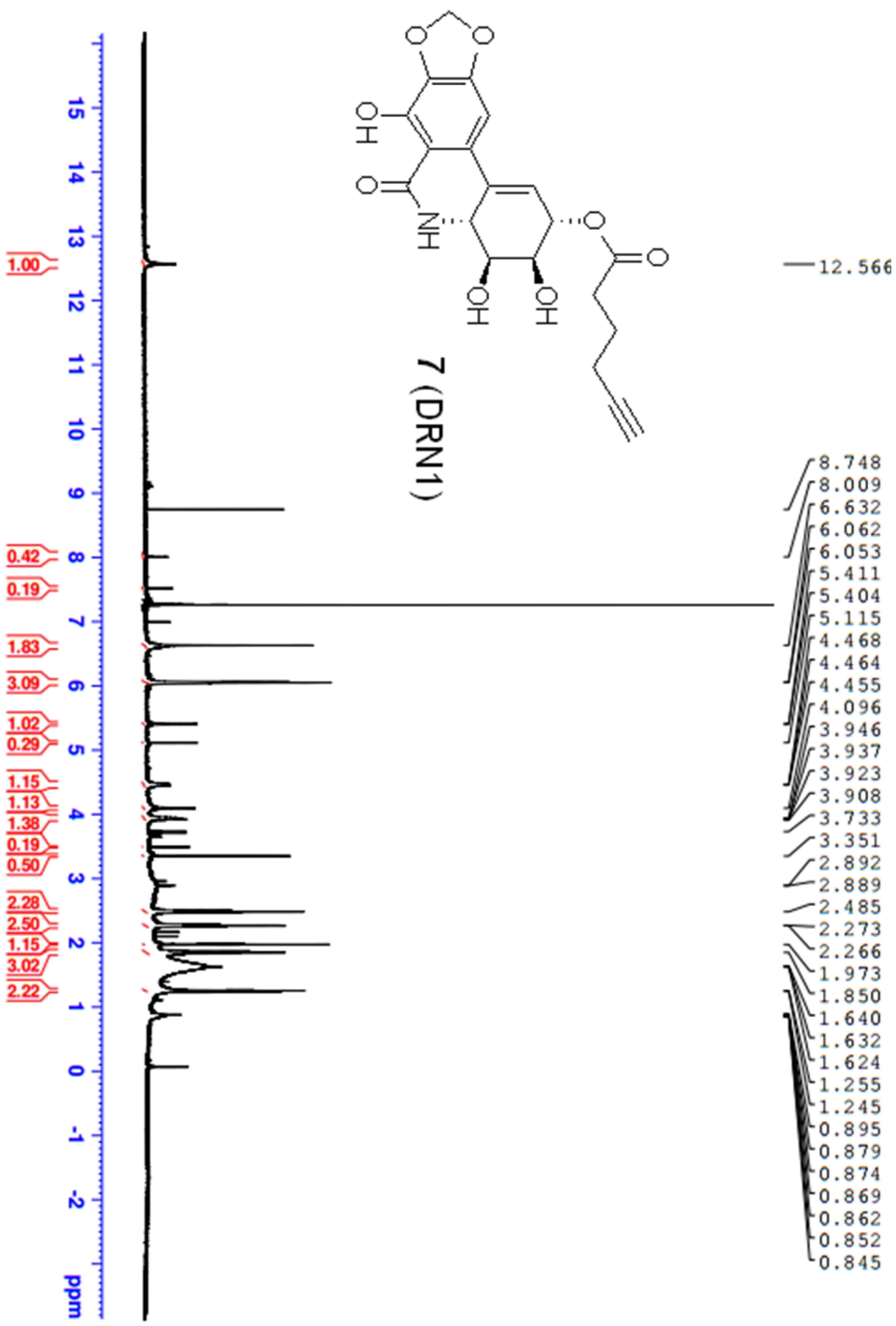
7 (DRN1)
12.566
8.748
8.009
6.632
6.062
6.053
5.411
5.404
5.115
4.468
4.464
4.455
4.096
3.946
3.937
3.923
3.908
3.733
3.351
2.892
2.889
2.485
2.273
2.266
1.973
1.850
1.640
1.632
1.624
1.255
1.245
0.895
0.879
0.874
0.869
0.862
0.852
0.845
1.00
0.42
0.19
1.83
3.09
1.02
0.29
1.15
1.13
1.38
0.19
0.50
2.28
2.50
1.15
3.02
2.22
ppm

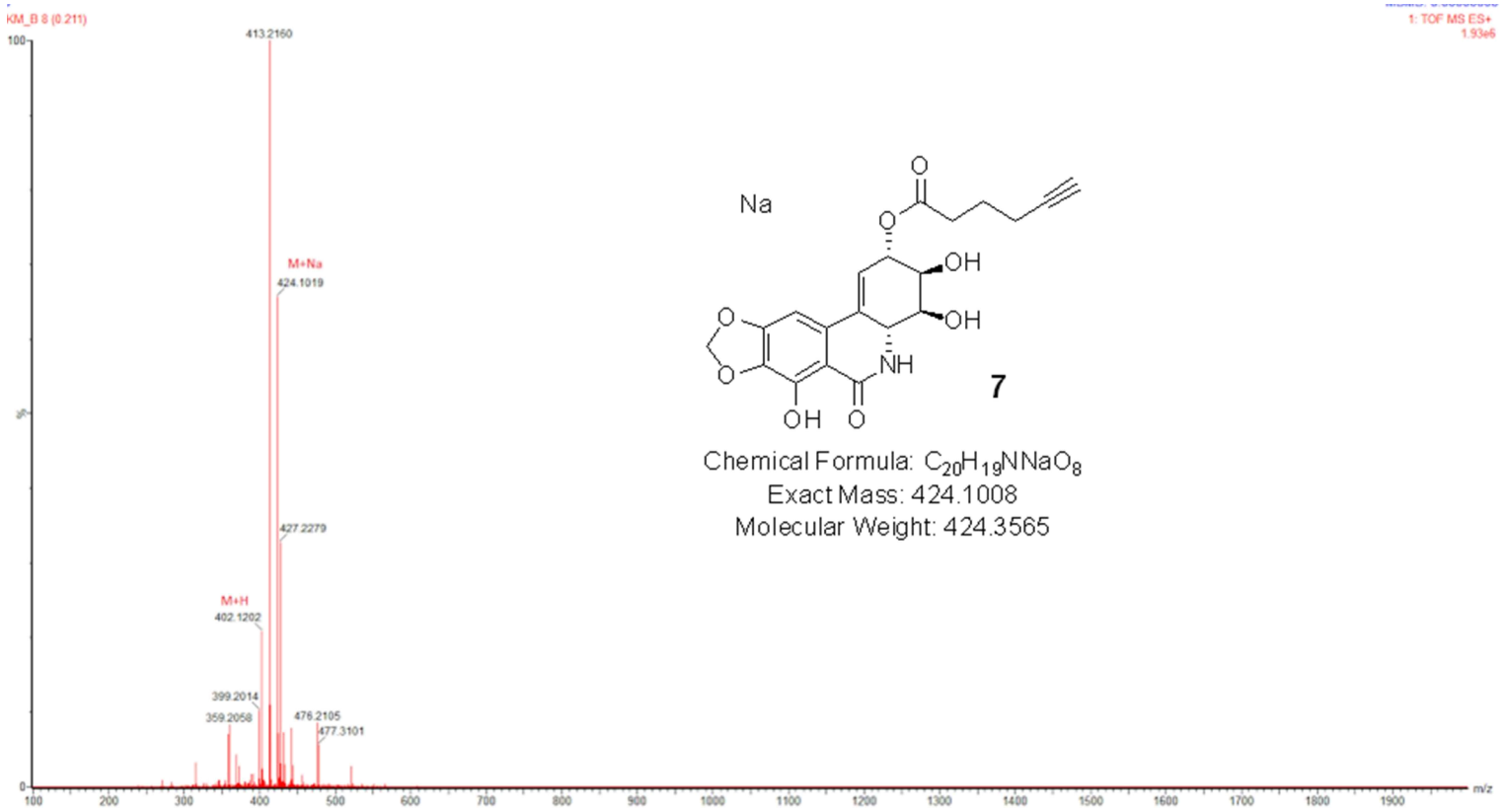

7

Chemical Formula: $C_{20}H_{19}NNaO_8$
Exact Mass: 424.1008
Molecular Weight: 424.3565

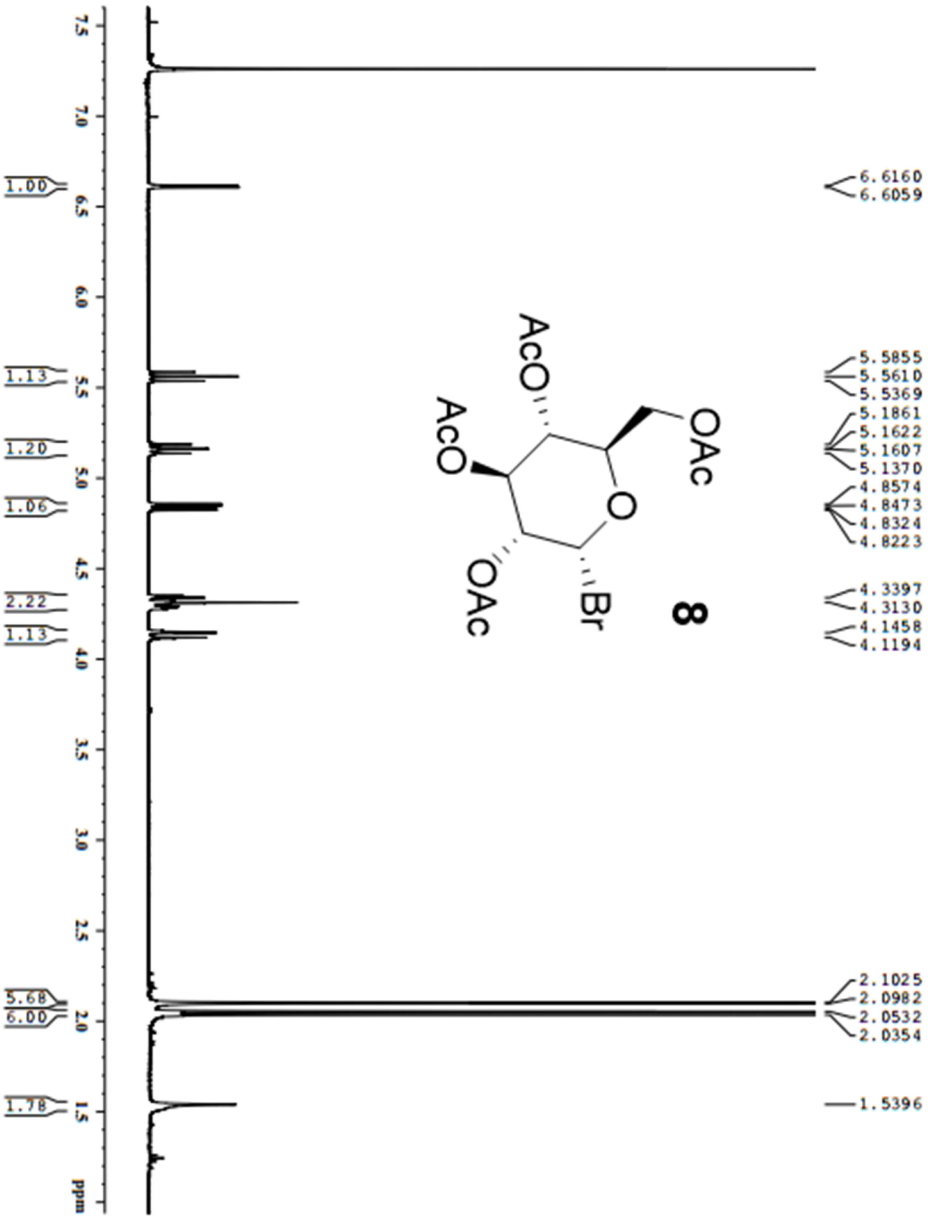
AcO
AcO
OAc
OAc
O
Br
8
6.6160
6.6059
5.5855
5.5610
5.5369
5.1861
5.1622
5.1607
5.1370
4.8574
4.8473
4.8324
4.8223
4.3397
4.3130
4.1458
4.1194
2.1025
2.0982
2.0532
2.0354
1.5396
1.00
1.13
1.20
1.06
2.22
1.13
5.68
6.00
1.78
ppm

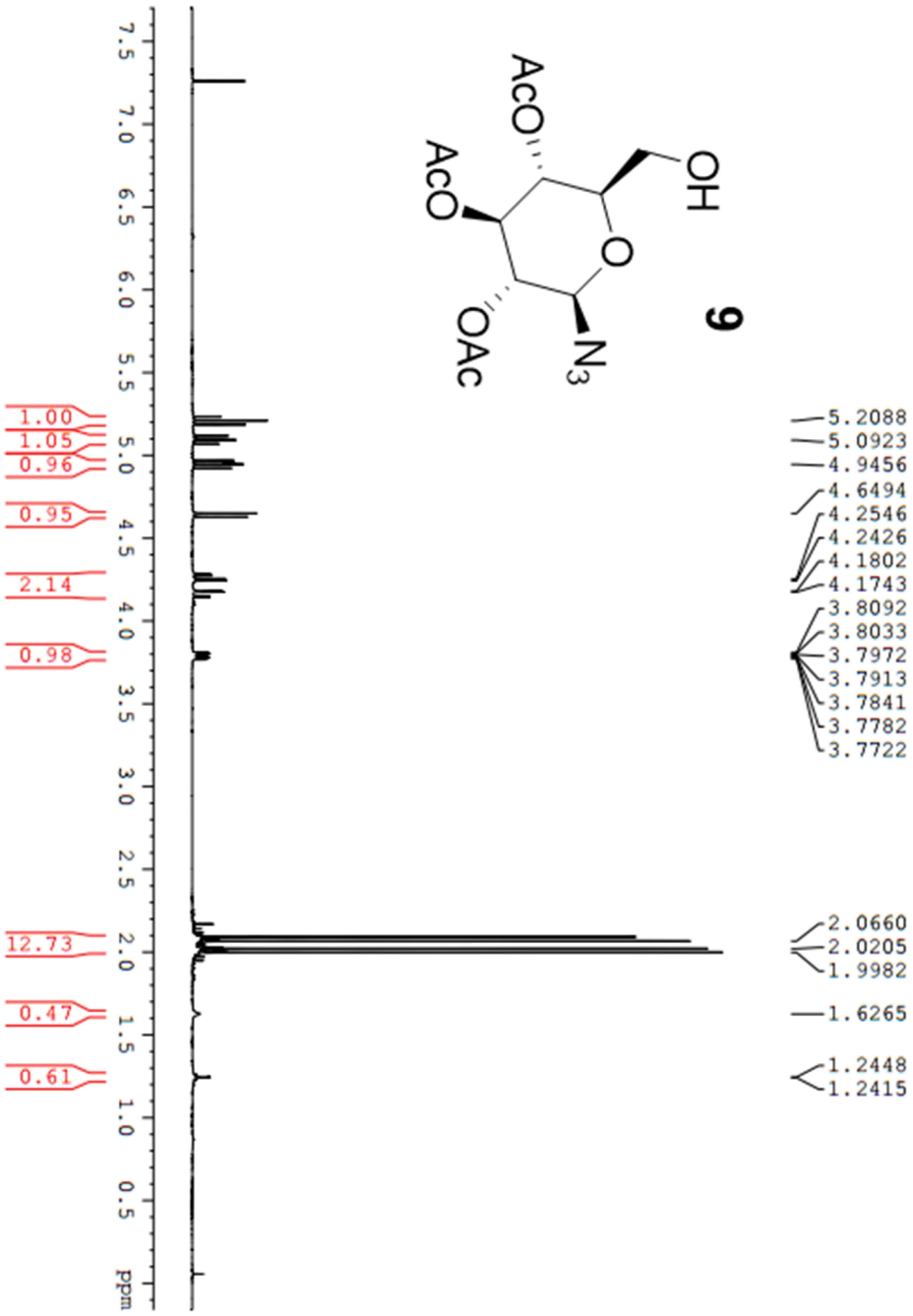
AcO
AcO
OAc
O
N3
OH
9
1.00
1.05
0.96
0.95
2.14
0.98
12.73
0.47
0.61
7.5
7.0
6.5
6.0
5.5
5.0
4.5
4.0
3.5
3.0
2.5
2.0
1.5
1.0
0.5
ppm
5.2088
5.0923
4.9456
4.6494
4.2546
4.2426
4.1802
4.1743
3.8092
3.8033
3.7972
3.7913
3.7841
3.7782
3.7722
2.0660
2.0205
1.9982
1.6265
1.2448
1.2415

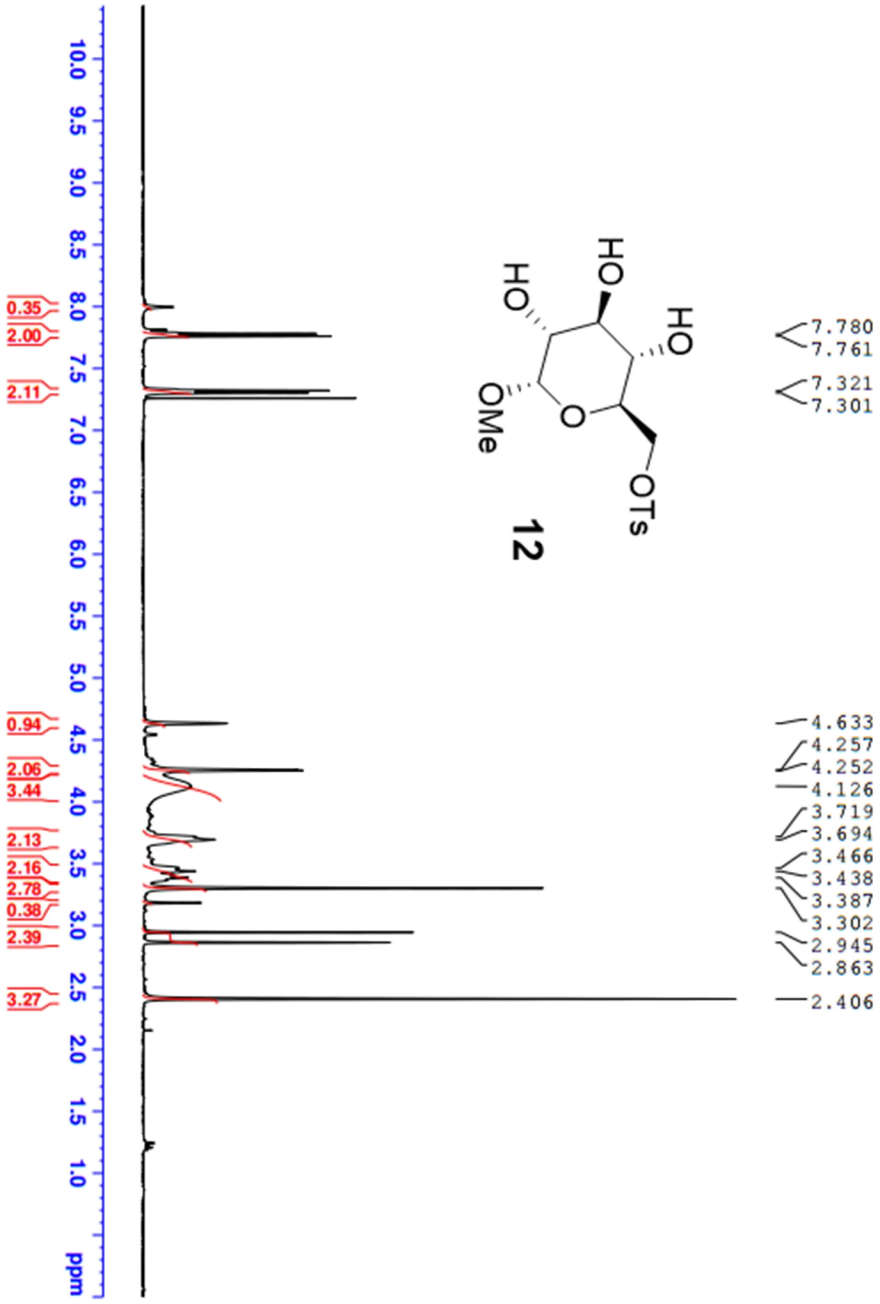
HO
HO
HO
OMe
O
OTs
12
7.780
7.761
7.321
7.301
4.633
4.257
4.252
4.126
3.719
3.694
3.466
3.438
3.387
3.302
2.945
2.863
2.406
0.35
2.00
2.11
0.94
2.06
3.44
2.13
2.16
2.78
0.38
2.39
3.27
10.0
9.5
9.0
8.5
8.0
7.5
7.0
6.5
6.0
5.5
5.0
4.5
4.0
3.5
3.0
2.5
2.0
1.5
1.0
ppm

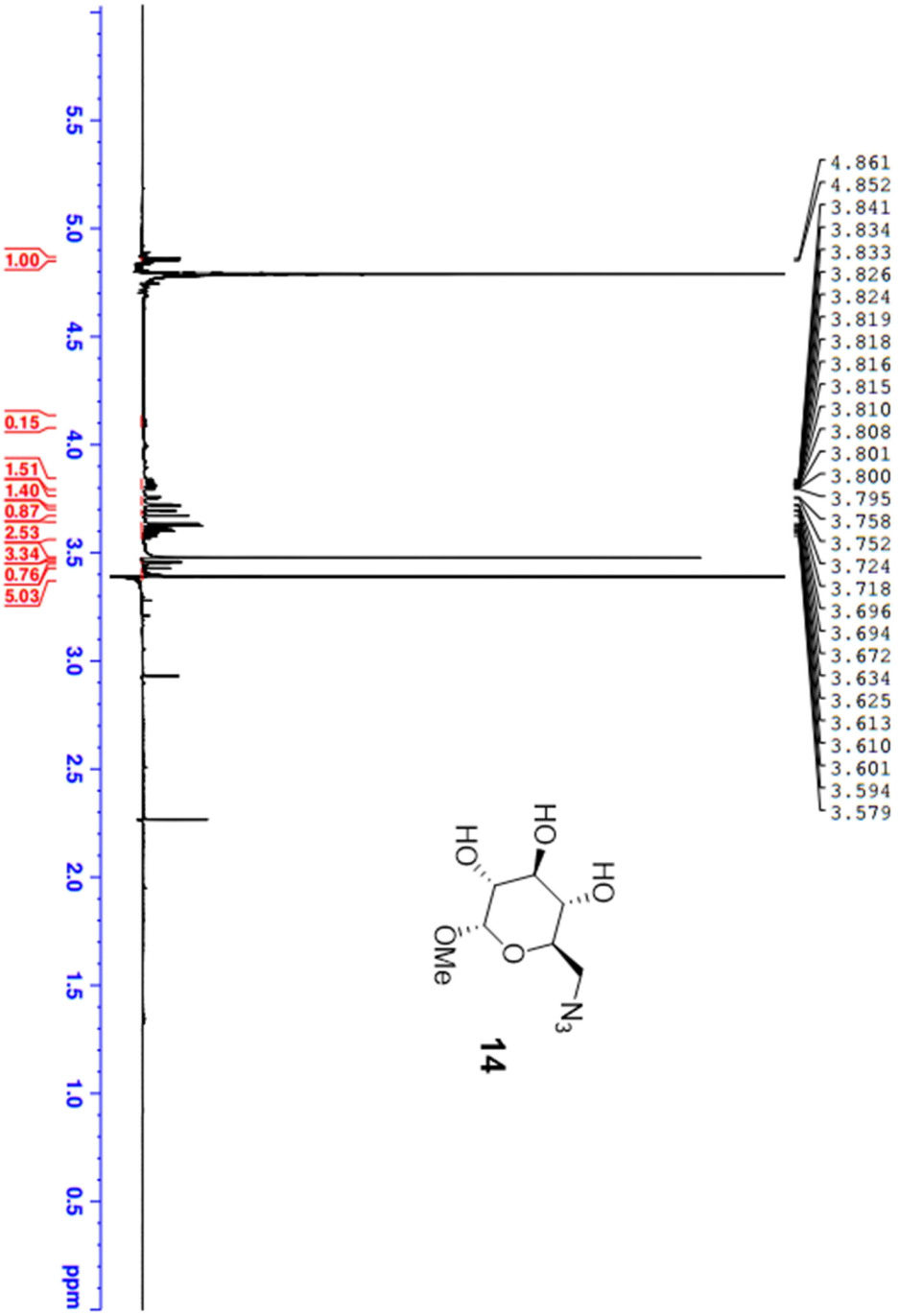
4.861
4.852
3.841
3.834
3.833
3.826
3.824
3.819
3.818
3.816
3.815
3.810
3.808
3.801
3.800
3.795
3.758
3.752
3.724
3.718
3.696
3.694
3.672
3.634
3.625
3.613
3.610
3.601
3.594
3.579
1.00
0.15
1.51
1.40
0.87
2.53
3.34
0.76
5.03
5.5
5.0
4.5
4.0
3.5
3.0
2.5
2.0
1.5
1.0
0.5
ppm
HO
HO
HO
OMe
O
N3
14

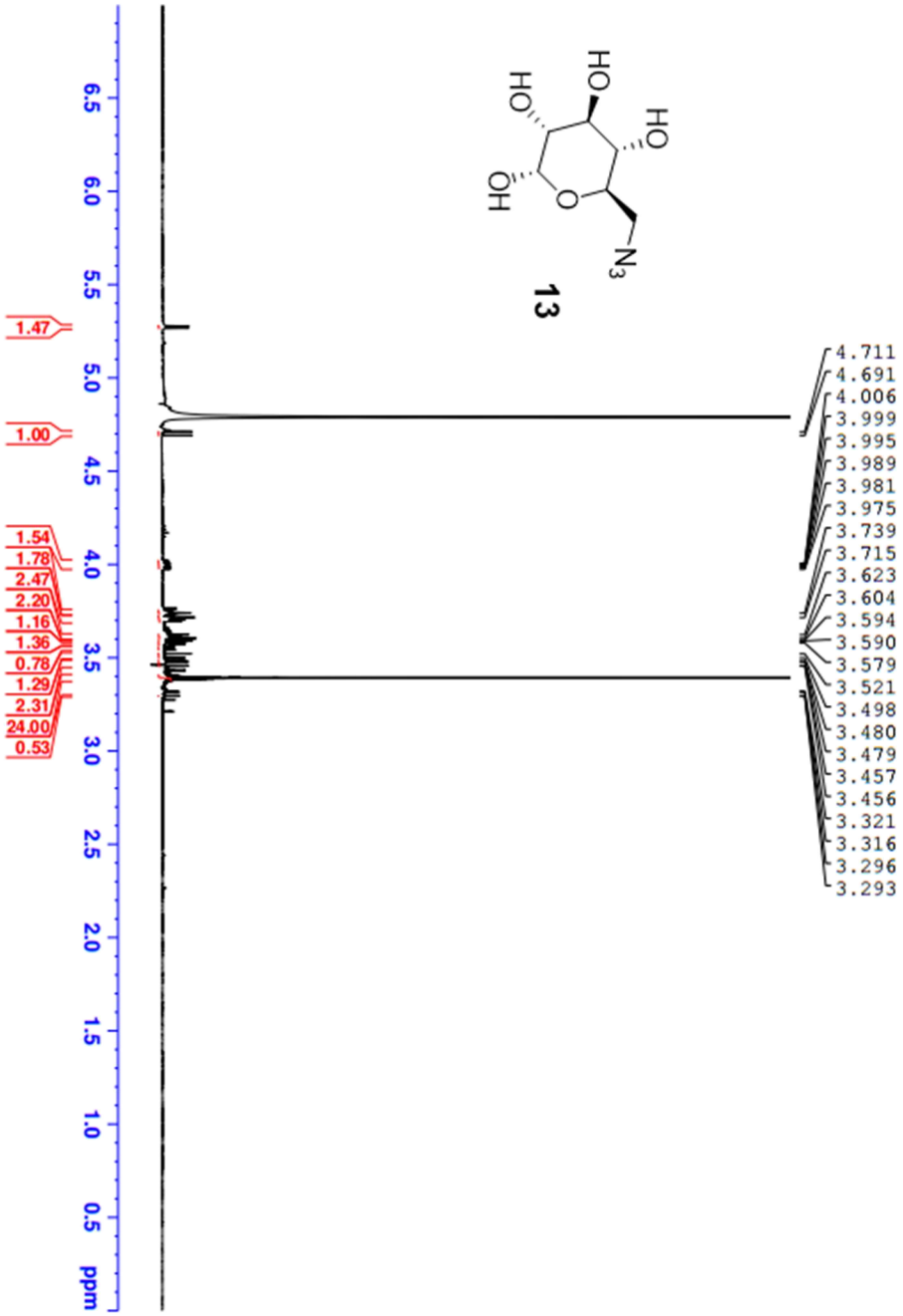
HO
HO
HO
OH
O
N3
13
1.47
1.00
1.54
1.78
2.47
2.20
1.16
1.36
0.78
1.29
2.31
24.00
0.53
4.711
4.691
4.006
3.999
3.995
3.989
3.981
3.975
3.739
3.715
3.623
3.604
3.594
3.590
3.579
3.521
3.498
3.480
3.479
3.457
3.456
3.321
3.316
3.296
3.293
6.5
6.0
5.5
5.0
4.5
4.0
3.5
3.0
2.5
2.0
1.5
1.0
0.5
ppm

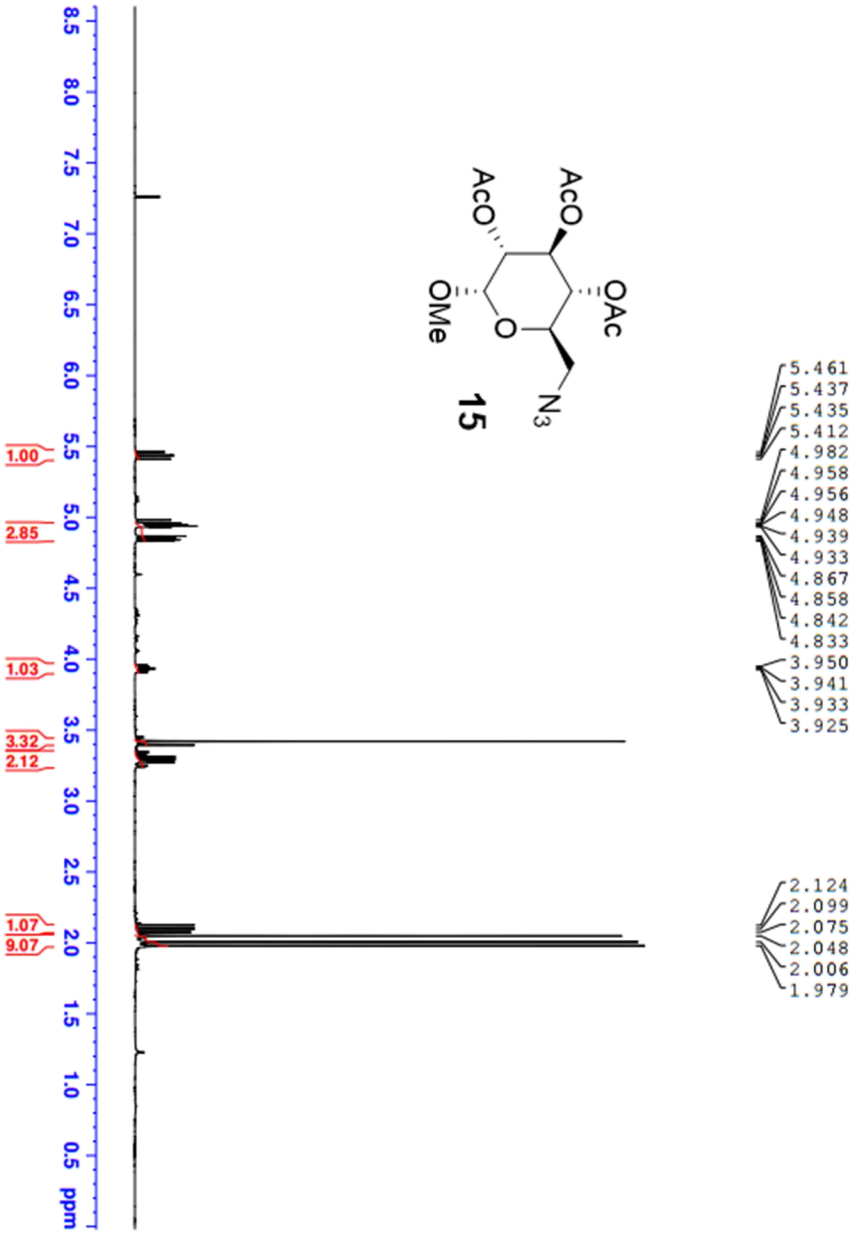
AcO
AcO
OAc
OMe
O
N3
15
5.461
5.437
5.435
5.412
4.982
4.958
4.956
4.948
4.939
4.933
4.867
4.858
4.842
4.833
3.950
3.941
3.933
3.925
2.124
2.099
2.075
2.048
2.006
1.979
1.00
2.85
1.03
3.32
2.12
1.07
9.07
8.5
8.0
7.5
7.0
6.5
6.0
5.5
5.0
4.5
4.0
3.5
3.0
2.5
2.0
1.5
1.0
0.5
ppm

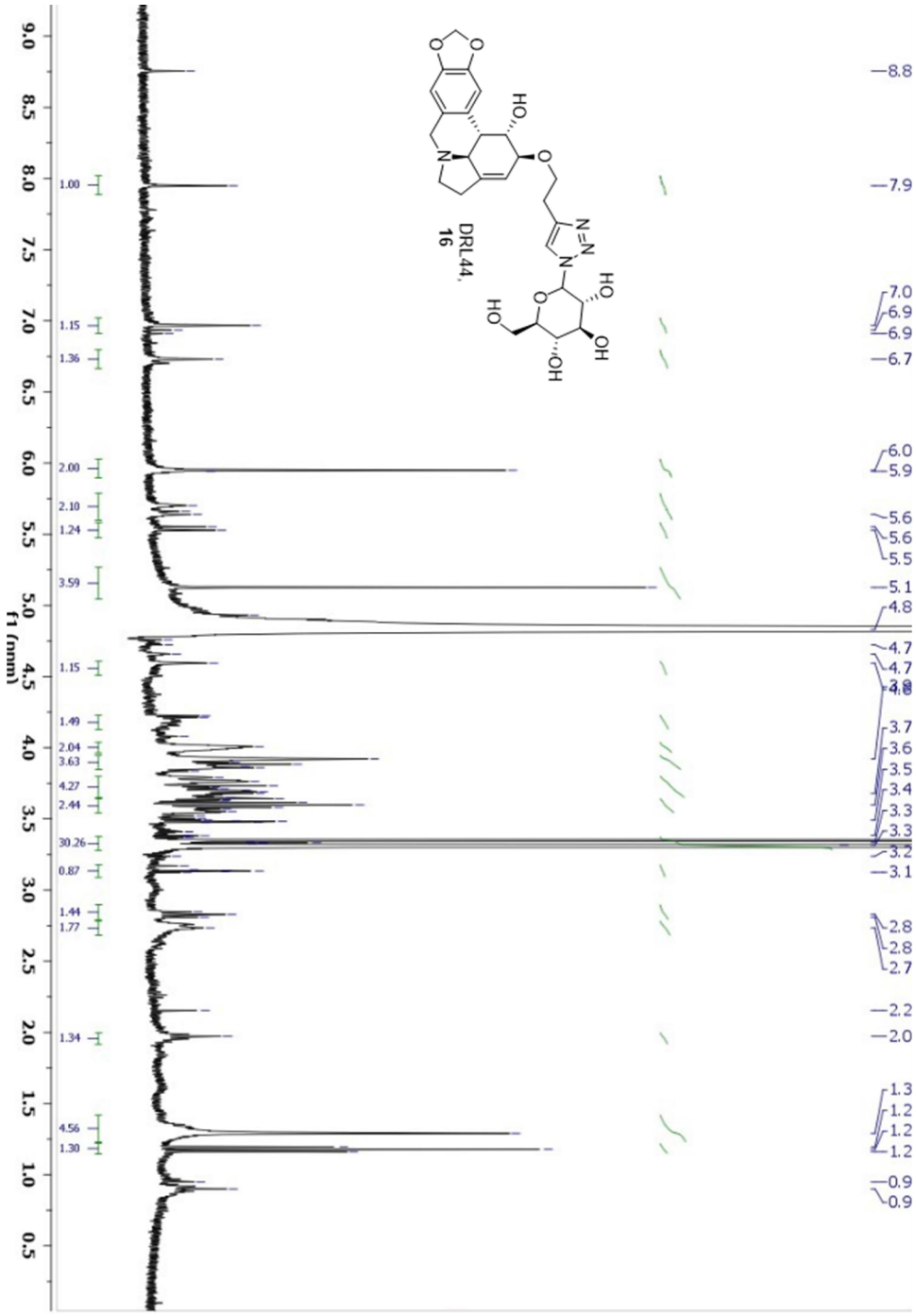
DRL44.
16
f1 (ppm)

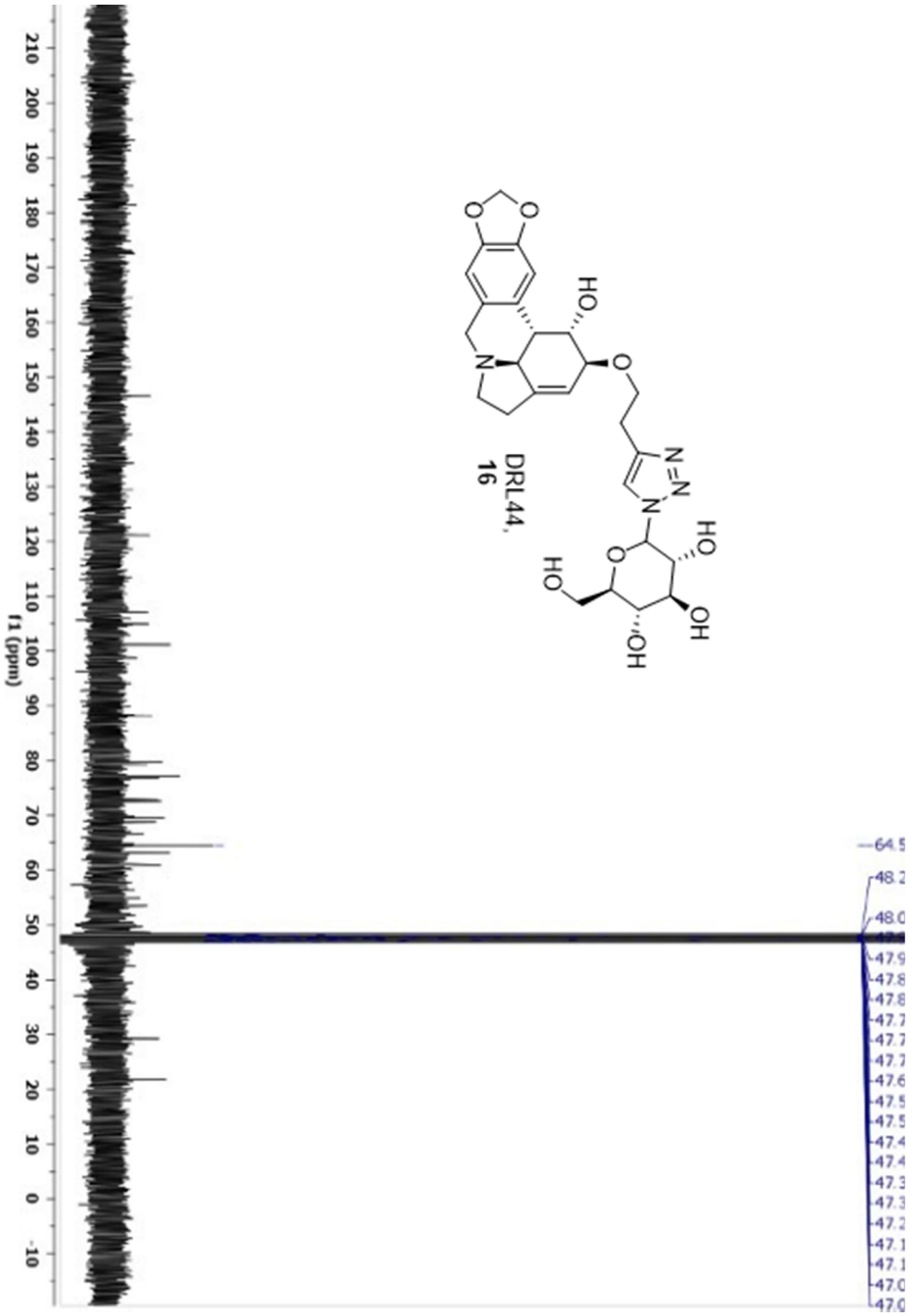
DRL44,
16
f1 (ppm)

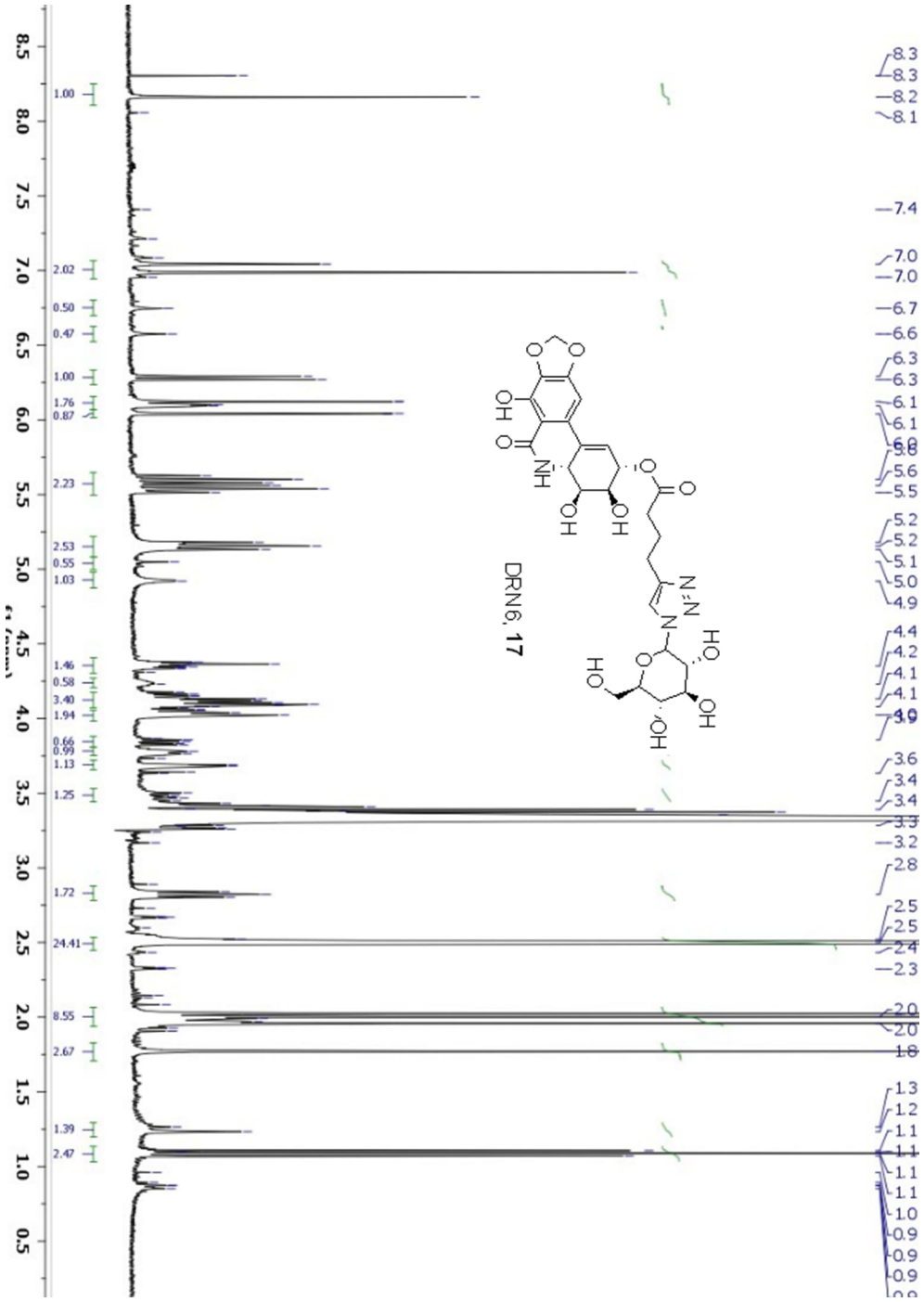
DRN6, 17

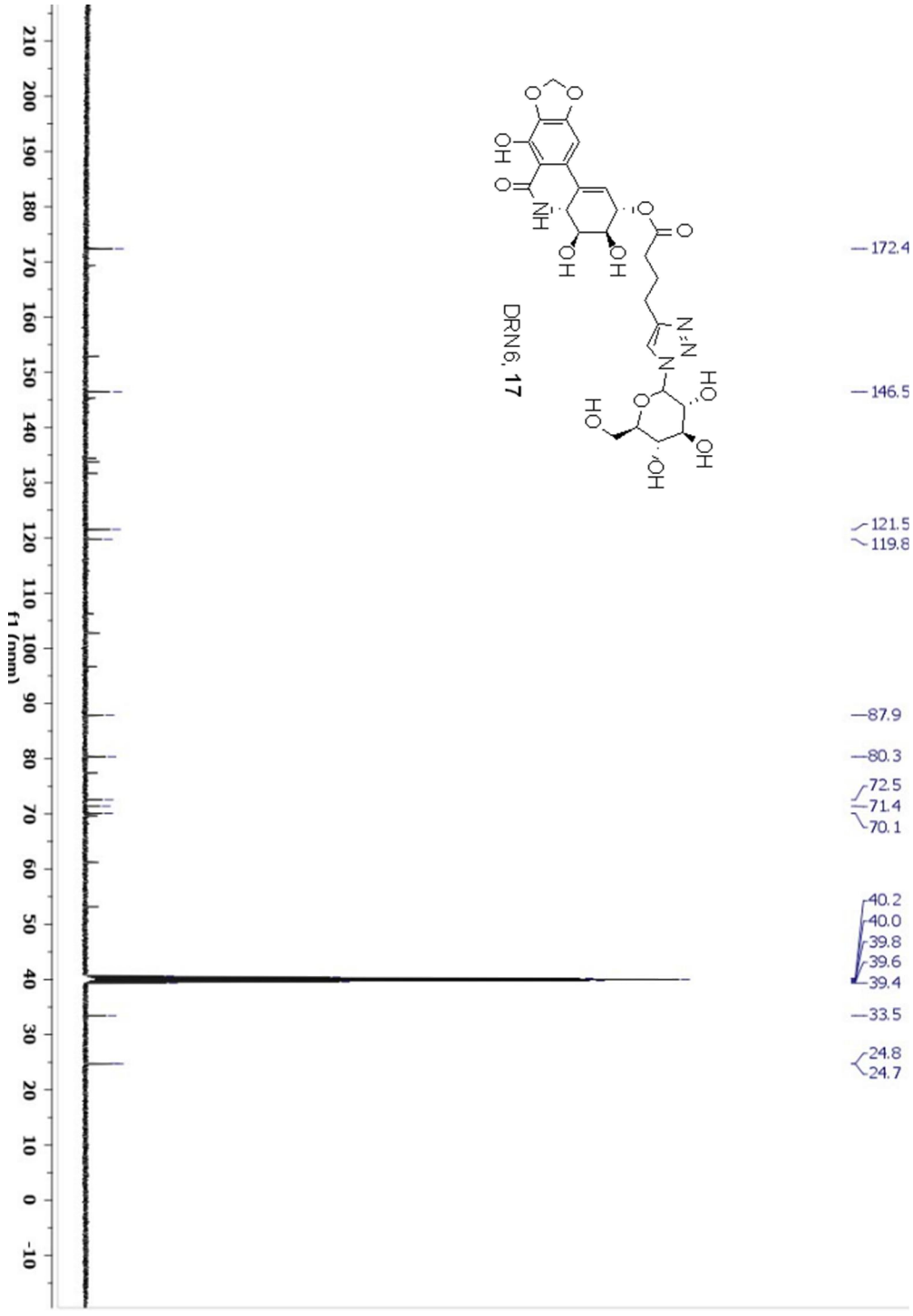
DRN6, 17
172.4
146.5
121.5
119.8
87.9
80.3
72.5
71.4
70.1
40.2
40.0
39.8
39.6
39.4
33.5
24.8
24.7
f1 (ppm)

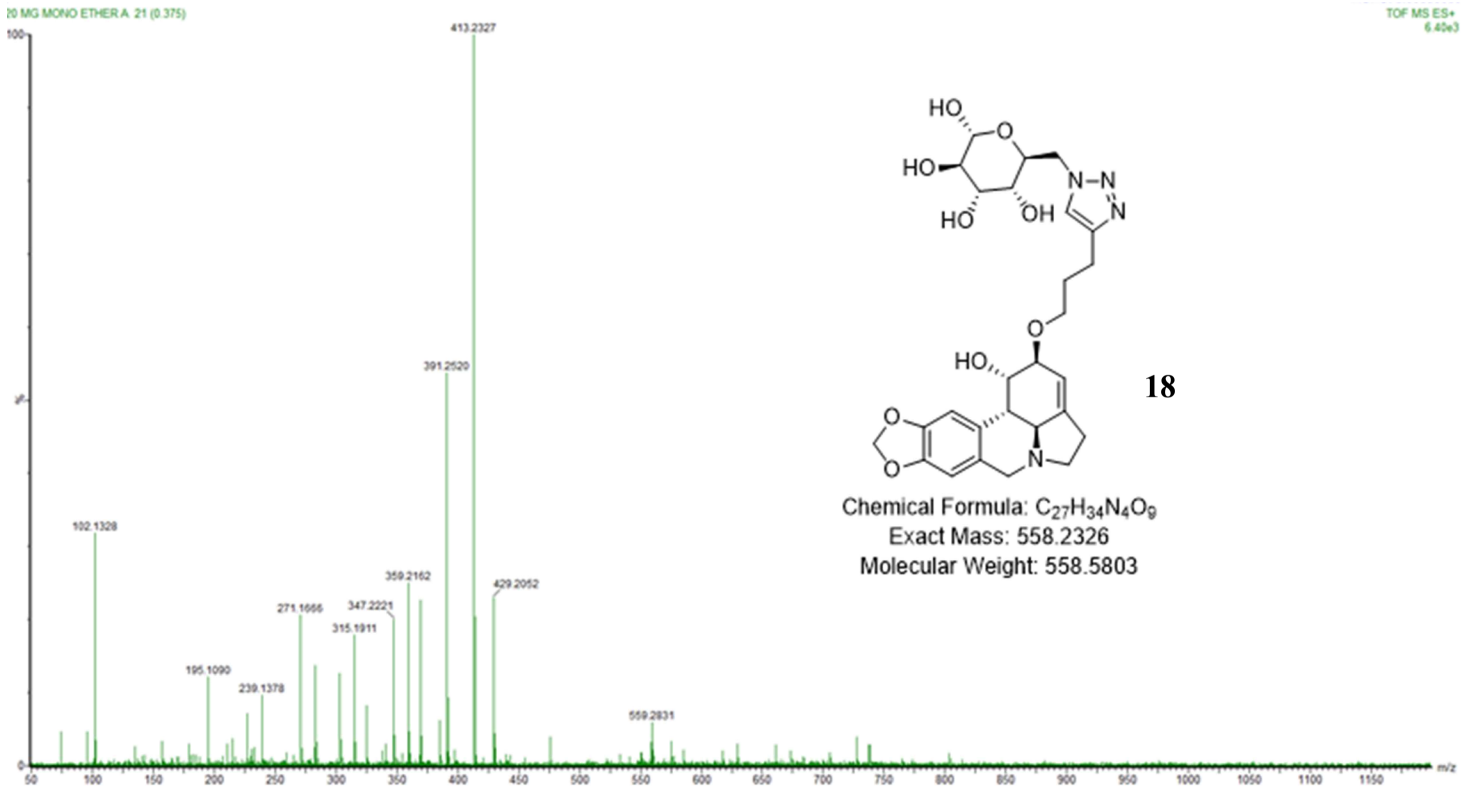

18

Chemical Formula: $C_{27}H_{34}N_4O_9$
Exact Mass: 558.2326
Molecular Weight: 558.5803

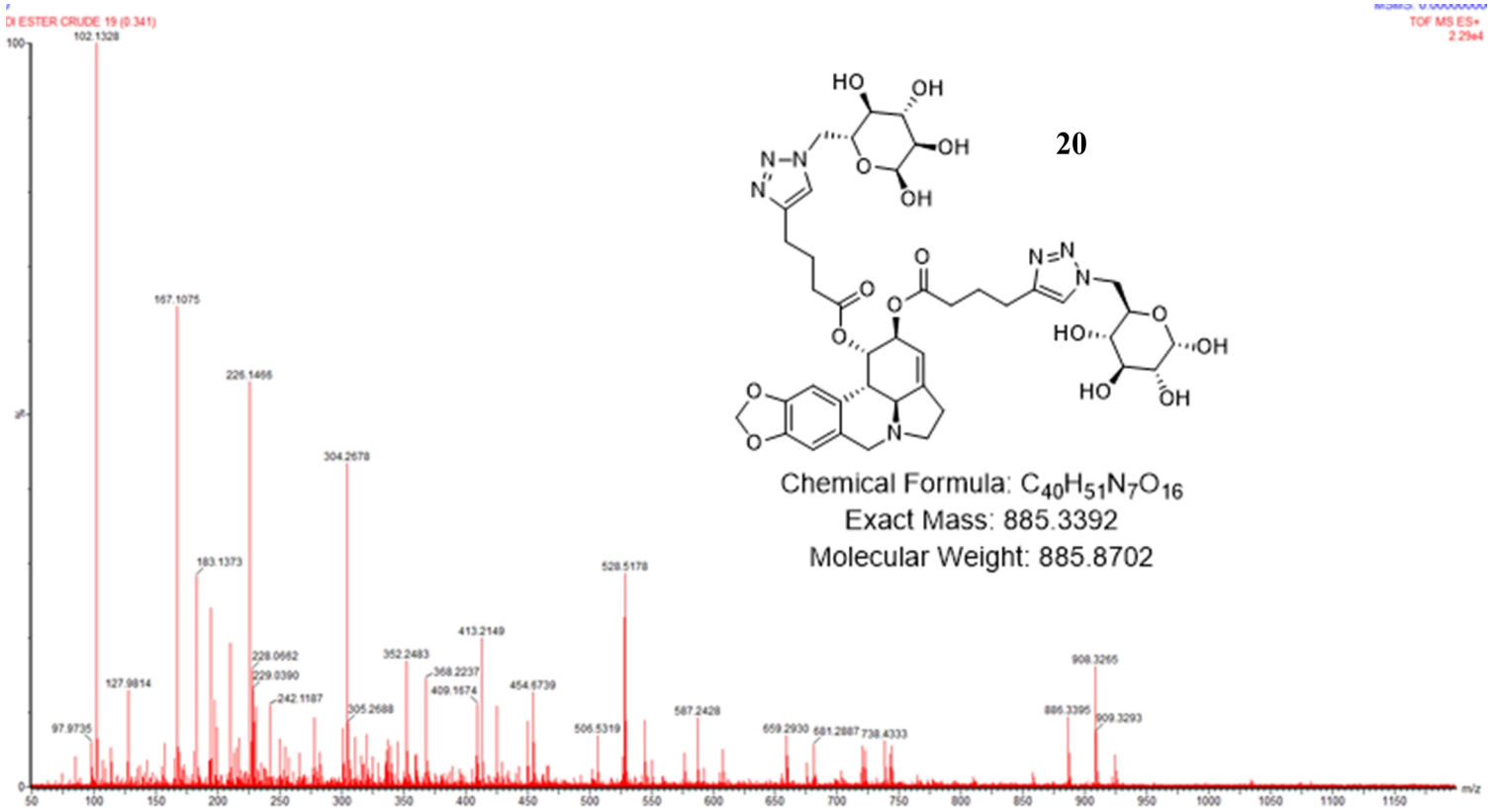
DI ESTER CRUDE 19 (0.341)
TOF MS ES+
2.29e4
100
%
0
102.1328
167.1075
226.1466
304.2678
183.1373
528.5178
413.2149
352.2483
228.0662
229.0390
368.2237
409.1674
454.6739
127.9814
242.1187
305.2688
97.9735
506.5319
587.2428
659.2930
681.2887
738.4333
908.3265
886.3395
909.3293
50
100
150
200
250
300
350
400
450
500
550
600
650
700
750
800
850
900
950
1000
1050
1100
1150
m/z
20
Chemical Formula: $C_{40}H_{51}N_7O_{16}$
Exact Mass: 885.3392
Molecular Weight: 885.8702

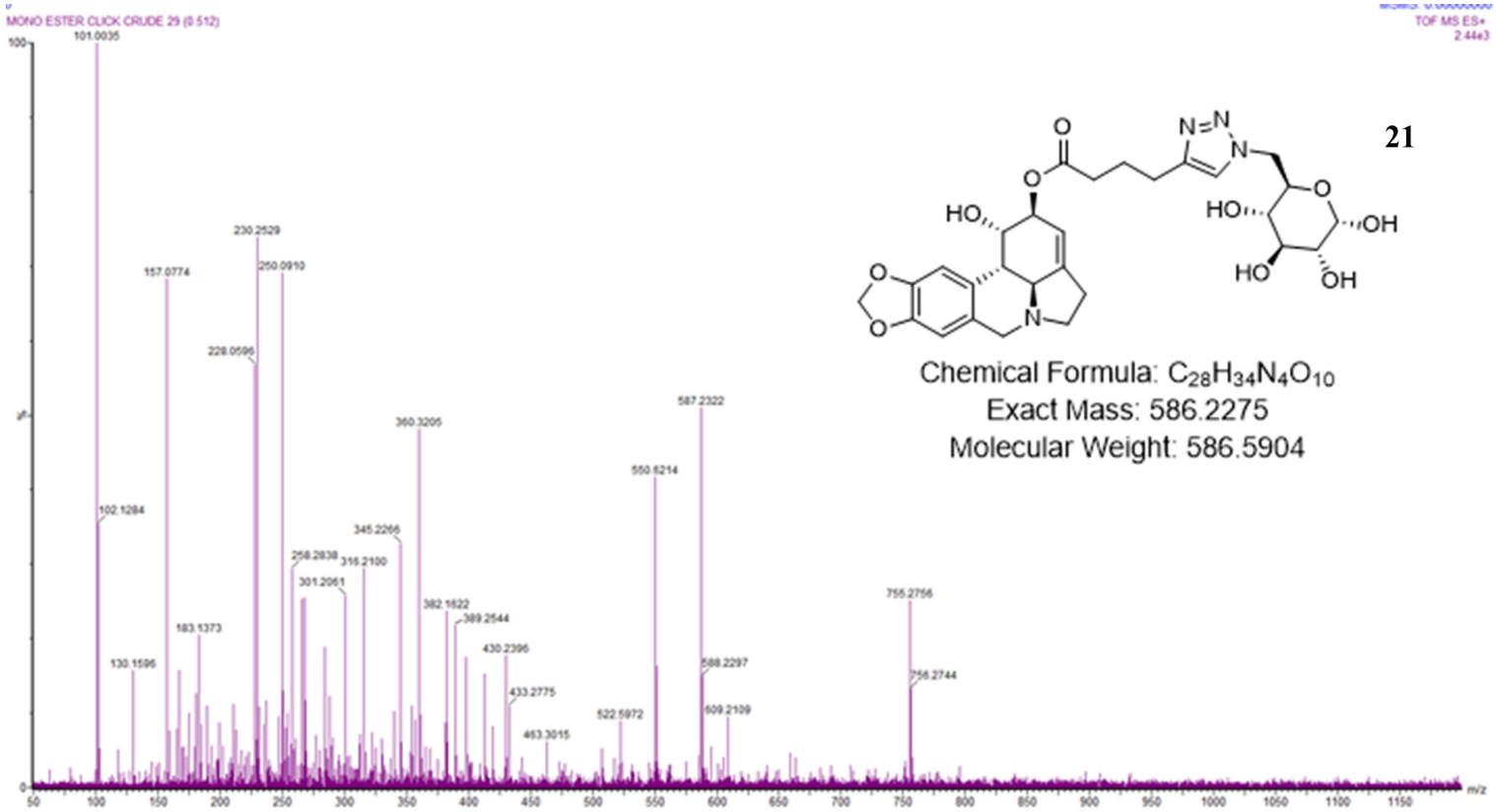
MONO ESTER CLICK CRUDE 29 (0.512)
TOF MS ES+
2.44e3
101.0035
230.2529
250.0910
157.0774
228.0596
360.3205
587.2322
550.6214
102.1284
345.2266
258.2838
316.2100
301.2061
382.1622
389.2544
755.2756
183.1373
430.2396
130.1596
588.2297
433.2775
756.2744
609.2109
522.5972
463.3015
m/z
21
Chemical Formula: $C_{28}H_{34}N_4O_{10}$
Exact Mass: 586.2275
Molecular Weight: 586.5904

VI. REFERENCES

1. Lefranc, F., J. Brotchi, and R. Kiss. Possible Future Issues in the Treatment of Glioblastomas: Special Emphasis on Cell Migration and the Resistance of Migrating Glioblastoma Cells to Apoptosis. *Journal of Clinical Oncology* **2005**. *23*(10): 2411-2422.

2. Alifieris, C. and D.T. Trafalis. Glioblastoma multiforme: Pathogenesis and treatment. *Pharmacology & Therapeutics* **2015**. *152*: 63-82.

3. Schimmer, A.D., et al. A Phase I Study of the Metal Ionophore Clioquinol in Patients With Advanced Hematologic Malignancies. *Clinical Lymphoma Myeloma and Leukemia* **2012**. *12*(5): 330-336.

4. Wen , P.Y. and S. Kesari. Malignant Gliomas in Adults. *New England Journal of Medicine* **2008**. *359*(5): 492-507.

5. Cheng, L., et al. Elevated invasive potential of glioblastoma stem cells. *Biochemical and Biophysical Research Communications* **2011**. *406*(4): 643-648.

6. Vokes, E.E., D.M. Brizel, and T.S. Lawrence. Concomitant Chemoradiotherapy. *J Clin Oncol.* **2007**. *25*(26): 4031-4032.

7. Juillerat-Jeanneret, L. The targeted delivery of cancer drugs across the blood–brain barrier: chemical modifications of drugs or drug-nanoparticles? *Drug Discovery Today* **2008**. *13*(23–24): 1099-1106.

8. Guo, L., J. Ren, and X. Jiang. Perspectives on brain-targeting drug delivery systems. *Curr Pharm Biotechnol* **2012**. *13*(12): 2310-8.

9. Dasari, R., et al. C1,C2-ether derivatives of the Amaryllidaceae alkaloid lycorine: Retention of activity of highly lipophilic analogues against cancer cells. *Bioorganic & Medicinal Chemistry Letters* **2014**. *24*(3): 923-927.

10. Kornienko, A. and A. Evidente. Chemistry, Biology, and Medicinal Potential of Narciclasine and its Congeners. *Chemical Reviews* **2008**. *108*(6): 1982-2014.

11. Lamoral-Theys, D., et al. Lycorine, the Main Phenanthridine Amaryllidaceae Alkaloid, Exhibits Significant Antitumor Activity in Cancer Cells That Display Resistance to Proapoptotic Stimuli: An Investigation of Structure−Activity Relationship and Mechanistic Insight. *Journal of Medicinal Chemistry* **2009**. *52*(20): 6244-6256.

12. Nakagawa, Y. and S. Uyeo. Stereochemistry of reduction products of 1-acetyl-lycorin-2-one. *Journal of the Chemical Society* **1959**. 3736-3741.

13. Ceriotti, G. Narciclasine: an Antimitotic Substance from Narcissus Bulbs. *Nature* **1967**. *213*(5076): 595-596.

14. Wang, P., et al. Novel Lycorine Derivatives as Anticancer Agents: Synthesis and In Vitro Biological Evaluation. *Molecules* **2014**. *19*(2): 2469.

15. Cao, Z., P. Yang, and Q. Zhou. Multiple biological functions and pharmacological effects of lycorine. *Science China Chemistry* **2013**. *56*(10): 1382-1391.

16. Ingrassia, L., et al. Structure−Activity Relationship Analysis of Novel Derivatives of Narciclasine (an Amaryllidaceae Isocarbostyril Derivative) as Potential Anticancer Agents. *Journal of Medicinal Chemistry* **2009**. *52(*4): 1100-1114.

17. Mégalizzi, V., et al. 4-IBP, a σ1 Receptor Agonist, Decreases the Migration of Human Cancer Cells, Including Glioblastoma Cells, In Vitro and Sensitizes Them In Vitro and In Vivo to Cytotoxic Insults of Proapoptotic and Proautophagic Drugs. *Neoplasia* **2007**. *9*(5): 358-369.

18. Serlin, Y., et al. Anatomy and physiology of the blood–brain barrier. *Seminars in Cell & Developmental Biology* **2015**. *38:* 2-6.

19. Löscher, W. and H. Potschka. Role of drug efflux transporters in the brain for drug disposition and treatment of brain diseases. *Progress in Neurobiology* **2005**. *76*(1): 22-76.

20. Pulicherla, K.K. and M.K. Verma. Targeting Therapeutics Across the Blood Brain Barrier (BBB), Prerequisite Towards Thrombolytic Therapy for Cerebrovascular Disorders—an Overview and Advancements. *AAPS PharmSciTech* **2015**. *16*(2): 223-233.

21. Hervé, F., N. Ghinea, and J.-M. Scherrmann. CNS Delivery Via Adsorptive Transcytosis. *The AAPS Journal* **2008**. *10*(3): 455-472.

22. Pohl, J., et al. D-19575—a sugar-linked isophosphoramide mustard derivative exploiting transmembrane glucose transport. *Cancer Chemotherapy and Pharmacology* **1995**. *35*(5): 364-370.

23. Stupp, R., et al. Effects of radiotherapy with concomitant and adjuvant temozolomide versus radiotherapy alone on survival in glioblastoma in a randomised phase III study: 5-year analysis of the EORTC-NCIC trial. *The Lancet Oncology* **2009**. *10*(5): 459-466.

24. Giaccone, G., et al. Glufosfamide administered by 1-hour infusion as a second-line treatment for advanced non-small cell lung cancer: a phase II trial of the EORTC-New Drug Development Group. *European Journal of Cancer* **2004**. *40*(5): 667-672.

25. Calvaresi, E.C. and P.J. Hergenrother. Glucose conjugation for the specific targeting and treatment of cancer. *Chemical Science* **2013**. *4*(6): 2319-2333.

26. Oliveri, V., et al. Gluconjugates of 8-hydroxyquinolines as potential anti-cancer prodrugs. *Dalton Transactions* **2012**. *41*(15): 4530-4535.

27. Grigsby, P.W., et al. Irradiation with or without misonidazole for patients with stages IIIb and IVa carcinoma of the cervix: final results of RTOG 80-05. *International Journal of Radiation Oncology*Biology*Physics* **1999**. *44*(3): 513-517.

28. Peltier-Pain, P., et al. Warfarin Glycosylation Invokes a Switch from Anticoagulant to Anticancer Activity. *ChemMedChem* **2011**. *6*(8): 1347-1350.

29. Gynther, M., et al. Glucose Promoiety Enables Glucose Transporter Mediated Brain Uptake of Ketoprofen and Indomethacin Prodrugs in Rats. *Journal of Medicinal Chemistry* **2009**. *52*(10): 3348-3353.

30. Warburg, O., F. Wind, and E. Negelein. THE METABOLISM OF TUMORS IN THE BODY. *The Journal of General Physiology* **1927**. *8*(6): 519-530.

31. Deng, D., et al. Crystal structure of the human glucose transporter GLUT1. *Nature* **2014**. *510*(7503): 121-125.

32. Zhou, J., et al. Transporter-mediated tissue targeting of therapeutic molecules in drug discovery. *Bioorganic & Medicinal Chemistry Letters* **2015**. *25*(5): 993-997.

33. Van Goietsenoven, G., et al. Amaryllidaceae Alkaloids Belonging to Different Structural Subgroups Display Activity against Apoptosis-Resistant Cancer Cells. *Journal of Natural Products* **2010**. *73*(7): 1223-1227.

34. Mosmann, T. Rapid colorimetric assay for cellular growth and survival: Application to proliferation and cytotoxicity assays. *Journal of Immunological Methods* **1983**. *65*(1): 55-63.

35. Tiwari, V.K., et al. Cu-Catalyzed Click Reaction in Carbohydrate Chemistry. *Chemical Reviews* **2016**. *116*(5): 3086-3240.

36. Temelkoff, D.P., M. Zeller, and P. Norris. N-Glycoside neoglycotrimers from 2,3,4,6-tetra-O-acetyl-β-d-glucopyranosyl azide. *Carbohydrate Research* **2006**. *341*(9): 1081-1090.

37. Fernández, C., et al. Synthesis and biological studies of glycosyl dopamine derivatives as potential antiparkinsonian agents. *Carbohydrate Research* **2000**. *327*(4): 353-365.

38. Mueckler, M. and C. Makepeace. Transmembrane Segment 6 of the Glut1 Glucose Transporter Is an Outer Helix and Contains Amino Acid Side Chains Essential for Transport Activity. *Journal of Biological Chemistry* **2008**. *283*(17): 11550-11555.

39. Mo, Y. Computational evidence that hyperconjugative interactions are not responsible for the anomeric effect. *Nat Chem* **2010**. *2*(8): 666-671.

40. Kumar, R., P.R. Maulik, and A.K. Misra. Significant rate accelerated synthesis of glycosyl azides and glycosyl 1,2,3-triazole conjugates. *Glycoconjugate Journal* **2008**. *25*(7): 595-602.

41. Wang, P., et al. Enzymes in oligosaccharide synthesis: active-domain overproduction, specificity study, and synthetic use of an .alpha.-1,2-mannosyltransferase with regeneration of GDP-Man. *The Journal of Organic Chemistry* **1993**. *58*(15): 3985-3990.

42. Overend, W.G., C.W. Rees, and J.S. Sequeira. Reactions at position 1 of carbohydrates. Part III. The acid-catalysed hydrolysis of glycosides. *Journal of the Chemical Society* **1962**: 3429-3440.

43. Matsuda, K., et al. Synthesis of 6-Amino-6-deoxy-L-idopyranosides. *Bulletin of the Chemical Society of Japan* **1986**. *59*(5): 1397-1401.

44. Kolb, H.C., M.G. Finn, and K.B. Sharpless. Click Chemistry: Diverse Chemical Function from a Few Good Reactions. *Angewandte Chemie International Edition* **2001**. *40*(11): 2004-2021.

45. Himo, F., et al. Copper(I)-Catalyzed Synthesis of Azoles. DFT Study Predicts Unprecedented Reactivity and Intermediates. *Journal of the American Chemical Society* **2005**. *127*(1): 210-216.

46. Aragão-Leoneti, V., et al. Application of copper(I)-catalysed azide/alkyne cycloaddition (CuAAC) 'click chemistry' in carbohydrate drug and neoglycopolymer synthesis. *Tetrahedron* **2010**. *66*(49): 9475-9492.

47. Worrell, B.T., J.A. Malik, and V.V. Fokin. Direct Evidence of a Dinuclear Copper Intermediate in Cu(I)-Catalyzed Azide-Alkyne Cycloadditions. *Science* **2013**. *340*(6131): 457-460.

48. Durrwachter, J.R. and C.H. Wong. Fructose 1,6-diphosphate aldolase-catalyzed stereoselective synthesis of C-alkyl and N-containing sugars: thermodynamically controlled C-C bond formations. *The Journal of Organic Chemistry* **1988**. *53*(18): 4175-4181.

49. Miyazawa, T., et al. Curdlan as a Polymeric Starting Material to Access C6-

Modified Glucose Derivatives. *Journal of Carbohydrate Chemistry* **2014**. *33*(5): 252-266.